MODELING AND OPTIMIZATION OF MATRIX ACIDIZING IN HORIZONTAL WELLS IN CARBONATE RESERVOIRS

A Thesis

by

HAU TRUNG TRAN

Submitted to the Office of Graduate Studies of
Texas A&M University
in partial fulfillment of the requirements for the degree of

MASTER OF SCIENCE

Approved by:

Chair of Committee,	Ding Zhu
Committee Members,	A. Daniel Hill
	Zhengdong Cheng
Head of Department,	A. Daniel Hill

May 2013

Major Subject: Petroleum Engineering

ABSTRACT

In this study, the optimum conditions for wormhole propagation in horizontal well carbonate acidizing was investigated numerically using a horizontal well acidizing simulator. The factors that affect the optimum conditions are rock mineralogy, acid concentration, temperature and acid flux in the formation. The work concentrated on the investigation of the acid flux. Analytical equations for injection rate schedule for different wormhole models.

In carbonate acidizing, the existence of the optimum injection rate for wormhole propagation has been confirmed by many researchers for highly reactive acid/rock systems in linear core-flood experiments. There is, however, no reliable technique to translate the laboratory results to the field applications. It has also been observed that for radial flow regime in field acidizing treatments, there is no single value of acid injection rate for the optimum wormhole propagation. In addition, the optimum conditions are more difficult to achieve in matrix acidizing long horizontal wells. Therefore, the most efficient acid stimulation is only achieved with continuously increasing acid injection rates to always maintain the wormhole generation at the tip of the wormhole at its optimum conditions.

Examples of acid treatments with the increasing rate schedules were compared to those of the single optimum injection rate and the maximum allowable rate. The comparison study showed that the increasing rate treatments had the longest wormhole

penetration and, therefore, the least negative skin factor for the same amount of acid injected into the formations.

A parametric study was conducted for the parameters that have the most significant effects on the wormhole propagation conditions such as injected acid volume, horizontal well length, acid concentration, and reservoir heterogeneity. The results showed that the optimum injection rate per unit length increases with increasing injected acid volume. And it was constant for scenarios with different lateral lengths for a given system of rock/ acid and injected volume. The study also indicated that for higher acid concentration the optimum injection rate was lower. It does exist for heterogeneous permeability formations.

Field treatment data for horizontal wells in Middle East carbonate reservoirs were also analyzed for the validation of the numerical acidizing simulator.

DEDICATION

To my family and my wife, Lien.

ACKNOWLEDGEMENTS

I would like to thank Dr. Ding Zhu and Dr. A. D. Hill for their patience, guidance and support throughout the course of this research, and Dr. Zhengdong Cheng for being a member of my advisory committee.

Thanks also go to my friends and colleagues and the department faculty and staff for making my time at Texas A&M University a great experience. I would also like to thank friends in office 712 for their kindness, friendship and sharing memorable moments of student life. Special thanks to Hari and Manabu for their help and discussions during the course of this work.

Thanks to my parents for their support and encouragement, and to my wife, Lien, for her patience and love.

I would like to acknowledge the financial support from the Middle East Carbonate Stimulation joint industry project and Qatar Petroleum Research project at Texas A&M University for this research work.

NOMENCLATURE

$a_{J\,x}$	coefficient defined in Eq. 2.28
A	pipe cross-sectional area, L^2, ft^2
$b_{J\,x}$	coefficient defined in Eq. 2.29
C_0	injection acid concentration, weight fraction
c_t	total compressibility, $M^{-1}L^{-1}T^2$, psi^{-1}
d_{core}	core diameter, L, inch
$d_{e,wh}$	effective wormhole radius, L, ft
d_{pipe}	pipe diameter, L, inch
d_{ci}	casing inside diameter, L, inch
d_{to}	tubing outside diameter, L, inch
f_f	fanning friction factor, dimensionless
g	acceleration of gravitation, LT^{-2}, ft/sec^2
g_c	gravitational dimensional constant
h	thickness, L, ft
I_{ani}	anisotropy ratio, dimensionless
k	permeability, L^2, md
k_d	damage permeability, L^2, md
k_H	horizontal permeability, L^2, md
k_V	vertical permeability, L^2, md
L	length, L, ft

L_{core}	core length, L, inch
m_{wh}	number of dominant wormholes per plane
N_{Ac}	acid capacity number, dimensionless
N_{Re}	Reynolds number, dimensionless
p	pressure, mLt^{-2}, psi
p_D	dimensionless pressure, dimensionless
p_i	initial reservoir pressure, mLt^{-2}, psi
$PV_{bt,opt}$	optimum pore volume to breakthrough, dimensionless
p_w	well pressure, mLt^{-2}, psi
Δp	pressure drop, MLT^{-2}, psi
Δp_F	frictional pressure drop, MLT^{-2}, psi
q	flow rate, L^3T^{-1}, ft^3/min
q_{sR}	specific reservoir outflow rate, L^2t^{-1}, bbl/min/ft
q_w	flow rate in the wellbore, L^3t^{-1}, bbl/min
r	radial coordinate, L, ft
r_d	damage radius, L, ft
r_e	reservoir radius, L, ft
r_w	wellbore radius, L, ft
r'_w	modified wellbore radius, L, ft
r_{we}	effective wellbore radius, L, ft
r_{wh}	wormhole penetration radius, L, ft
s	skin factor, dimensionless

s_d	damage skin factor, dimensionless
s_{app}	apparent skin factor, dimensionless
$s_{overall}$	overall skin factor, dimensionless
t	time, T, minute
t_D	dimensionless time, dimensionless
v	velocity, LT^{-1}, ft/min
v_i	interstitial velocity, LT^{-1}, ft/min
$v_{i,opt}$	optimum interstitial velocity, LT^{-1}, cm/min
$v_{i,tip}$	interstitial velocity at the tip of wormholes, LT^{-1}, cm/min
v_{wh}	wormhole propagation rate, LT^{-1}, ft/min

Greek

α_z	wormhole axial spacing coefficient
γ	specific gravity, dimensionless
ε	roughness, dimensionless
μ	viscosity, $ML^{-1}T^{-1}$, cp
ρ	density, ML^{-3}, g/cm^3
ρ_{acid}	acid density, ML^{-3}, g/cm^3
ρ_{rock}	rock density, ML^{-3}, g/cm^3
ϕ	porosity, fraction

TABLE OF CONTENTS

Page

LIST OF FIGURES

Page

LIST OF TABLES

Page

1 INTRODUCTION

1.1 Research Background

Matrix acidizing is a stimulation technique that involves injecting a reactive fluid into the formation matrix rock below the fracturing pressure. In carbonate acidizing, the acid dissolves the reservoir rock to form conductive channels that are commonly referred to as wormholes, in which the pressure drop is assumed to be neglected. The effectiveness of an acid treatment depends greatly on the efficiency of the wormholing process in carbonate rocks. To optimize an acid treatment one needs to understand the mechanism of the wormhole propagation and the factors that affect its efficiency.

In general, the acid/rock interaction involves the following processes: the acid mass transfer to the rock surface, the surface reaction and the transport of the reaction products from the rock surface. The mass transfer occurs because of the acid diffusion and convection. The acid diffusion depends on the acid concentration and the convection of acid is governed by the injection rate. The surface reaction rate is a function of type of acid/rock systems, temperature at the time of reaction and the surface contact area of acid and rock.

As observed by many researchers, the reaction of highly reactive acids, for example hydrochloric acid, with carbonate rocks is controlled by mass-transfer limited kinetics. For such acid/rock systems, for a given reservoir conditions and acid concentration, the formation of wormhole patterns and the wormholing efficiency are acid injection rate dependent. At low injection rates, the wormhole pattern is of compact

dissolution. At high injection rates, the wormholes have ramified structures. Dominant wormhole pattern is obtained at intermediate injection rates. An example of wormhole pattern dissolution created by hydrochloric acid is shown in **Fig. 1.1** from Fred and Fogler (1998a). Compared to other wormhole patterns, the dominant wormhole structure propagates the longest wormhole penetration depth with the least amount of acid injected. Therefore, it is the most desirable wormhole pattern in carbonate matrix stimulation.

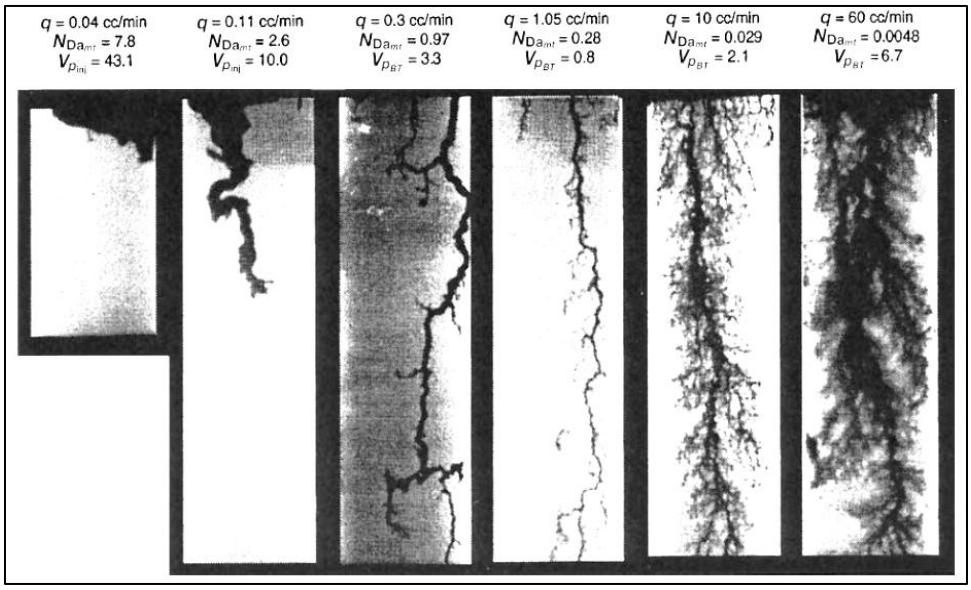

Fig. 1.1—Wormhole patterns created by different injection rates (Fredd and Fogler, 1998a)

The injection rate, at which the dominant wormhole pattern is obtained, is called the optimum injection rate on an acid treatment. For highly reactive acid/rock systems, the optimum injection rate does exist and it depends on the rock mineralogy, acid concentration and reaction temperature (Wang et al., 1993). The CT scanned image in

Fig. 1.2 from McDuff et al. (2010) shows the changes in wormhole structures with changing acid injection rate. The wormholes have a large tube structure at relatively low injection rates, much narrower channel with few branches at intermediate rates, and highly branched structure at high injection rates.

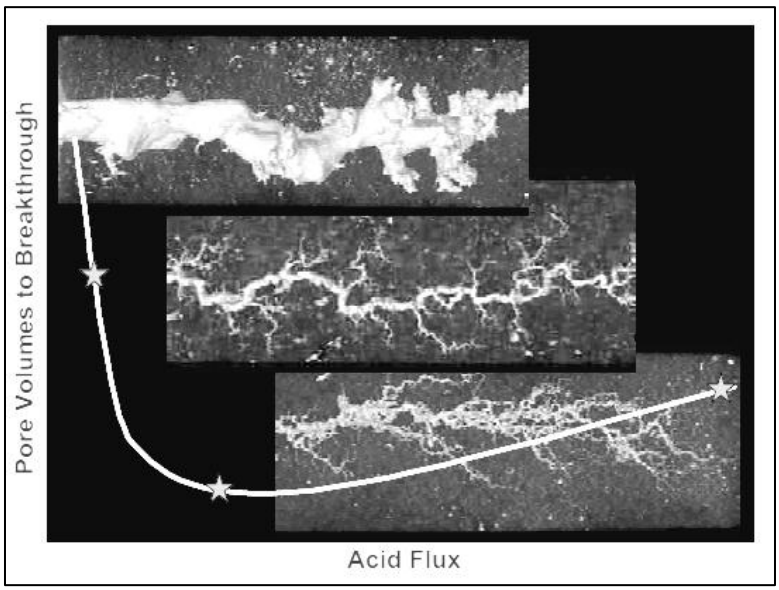

Fig. 1.2—Wormhole morphology at different injection rates (McDuff et al., 2010)

The wormhole structures also depend on the flow geometry. The wormhole structure shown in **Fig. 1.3** is created by injecting acid into a large rock sample with radial acid flow from the wellbore (McDuff et al., 2010). It has a symmetric wormhole pattern extending radially from the wellbore wall. This radial wormhole structure is observed in field treatment conditions.

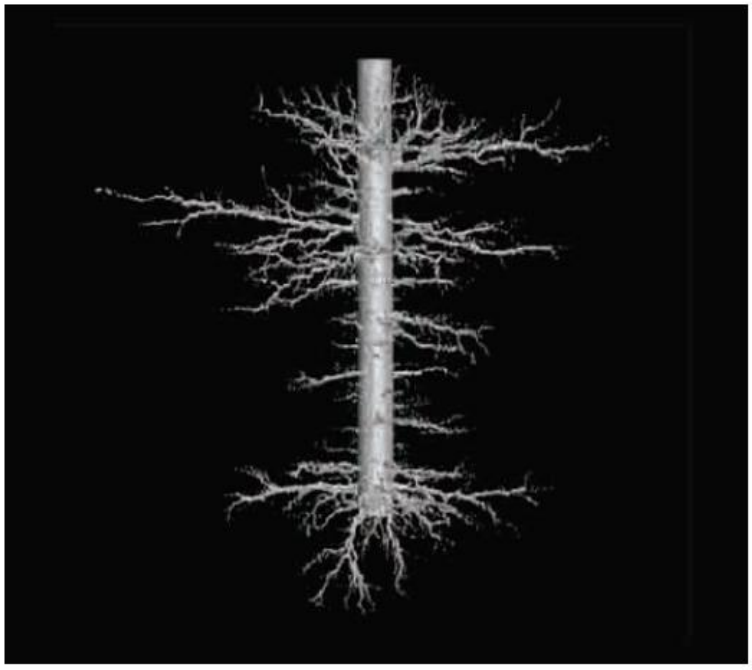

Fig. 1.3—Wormhole created in a large rock sample with radial wormhole propagation (McDuff et al., 2010)

In carbonate acidizing, the high degree of reservoir heterogeneity further complicates the design of the field treatments. It is essential to have reliable numerical models to design and optimize acidizing treatments.

1.2 Literature Review

In this section, a comprehensive review of the state of the art in matrix acidizing in carbonate reservoirs. The review focuses on the historical development in experimental and modeling works of wormhole propagation process, as well as the investigation of factors that affect its efficiency.

When acid is injected into carbonate formations and reacts with rocks, the conductive channels are created (Williams et al., 1979), which are normally referred to as wormholes. The wormhole propagation occurs as the result of two processes: the chemical reaction between acid and carbonate rocks; the fluid loss from the wall of wormholes to the formation and the fluid distribution in a multiple wormhole geometry (Buijse, 1997).

Hoefner and Fogler (1987; 1988; 1989) studied the wormholing process experimentally and numerically with a random network model taking into account the acid diffusion, convection and reaction. The studies showed that the diffusion effect was important for micro-emulsion acid systems because of the retarded reaction rate. The acid convection became more important for highly reactive systems such as regular hydrochloric acid. The authors investigated the conditions under which the wormholes were formed and the parameters that affected the wormhole structures and growth rate. The important parameter that controlled the wormhole propagation and structures is the ratio of the reaction rate over the acid convective transport rate, which is called the Damkoler number. The effect of fluid loss on wormholing process was not taken into account in their studies.

Hung et al. (1989) developed a mechanistic model to study the wormhole growth and their competition during an acid treatment with the initial distribution of pores. The wormhole dimensions and distribution were found to be controlled by the injection rate, fluid loss and diffusion.

Daccord et al. (1989) examined the wormhole phenomenon both experimentally with a plaster/water model and numerically with a computer model and fractal theory. They studied the linear and radial flow geometries and concluded that the wormhole growth depends on geometry of the system and that the results obtained from one type of geometry cannot be directly applied to another without taking into account the change in fractal dimension. Another conclusion drawn was that the optimum injection rate did exist for highly reactive systems and the rates typically used in the field treatments were much too high.

Wang et al. (1993) investigated the optimum injection rate for limestone and dolomite. A model to predict the optimum injection rate was developed and confirmed by the experimental results. However, an up-scaling treatment for field application was not carried out. One of the conclusions drawn was that the optimum injection rate exists for highly reactive rock/acid systems. This optimum value of injection rates is a function of rock mineralogy, acid concentration and reaction temperature, of which rock mineralogy has the largest effect. In addition, as the temperature increases the optimum injection rate increases for both limestone and dolomite formations.

Fredd and Fogler (1998b) showed that the optimum injection rate for a given acid-rock system and temperature exists at which a minimum volume of acid is required to propagate a wormhole through the core.

The results of linear core-flood experiments are difficult to apply directly to field treatment design because of the flow geometry and core size dependency. This fact motivated many researchers to conduct radial experiments, although they are more

complicated to conduct and more expensive (Daccord et al., 1989; Frick et al., 1994; McDuff et al. 2010; Mostofizadeh and Economides, 1994). They made attempts to find the relationship between radial core-flood experimental results with the ones of linear experiments, from which a correlation can be developed to convert laboratory data to field application.

Frick et al. (1994) performed radial experiments for low permeability limestone and hydrochloric acid under different conditions of temperature, acid concentration and permeability. As the result, they confirmed the existence of the optimum injection rate that corresponds to the generation of dominant wormholes.

Mostofizadeh and Economides (1994) further investigated radial laboratory experiments with the same experimental setup and proposed a simple technique to upscale the experimental results to the field scale conditions. They also found that the optimum injection rate depends on the permeability. Higher permeability requires higher optimum injection rate.

Another important aspect of wormhole study is the density and distribution of the wormholes around the wellbore region and along the wellbore axis (Buijse, 1997; Huang et al., 1999). One can estimate how much acid is needed to propagate a certain number of wormholes with their distribution status. Gdanski (1999) presented a method to approximate the wormhole density based on the experimental observation of the symmetry of wormholing process under radial flow geometry. The author concluded that the penetration length of the wormhole is controlled by the volume of acid injected and

the formation porosity; the wormhole diameter and the stimulated permeability are controlled by the kinetics of reaction and the time in contact with acid.

Huang et al. (2000) developed design charts based on optimum flux theory that can be used as a guide tool for acid selection based on treating temperature. The important highlight of this research work was that the optimum injection rate strongly depends on the temperature.

Fredd (2000) investigated the wormhole propagation with optimum injection strategies and indicated that to keep wormhole evolution efficiency the Damkohler number is maintained at optimum value by means of increasing injection rate or decreasing the dissolution rate as the depth of penetration increases (Fredd, 2000; Fredd and Fogler, 1998a; Fredd and Fogler, 1998b; Fredd et al., 1997).

Buijse (2000) examined the wormholing mechanism and showed that the optimum injection rate depends on the wormhole length. He also observed the core-size dependence of wormhole propagation process during core flood experiments. Buijse and Glasbergen (2005) presented a semi-empirical wormhole model and showed that the wormhole length is a function of acid volume, acid coverage and injection rate. The advantage of this model is that it requires only two empirical parameters from core flood experiments, the optimum pore volume to breakthrough and the optimum interstitial velocity. They also suggested a way of scaling up experimental results to field conditions for radial flow in openhole completion and flow regimes existing in cased perforated completion.

Bazin (2001) performed a laboratory evaluation of acid/rock interactions to determine the optimum injection rate of carbonate matrix acidizing and its variation with core length, temperature, acid concentration and reservoir permeability. He confirmed that the optimum injection rate does exist for straight acids and is related to the maximum wormhole penetration distance. In addition, the optimum injection rate increases with increasing acid concentration, temperature and rock permeability. The author also indicated that the translation of laboratory results to the reservoir cannot be obtained directly and not reliable.

Furui et al. (2010) analyzed more than 400 well treatments in carbonate reservoirs and observed that the previously published acidizing models under-predicted the wormhole penetration and the stimulation effects by analyzing treatment data in Middle East and North Sea Fields. They presented a new wormhole model based on the Buise and Glasbergen (2005) semi-empirical model. The new wormhole model estimates the wormhole evolution with the consideration of acid flux at the tip of the wormhole and core size dependencies. The results showed that wormhole predicted by Furui et al.'s model penetrates deeper into the formation compared to that of Buijse and Glasbergen's model (2005).

Many researchers have indicated that the core flood experimental data could not be used directly for the field treatment design because of the linear flow nature. The conversion of optimum injection rate from core scale to field application is not trivial and that reliable up-scaling models and procedures are desired (Glasbergen et al., 2009).

1.3 Research Objectives and Approach

The objectives of this work are to investigate the optimum design of acid treatments in horizontal wells in carbonate reservoirs using a developed numerical acidizing simulator. The simulator couples the transient reservoir flow and the wellbore flow to model the fluid placement and diversion of acids in horizontal wells. The optimum treatment design in carbonate acidizing is desired to achieve the stimulation benefit with the least amount of injected acid into the well. To always keep the wormhole propagation at its optimum conditions at the tip of the wormhole, the acid treatment is executed with an increasing injection rate. The equations for the increasing rate schedule were derived for three wormhole model used in the acidizing simulator. This increasing rate acid stimulation is then compared to the treatment with a single optimum injection rate and the maximum allowable injection rate.

We started the study with a comprehensive literature review of the research studies that have been done in wormhole propagation modeling, of which the optimum wormhole propagation conditions are the ultimate goal. A brief description of an acidizing simulator is provided that includes a reservoir flow model, a wellbore flow model, a wellbore fluid interface tracking model, a wormhole model, and a viscous diversion skin model. We then used the developed acidizing simulator to perform a parametric study to investigate the optimum injection rate and the parameters that affect its variation for the same acid/rock systems.

Based on the parametric study, we determined the optimum injection rate for a given volume of injected acid. We conducted acid treatments with this increasing rate

schedule and compared to the single optimum injection rate treatment. The skin factor was selected as a criterion for the evaluation of acid treatment effectiveness. The wormhole growth was tracked throughout the entire injection period and the stimulation effect contributed by the wormholes was then evaluated by a local skin factor. The total equivalent skin factor for the horizontal well is calculated using Furui et al.'s damaged skin model (Furui et al., 2003).

We also analyzed field treatment data for horizontal wells in carbonate reservoirs validate the numerical acidizing simulator.

2 MATRIX ACIDIZING MODELING

2.1 Acid Placement Model

2.1.1 Introduction

The numerical acidizing simulator used in this study was developed based on the Mishra et al. (2007) with the extension of the viscous diversion Nozaki and Hill (2009) for radial flow in openhole completion.

The acidizing model consists of a wellbore flow model, a wellbore fluid interface tracking model, a transient reservoir outflow model, a wormhole growth model and a skin model. The wellbore flow model accounts for pressure drop and material balance inside the wellbore. The fluid interface tracking monitors the interface between injected fluids in the horizontal wellbore. The transient reservoir outflow model captures the transient effect of the varying injection rates that are often seen in well test problems. The wormhole model predicts the wormhole penetration in the formation during the entire acid injection period. The apparent skin model accounts for well completions damaged region, wormholes, reservoir mobility and injected fluids mobility. The final skin factor is a function of the wormhole penetration depth with the assumption that the wormholes extend beyond the damage zone at the end of the treatment.

2.1.2 Wellbore Flow Model

The wellbore flow model consists of wellbore pressure drop and wellbore material balance calculations. To develop pressure drop and material balance equations the fluid injection is assumed to be single phase and injected fluid is incompressible.

2.1.2.1 Wellbore Material Balance

It is assumed that the horizontal well fully penetrates the reservoir length and flow from the wellbore into the reservoir is perpendicular to the well axis. **Fig. 2.1** shows a segment of the horizontal wellbore under consideration. p_w, q_w and q_R are pressure, flow rate and specific reservoir outflow as functions of time t and location x.

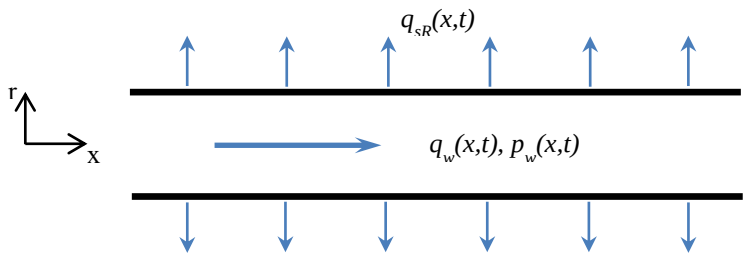

Fig. 2.1—Schematic of a horizontal wellbore segment

The specific reservoir outflow is equal to the change in wellbore flow rate as in following equation,

$$\frac{\partial q_w}{\partial x} = -q_R \tag{2.1}$$

2.1.2.2 Wellbore Pressure Drop

Total pressure loss in pipes is caused by friction, vertical pipe elevation and change in kinetic energy. With the assumption that the well is relatively horizontal, the vertical elevation changes are neglected. The change in kinetic energy is also negligible for single phase incompressible flow. Therefore, the friction pressure drop is the sole component that contributes to the pressure loss.

Based on the assumption that the fluid flow in the horizontal wellbore is single phase and incompressible, friction pressure drop can be calculated by the Fanning equation (Economides et al., 1994),

$$\Delta P_F = \frac{2 f_f \rho v^2 L}{d} \tag{2.2}$$

where, f_f is the Fanning friction factor, v is the fluid velocity in the wellbore and is defined as,

$$v = \frac{q_w}{A} \tag{2.3}$$

where, A is the cross-section area of pipe.

In **Eq. 2.2,** the Fanning friction factor depends on the fluid flow regime and pipe roughness. The fluid flow regime is determined based on the Reynolds number, N_{Re}. The Reynolds number is the dimensionless number that represents the ratio of inertial forces to viscous forces for a given flow conditions. For flow in pipe,

$$N_{\mathrm{Re}} = \frac{dv\rho}{\mu} \tag{2.4}$$

where, d - pipe inside diameter, v - average velocity, ρ - fluid density, and μ - fluid viscosity.

When N_{Re} < 2000 the flow is laminar, N_{Re} > 4000 the flow is turbulent. For N_{Re} from 2000 to 4000, the flow regime is the transition between laminar and turbulent flows.

For laminar flow, the friction factor is calculated as,

$$f_f = \frac{16}{N_{\mathrm{Re}}} \tag{2.5}$$

For turbulent flow, the Fanning friction factor is commonly estimated from the Moody diagram. For computational purposes, the Fanning friction factor can be calculated explicitly using Chen's equation (1979),

$$\frac{1}{\sqrt{f_f}} = -4\log_{10}\left\{\frac{\varepsilon}{3.7065} - \frac{5.0452}{N_{\mathrm{Re}}}\left[\frac{\varepsilon^{1.1098}}{2.8257} + \left(\frac{7.149}{N_{\mathrm{Re}}}\right)^{0.8981}\right]\right\} \tag{2.6}$$

Rewriting Eq. 2.2 in the differential form,

$$\frac{\partial p_w}{\partial x} = -\frac{2 f_f \rho v^2}{d}\,\mathrm{sgn}(v) \tag{2.7}$$

where, sgn(x) is the sign function and is defined as

$$\mathrm{sgn}(x) = \begin{cases} -1 & if \quad x < 0 \\ 0 & if \quad x = 0 \\ 1 & if \quad x > 0 \end{cases} \tag{2.8}$$

Eq. 2.7 in oil field units has the form,

$$\frac{\partial p_w}{\partial x} = -1.525 f_f \frac{\rho q_w^{\,2}}{d^5}\mathrm{sgn}(q_w) \tag{2.9}$$

Eq. 2.9 can be written for flow in the casing,

$$\frac{\partial p_w}{\partial x} = \left(-1.525 f_f \frac{\rho q_w}{d_{ci}^5} \operatorname{sgn}(q_w) \right) q_w \tag{2.10}$$

It can also be re-written as,

$$\frac{\partial p_w}{\partial x} = -\xi q_w \tag{2.11}$$

where,

$$\xi = 1.525 f_f \frac{\rho q_w}{d^5} \operatorname{sgn}(q_w) \tag{2.12}$$

To obtain the flow distribution and pressure profiles along the horizontal wellbore the system of equation, which consists of **Eq. 2.1** and **Eq. 2.11**, is solved simultaneously,

$$\begin{cases} \dfrac{\partial q_w}{\partial x} = -q_{sR} \\ \dfrac{\partial p_w}{\partial x} = -\xi q_w \end{cases} \tag{2.13}$$

To solve the system of differential **Eq. 2.13 t**he initial and boundary conditions are required.

$$q_w(x,0) = 0\,,\ p_w(x,0) = p_i \tag{2.14}$$

$$q_w(0,t) = 0\,,\ q_w(x \geq L, t) = 0 \tag{2.15}$$

where,

$$Q_w(x_{tubing}, t) \text{ or } p_w(x_{tubing}, t) \tag{2.16}$$

must be specified, and, L - wellbore length, Q_w - injected fluid volumetric flow rate, and x_{tubing} - tubing location.

2.1.3 Reservoir Flow Model

In matrix acidizing, during the acid injection period, the injection rate is normally varying with time. The superposition theory for reservoir outflow is used to account for the transient effects of acid injection rate. From Lee et al. (2003) we have the superposition equation for transient flow,

$$-\frac{2\pi kl}{\mu}\left(p_i - p_w^n\right) = \sum_{i=1}^{n} \Delta q^j [\, p_D(t_D^n - t_D^{j-1})] + q^n s^n \tag{2.17}$$

Manipulating the equation to rearrange it into the desired form,

$$-\frac{2\pi kl}{\mu}\left(p_i - p_w^n\right) = \sum_{i=1}^{n-1} \Delta q^j [\, p_D(t_D^n - t_D^{j-1})] - q^{n-1} p_D(t_D^n - t_D^{n-1}) + q^n p_D(t_D^n - t_D^{n-1}) + q^n s^n \tag{2.18}$$

Dividing both sides by l and rearranging to have,

$$-\frac{2\pi k}{\mu}\left(p_i - p_w^n\right) = \sum_{j=1}^{n-1} \Delta q_{sR}^j p_D(t_D^n - t_D^{j-1}) - q_{sR}^{n-1} p_D(t_D^n - t_D^{n-1}) + q_{sR}^n [\, p_D(t_D^n - t_D^{n-1}) + s^n] \tag{2.19}$$

where,

$$q_{sR}^n = -a_{Jx}\left(p_i - p_w^n\right) - b_{Jx} \tag{2.20}$$

and,

$$a_{Jx} = \frac{4.91816 \times 10^{-6} k}{\mu [\, p_D(t_D^n - t_D^{n-1}) + s^n]} \tag{2.21}$$

$$b_{Jx} = \frac{\sum_{j=1}^{n-1} \Delta q_{sR}^j p_D(t_D^n - t_D^{j-1}) - q_{sR}^{n-1} p_D(t_D^n - t_D^{n-1})}{p_D(t_D^n - t_D^{n-1}) + s^n} \tag{2.22}$$

where, k is in md, μ - cP, and q_{sR} - bpm/ft

2.1.4 Interface Tracking Model

The interfaces between wellbore fluid and injected fluids, between injected fluids themselves can be tracked by the model proposed by Eckerfield et al. (1998). **Fig. 2.2** shows the interface tracking for the time Δt from t to $t+\Delta t$.

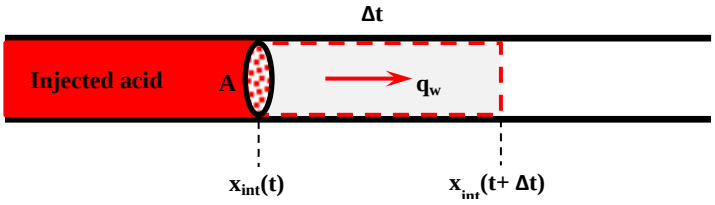

Fig. 2.2—Interface tracking from t to t+Δt

The fluid interface movement velocity is calculated by,

$$\frac{dx_{\text{int}}}{dt} = \left.\frac{q_w}{A}\right|_{x=x_{\text{int}}} \tag{2.23}$$

Eq. 2.23 can be rewritten in discrete form,

$$x_{\text{int}}\big|_{t+\Delta t} = x_{\text{int}}\big|_t + \left.\frac{q_w}{A}\right|_{x=x_{\text{int}}} \Delta t \tag{2.24}$$

where, A is the cross-sectional area of flow.

2.1.5 Wormhole Models

2.1.5.1 Volumetric Model

This is a simple wormhole model and was first presented by (Economides et al., 1994). For radial flow, the wormhole radius is calculated as a function of injected acid volume by the equation,

$$r_{wh} = \sqrt{r_w^{\,2} + \frac{V}{\pi\phi LPV_{bt}}} \tag{2.25}$$

where, PV_{bt} is the number of pore volumes of injected acid at the time of wormhole breakthrough at the end of the core. This model assumes a fixed number of pore volumes of acid that are required to propagate wormholes to a given distance.

2.1.5.2 Buijse and Glasbergen's Model

Buijse and Glasbergen (2005) presented an empirical model to predict wormhole propagation that requires only two parameters from core flood experiments: optimum pore volume to breakthrough and optimum interstitial velocity. These two parameters characterize the optimum conditions of wormhole propagation process in carbonate rocks and can be obtained from core flood experiments for acid-rock systems (**Fig. 2.3**).

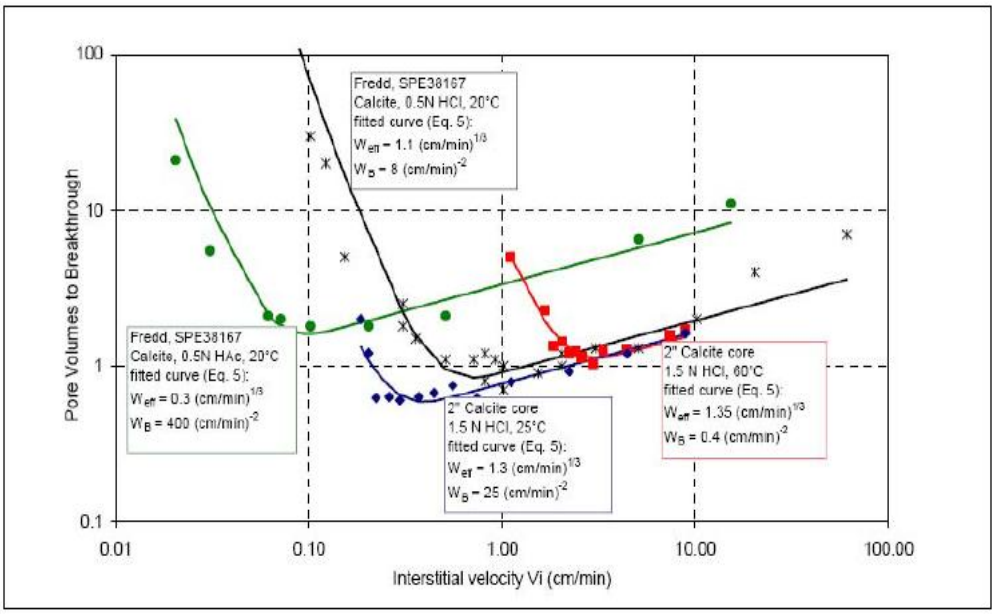

Fig. 2.3—Pore volume to breakthrough (PV_{bt}) vs. interstitial velocity (v_i) (from Buijse and Glasbergen 2005).

The wormhole growth rate is calculated by the equation,

$$v_{wh} = \left(\frac{v_i}{PV_{bt,opt}}\right) \times \left(\frac{v_i}{v_{i,opt}}\right)^{-\gamma} \times \left\{1 - \exp\left[-4\left(\frac{v_i}{v_{i,opt}}\right)^2\right]\right\}^2 \tag{2.26}$$

where, the interstitial velocity is determined by

$$v_i = \frac{q}{2\pi\phi L} \tag{2.27}$$

In the developed acidizing model the equation is re-written in terms of two parameters, the optimum pore volume to breakthrough and optimum interstitial velocity, as the followings,

$$v_{wh} = W_{eff} v_i^{2/3} B \tag{2.28}$$

where,

$$B = \left[1 - e^{-W_B v_i^2}\right]^2 \tag{2.29}$$

$$W_{eff} = \frac{v_{iopt}^{1/3}}{PV_{btopt}} \tag{2.30}$$

$$W_B = \frac{4}{v_{iopt}^2} \tag{2.31}$$

This model is easy to use because it requires only two parameters that can be obtained from experimental data in the literature. The authors also proposed equations for scaling up the laboratory data to the field condition for radial flow in openhole completion and for flow regimes in cased perforated completion.

2.1.5.3 Furui et al.'s Wormhole Model

Furui et al. (2010) analyzed field treatment data and showed that the current wormhole models under-predicted the wormhole penetration compared to field treatments responses. **Fig. 2.4** shows experimental results conducted by Furui et al. (2010) using outcrop samples. The experimental results indicated the core size dependency of the wormhole propagation. The larger core experiments give smaller optimum pore volume to breakthrough and optimum interstitial velocity.

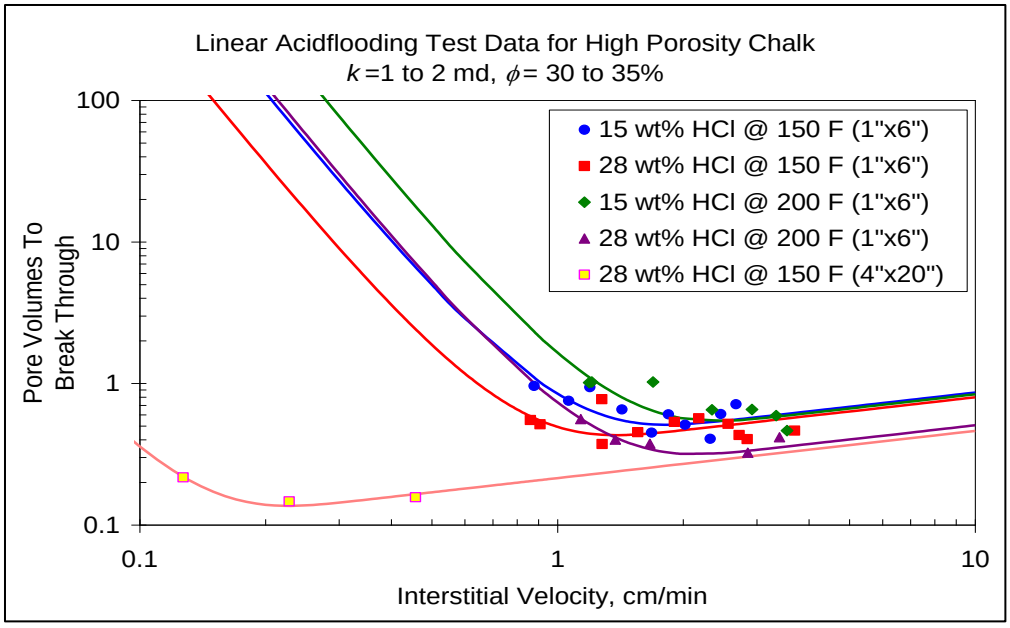

Fig. 2.4—Linear core flooding experiment results for high porosity outcrop chalk samples (from Furui et al. 2010).

They also studied the acid wormholing process using a finite element numerical model and showed that the interstitial velocity at the tip of the wormhole has a strong effect on the wormhole propagation process.

They developed a new wormhole model based on the Buijse and Glasbergen (2005) semi-empirical model.

The wormhole flow rate is approximated by the equation

$$v_{wh} = v_{i,tip} N_{Ac} \left(\frac{v_{i,tip} PV_{bt,opt} N_{Ac}}{v_{i,opt}} \right)^{-\gamma} \left\{ 1 - \exp\left[-4 \left(\frac{v_{i,tip} PV_{bt,opt} N_{Ac} L_{core}}{v_{i,opt} r_{wh}} \right)^2 \right] \right\}^2 \quad (2.32)$$

where, the interstitial velocity at the tip of the wormhole is calculated for radial flow by **Eq. 2.33**,

$$v_{i,tip} = \frac{q}{\phi h\sqrt{\pi m_{wh}}}\left[(1-\alpha_z)\frac{1}{\sqrt{d_{e,wh}r_{wh}}} + \alpha_z\left(\frac{1}{d_{e,wh}}\right)\right] \tag{2.33}$$

and for spherical flow by,

$$v_{i,tip} = \frac{q}{4\pi\phi d_{e,wh}hr_{wh}} \tag{2.34}$$

where, the effective wormhole diameter and the acid capacity number are defined as

$$d_{e,wh} = d_{core}PV_{bt,opt}N_{Ac} \tag{2.35}$$

and,

$$N_{Ac} = \frac{\phi\beta C_0\rho_{acid}}{(1-\phi)\rho_{rock}} \tag{2.36}$$

The wormhole growth rate v_{wh} is in cm/min, $v_{i,tip}$ is the interstitial velocity at the wormhole tip in cm/min, N_{Ac} is the acid capacity number (dimensionless), L_{core} is the core length of the linear core flood experiments in cm, α_z is the wormhole axial spacing coefficient (dimensionless), $d_{e,wh}$ is the effective wormhole radius in cm, d_{core} is the core diameter of the linear core flood experiments in cm, β is the acid dissolving power, C_0 is the injection acid concentration in weight fraction, ρ_{acid} is the acid density in g/cm^3, and ρ_{rock} is the density of the formation rock in g/cm^3. For horizontal wells, the value of α_z ranges from 0.5 to 0.75 and from 0.25 to 0.5 for vertical wells.

2.1.6 Skin Factor

2.1.6.1 Damage Skin and Wormhole Effect

For radial flow in openhole completion, the damage skin without stimulation effect is calculated by the following Hawkins' equation,

$$s_d = \left(\frac{k}{k_d} - 1 \right) \ln \frac{r_d}{r_w} \tag{2.37}$$

When the stimulation starts, the wormhole creation contributes to the skin factor and the wormhole region is still inside the damaged zone (**Fig. 2.5**).

$$s_{da} = \frac{k}{k_d} \ln \frac{r_d}{r_{wh}} - \ln \frac{r_d}{r_w} \quad \text{for} \quad r_{wh} < r_d \tag{2.38}$$

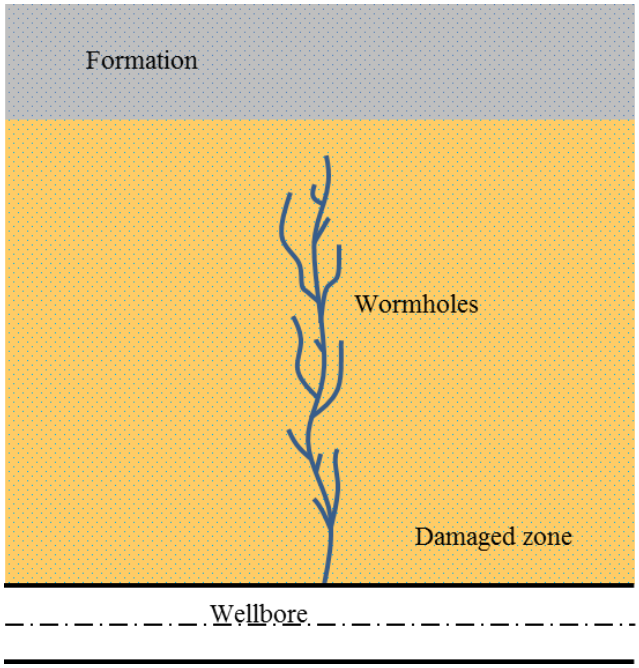

Fig. 2.5—Wormhole region inside the damaged zone

Once wormholes break through the damage zone (**Fig. 2.6**), the wormhole effect is dominant with the assumption that the pressure drop inside the wormhole is neglected, in other words, the wormhole has relatively high permeability.

$$s_{da} = -\ln \frac{r_{wh}}{r_w} \quad \text{for} \quad r_d < r_{wh} \tag{2.39}$$

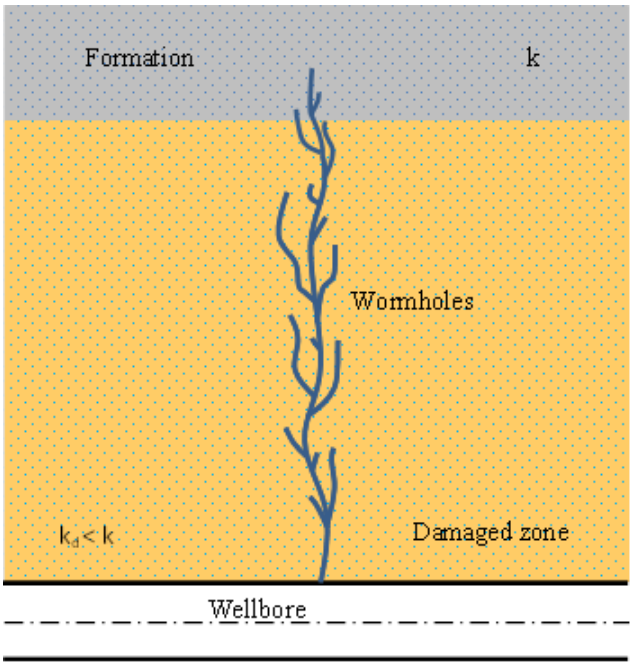

Fig. 2.6—Wormhole region breaks through the damaged zone

2.1.6.2 Apparent Skin Factor for Viscous Diversion for Radial Flow

Hill and Rossen (1994) first introduced a simple skin model (**Eq. 2.40**) to account for the viscous diversion effect for the case in which the reservoir fluid was displaced by a higher viscous fluid/acid (**Fig. 2.7**). However, **Eq. 2.40** can be used for

single fluid injection and does not account for the effects of the wormhole propagation and the formation damage.

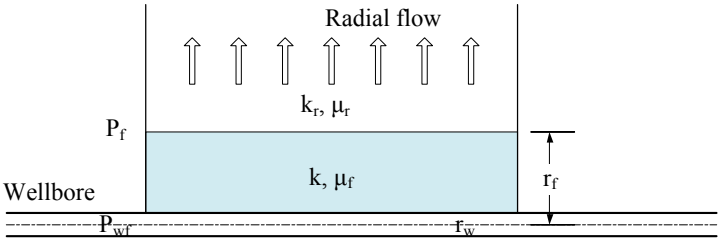

Fig. 2.7—Radial flow with the reservoir fluid being displaced by the injected higher viscous acid

$$s_{app} = \left(\frac{\mu_f}{\mu_r} - 1 \right) \ln \frac{r_f}{r_w} \tag{2.40}$$

For multiple fluids injection case (Fig. 2.8) has the form of **Eq. 2.41**.

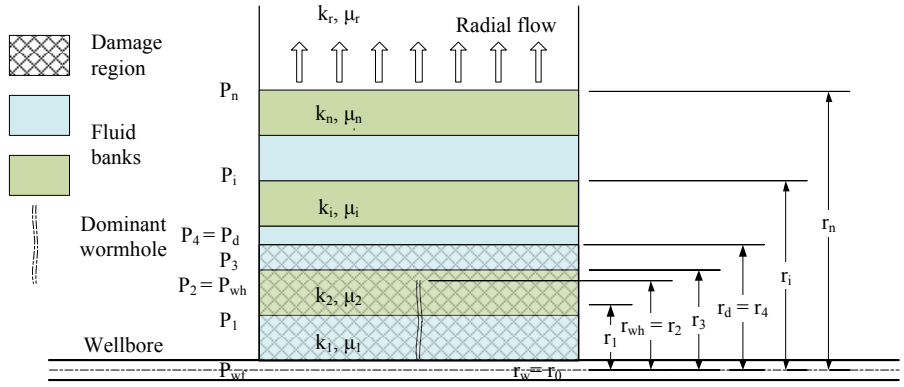

Fig. 2.8—Radial flow in one grid block with the damaged zone, the wormhole region and multiple injected fluids with different viscosities

$$s_{app} = \sum_{i=1}^{n} \frac{M_r}{M_i} \ln \frac{r_i}{r_{i-1}} - \ln \frac{r_n}{r_0} \tag{2.41}$$

In **Eq. 2.41** the r_n is smaller or equal to half of the formation thickness assuming the horizontal well is completed at the center of the pay zone.

$$M = \frac{k}{\mu} \tag{2.42}$$

where, M, calculated by **Eq. 2.42** is fluid mobility, r_0 is wellbore radius. The i-th fluid radius is calculated by **Eq. 2.43**,

$$r_i = \sqrt{r_{i-1}^2 + \frac{V_i}{\pi L \phi}} \tag{2.43}$$

where, V_i is the volume injected of i-th fluid, - ϕ is the reservoir porosity, L – is the length of the wellbore interval

It is important to note that when the wormholes break through the damage zone and extend beyond the fluid banks, **Eq. 2.41** reduces to **Eq. 2.44** and the skin factor only depends on the wormhole length,

$$s_{app} = -\ln \frac{r_{wh}}{r_w} \tag{2.44}$$

The smallest skin factor can be achieved as shown in **Fig. 2.9** for limitation of radial flow in vertical direction of the plane perpendicular to the wellbore.

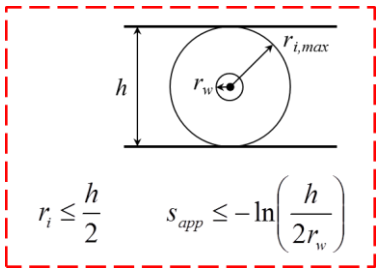

Fig. 2.9—Radial flow geometry and its limit in vertical direction

2.1.6.3 Horizontal Well Overall Skin Factor

From Furui et al (2003), the overall skin factor of the horizontal well is approximated by **Eq. 2.45**

$$s_{overall} = \frac{\sum_{i=1}^{n} k_i \Delta L_i}{\sum_{i=1}^{n} \frac{k_i \Delta L_i}{\ln(I_{ani} h / [(I_{ani}+1) r_w] + s_i}} - \ln \frac{I_{ani} h}{(I_{ani}+1) r_w} \tag{2.45}$$

where,

$s_{overall}$ - overall (equivalent) horizontal well skin factor,

s_i - local skin of i-th zone,

k_i - permeability of i-th zone, mD

ΔL_i - length of i-th zone, ft

h - net pay thickness, ft

I_{ani} - index of anisotropy.

2.2 Horizontal Well Acidizing Simulator

In this section, the developed acidizing simulator is implemented in a computer code, which is written in FORTRAN language, to simulate acid treatments. **Fig. 2.10** shows the schematic of the acidizing simulator.

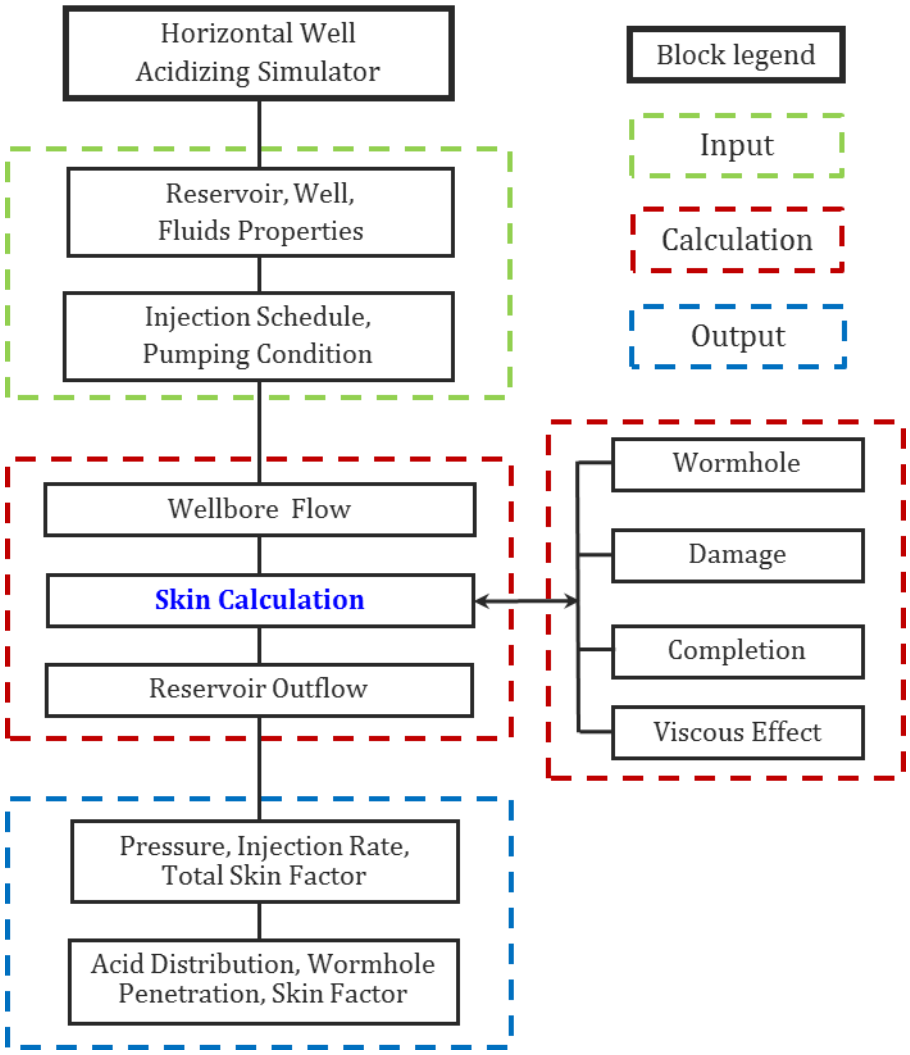

Fig. 2.10—Schematic of horizontal well acidizing simulator

The horizontal well acidizing simulator consists of blocks: input, calculation, and output. Input block has reservoir properties, well parameter, properties of fluids to be injected, injection schedule, and pumping condition. The calculation block consists of wellbore flow module, skin calculation module, and reservoir outflow module. The wellbore flow module includes the wellbore fluid interface tracking procedure. The skin

calculation module takes into account the effects of formation damage, well completion, wormhole penetration, and the mobility of reservoir and injected fluids. The output block has the global pumping parameters as functions of pumping time or injected acid volume and local parameters as functions of position along the horizontal well. The global parameters are pressure, injection rate and total skin factor. The local parameters are acid distribution, wormhole penetration, and skin factor profile.

The development of the acidizing simulator is presented in **Appendix A**.

3 MATRIX ACIDIZING OPTIMIZATION

The wormhole growth rate decreases as the acid spends in the formation that causes less efficient wormhole propagation over time. If we inject acid at a constant (even the optimum) injection rate, the interstitial velocity at the tip of the wormhole decreases towards the end of the treatment. To keep the wormhole growth process at the optimum conditions, the interstitial velocity needs to be maintained at or close to its optimum value. To achieve that, the injection rate has to be increasing as the wormhole radius increases.

For radial flow of fluid from the wellbore, the interstitial velocity at the tip of the wormhole is calculated by

$$v_i(r_{wh}) = \frac{q}{2\pi\phi L r_{wh}} \tag{3.1}$$

Rearranging **Eq. 3.1** to obtain injection rate as a function of wormhole radius and interstitial velocity at that radius,

$$q = 2\pi\phi L r_{wh} v_i(r_{wh}) \tag{3.2}$$

The goal of the optimum acidizing treatment design is to maintain the wormhole propatagion at its optimum conditions. In other words, the pore volume to breakthrough and interstitial velocity are maintaned at their optimum values, or

$$v_i(r_{wh}) = v_{i,opt} \tag{3.3}$$

and,

$$PV_{bt} = PV_{bt,opt} \tag{3.4}$$

For each of the wormhole models, we derive an equation for the injection rate schedule that which the acid treatment is achieved with the best stimulation benefits.

3.1 Equation Derivation for Volumetric Wormhole Model

For the volumetric model, the wormhole radius is calculated by **Eq. 3.5**,

$$r_{wh} = \sqrt{r_w^{\,2} + \frac{V}{\pi\phi LPV_{bt}}} \tag{3.5}$$

From **Eq. 3.2**, the injection rate per unit length for this model is calculated by **Eq. 3.6**,

$$\frac{q}{L} = 2\pi\phi v_i(r_{wh}) \times \sqrt{r_w^{\,2} + \frac{V}{\pi\phi LPV_{bt}}} \tag{3.6}$$

To maintain the wormhole propagation at its optimum conditions we have to inject acid with the injection increasing as a function of injected acid volume,

$$\frac{q}{L} = 2\pi\phi v_{i,opt} \times \sqrt{r_w^{\,2} + \frac{V}{\pi\phi LPV_{bt,opt}}} \tag{3.7}$$

It is noticed that the only parameter that changes in **Eq. 3.7** is the injected acid volume. This leads to the thinking that, the injection rate seems to only depend on the acid volume injected. In fact, when the injection rate changes the pore volume to breakthrough will change. However, the pore volume to breakthrough is an input for this wormhole model. Therefore, in the example the rate series is calculated for different values of the pore volume to breakthrough and simulation runs are conducted for a comparison study.

3.2 Equation Derivation for Buijse-Glasbergen Wormhole Model

In **Section 2.1.5.2**, for Buijse and Glasberger (2005), the growth rate of a wormhole region extending around the wellbore is calculated by **Eq. 2.26**, which is repeated here for the convenience by **Eq. 3.8**.

$$v_{wh} = \left(\frac{v_i}{PV_{bt,opt}} \right) \times \left(\frac{v_i}{v_{i,opt}} \right)^{-\gamma} \times \left\{ 1 - \exp\left[-4 \left(\frac{v_i}{v_{i,opt}} \right)^2 \right] \right\}^2 \tag{3.8}$$

With the fluid loss limited wormholing parameter $\gamma = 1/3$ **Eq. 3.8** becomes,

$$v_{wh} = v_i^{\frac{2}{3}} \left(\frac{v_{i,opt}^{\frac{1}{3}}}{PV_{bt,opt}} \right) \times \left\{ 1 - \exp\left[-4 \left(\frac{v_i}{v_{i,opt}} \right)^2 \right] \right\}^2 \tag{3.9}$$

At the tip of the wormhole,

$$v_{wh}(r_{wh}) = v(r_{wh})_i^{\frac{2}{3}} \left(\frac{v_{i,opt}^{\frac{1}{3}}}{PV_{bt,opt}} \right) \times \left\{ 1 - \exp\left[-4 \left(\frac{v_i(r_{wh})}{v_{i,opt}} \right)^2 \right] \right\}^2 \tag{3.10}$$

Substituting the optimum value of the interstitial velocity into **Eq. 3.10** for interstitial velocity at the tip of the wormholes yields,

$$v_{wh}(r_{wh}) = v_{i,opt}^{\frac{2}{3}} \left(\frac{v_{i,opt}^{\frac{1}{3}}}{PV_{bt,opt}} \right) \times \left\{ 1 - \exp\left[-4 \left(\frac{v_{i,opt}}{v_{i,opt}} \right)^2 \right] \right\}^2 \tag{3.11}$$

or,

$$v_{wh}(r_{wh}) = \left(\frac{v_{i,opt}}{PV_{bt,opt}} \right) \times \left\{ 1 - \exp\left[-4 \right] \right\}^2 \tag{3.12}$$

and the final form of wormhole growth rate,

$$v_{wh}(r_{wh}) \cong 0.96 \times \left(\frac{v_{i,opt}}{PV_{bt,opt}} \right) \tag{3.13}$$

For Buijse and Glasbergen's model the wormhole growth rate at the optimum wormhole propagation conditions is constant. The wormhole radius at the time t+Δt can be calculated as

$$r_{wh}^{n+1} = r_{wh}^{n} + v_{wh}\Delta t \tag{3.14}$$

From the wormhole penetration radius we can calculate the injection rate as a funtion of time or injected acid volume,

$$\left(\frac{q}{L} \right)^{n+1} = 2\pi\phi v_{i,opt} r_{wh}^{n+1} \tag{3.15}$$

The cumulative injected acid volume is calculated by **Eq. 3.16**,

$$\left(\frac{V}{L} \right)^{n+1} = \left(\frac{V}{L} \right)^{n} + \Delta t \left(\frac{q}{L} \right)^{n+1} \tag{3.16}$$

3.3 Equation Derivation for Furui et al. Wormhole Model

In **Section 2.1.5.3**, for Furui et al. (2010), the growth rate of a wormhole region extending around the wellbore is calculated by **Eq. 2.32**, which is repeated here for the convenience by **Eq. 3.17**.

$$v_{wh} = v_{i,tip} N_{Ac} \left(\frac{v_{i,tip} PV_{bt,opt} N_{Ac}}{v_{i,opt}} \right)^{-\gamma} \left\{ 1 - \exp\left[-4 \left(\frac{v_{i,tip} PV_{bt,opt} N_{Ac} L_{core}}{v_{i,opt} r_{wh}} \right)^{2} \right] \right\}^{2} \tag{3.17}$$

For radial flow, the tip velocity is calculated as

$$v_{i,tip} = \frac{q}{\phi L\sqrt{\pi m_{wh}}}\left[(1-\alpha_z)\frac{1}{\sqrt{d_{e,wh}r_{wh}}} + \alpha_z\left(\frac{1}{d_{e,wh}}\right)\right] \tag{3.18}$$

where, the effective wormhole diameter and acid capacity number are defined as **Eq. 3.19** and **Eq. 3.20** respectively,

$$d_{e,wh} = d_{core}PV_{bt,opt}N_{Ac} \tag{3.19}$$

and,

$$N_{Ac} = \frac{\phi\beta C_0\rho_{acid}}{(1-\phi)\rho_{rock}} \tag{3.20}$$

To maintain the optimum wormhole propagation conditions at the tip of the wormhole, the tip velocity needs to be keep at its optimum value.

Furui et al. (2010) showed that for tip splitting and side branching, the optimum tip velocity is,

$$v_{i,tip,opt} = \frac{v_{i,opt}}{PV_{bt,opt}N_{Ac}} \tag{3.21}$$

and for the difusion limited wormholing,

$$v_{i,tip,opt} = \frac{v_{i,opt}}{PV_{bt,opt}N_{AC}}\frac{r_{wh}}{L_{core}} \tag{3.22}$$

Assuming the dominant wormholes are formation and the difussion limited wormholing is the dominant process, **Eq. 3.22** is used for the optimum tip velocity. Substituting its value from **Eq. 3.22** into **Eq. 3.17** we have,

$$v_{wh}(r_{wh}) = \frac{v_{i,opt}}{PV_{bt,opt}}\left(\frac{r_{wh}}{L_{core}}\right)^{\frac{2}{3}}\left[1-\exp(-4)\right]^2 \tag{3.23}$$

or,

$$v_{wh}(r_{wh}) \cong 0.96 \frac{v_{i,opt}}{PV_{bt,opt}} \left(\frac{r_{wh}}{L_{core}} \right)^{\frac{2}{3}} \tag{3.24}$$

From the **Eq. 3.24**, it is noticed that the wormhole growth rate is not constant for Furui et al.'s wormhole model. It does depend on the wormhole penetration radius and the length of the core. Assuming in a time increment Δt during which the wormhole growth rate v_{wh} is constant, the wormhole penetration can be calculated by **Eq. 3.14**,

From the wormhole penetration we can calculate the injection rate as a function of time or injected acid volume,

Rearranging the tip velocity **Eq. 3.18** to solve for length-normalized injection rate for radial flow (**Eq. 3.25**),

$$\left(\frac{q}{L} \right)^{n+1} = v_{i,tip} \phi \sqrt{\pi n_{wh}} \frac{1}{\left[(1-\alpha_z) \frac{1}{\sqrt{d_{e,wh} r_{wh}^{n+1}}} + \alpha_z \left(\frac{1}{d_{e,wh}} \right) \right]} \tag{3.25}$$

At the optimum conditions **Eq. 3.25** becomes,

$$\left(\frac{q}{L} \right)^{n+1} = v_{i,tip,opt} \phi \sqrt{\pi n_{wh}} \frac{1}{\left[(1-\alpha_z) \frac{1}{\sqrt{d_{e,wh} r_{wh}^{n+1}}} + \alpha_z \left(\frac{1}{d_{e,wh}} \right) \right]} \tag{3.26}$$

From **Eq. 3.26,** the injection rate is a function of the wormhole penetration radius assuming that all other parameters are constant.

The cumulative volume of injected acid can be calculated by **Eq. 3.16**.

4 RESULTS

4.1 Introduction

In this section, we conducted a parametric study of the optimum injection rate with varying the injected acid volume, the wellbore length, the acid concentration, and the reservoir heterogeneity. We alse presented examples of increasing rate schedule calculation for all three wormhole models: volumetric, Buijse and Glasbergen, and Furui et al's by the equations derived in **Section 3**. A comparison study was then done for acid treatments of the single optimum injection rate, the maximum allowable rate, and the increasing rate schedule for all three wormhole models. Finally, we used the acidizing simulator to history match field data of acid treatments for horizontal wells in Middle East carbonate reservoirs.

4.2 Parametric Study on the Optimum Injection Rate

The objective of this parametric study is to find the optimum injection rate that gives the best stimulation benefit, in other words, the least negative final skin factor for each of the scenarios with different values of injected acid volume, wellbore length, acid concentration, and reservoir permeability profile.

Input data for all cases of the parametric study is presented in **Table 4.1**. In **Table 4.1**, the parameters for wormhole modeling are taken from the published work of Furui et al. (2010).

Table 4.1—Input data for parametric study

Reservoir data	
Initial reservoir pressure, psi	2500
Porosity	0.2
Total compressibility, 1/psi	3.50E-06
Formation thickness, ft	50
Reservoir fluid viscosity, cp	0.5
Permeability, md	10
Well data	
Wellbore radius, ft	0.25
Pipe relative roughness	0.0001
Horizontal wellbore length, ft	1000
Wellbore fluid density, lb/ft^3	63.58
Wellbore fluid viscosity, cp	0.5
Fluid data	
wt% 15 HCl volume, gal/ft	5 - 100
Viscosity, cp	0.5
Density, lb/ft^3	63.58
Data for wormhole modeling	
Optimum porevolume to breakthrough, PV_{btopt}	0.53*
Optimum interstitial velocity (ν_{iopt}), cm/min	1.75*

(*) Values are taken from Furui et al. (2010)

In all the examples of this parametric study, the cases were performed with bullheading of wt%15 hydrochloric acid through tubing. Reservoir is homogeneous with permeability 10 md (**Table 4.1**). The damage penetration from the wellbore is in the range of 0.5 to 3.5 ft depending on the injected acid volume.

4.2.1 Effect of Injected Acid Volume

In this section, the effect of injected acid volume on the optimum injection rate was studied. The horizontal well acidizing simulator was used to run different scenarios, each with a given acid volume ranging from 5 to 100 gal/ft for the same reservoir and well conditions.

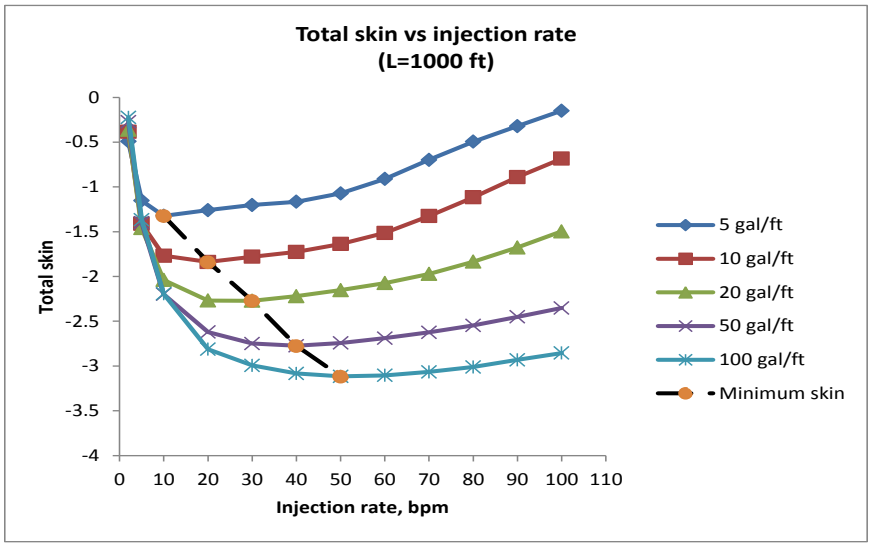

Fig. 4.1—Total skin factor for different injected acid volume for the same reservoir and conditions

Fig. 4.1 is the plot of total skin factor of the horizontal well for different values of injected acid volume: 5, 10, 20, 50, and 100 gal/ft. From the plot, the optimum injection rate is the one that gives the least (negative) skin factor on each skin curve and has the values from 10 to 50 bpm for acid volume from 5 to 100 gal/ft. This result shows that the optimum injection rate does exist for each of the given acid volume and it increases as the injected acid volume increases.

4.2.2 Effect of Wellbore Length

In this section, the optimum injection rate was determined for different values of the horizontal wellbore length for the injected acid volume of 20 gal/ft. The horizontal wellbore length selected for this study is of the range between 500 and 4000 ft.

The plots on **Fig. 4.2 a, b, c, d, e** show that with increasing wellbore length and acid volume injected the optimum injection rate increases and can be very high for longer wellbore length and larger acid volume, for example, for wellbore length of 3000 ft to 4000ft, and more than 50 gal/ft of injected acid, the optimum injection rate exceeds 100 bpm.

Fig. 4.2 f shows that for the same volume of acid injected, 20 gal/ft, the optimum injection rate increases proportionally to the increasing wellbore length. If we plot the total skin factor for this case as a function of length-normalized injection rate (**Fig. 4.3)**, the minimum skin factor was achieved at the injection rate from 0.021 to 0.029 bpm/ft. The average value of the optimum injection rate per unit length is 0.025 bpm/ft.

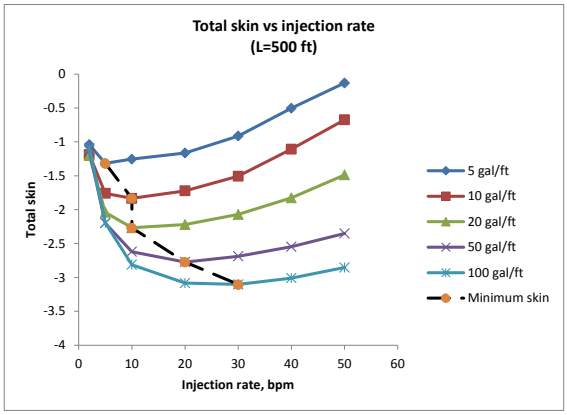

a) L = 500 ft

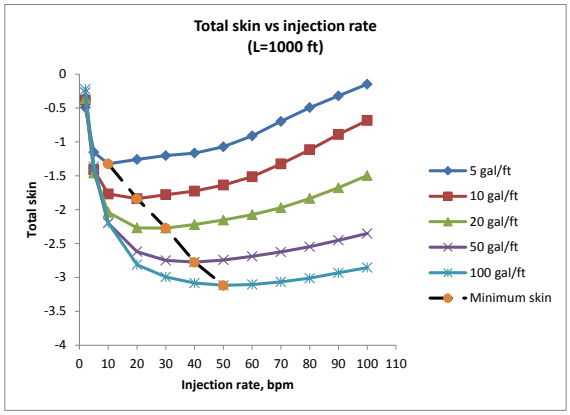

b) L = 1000 ft

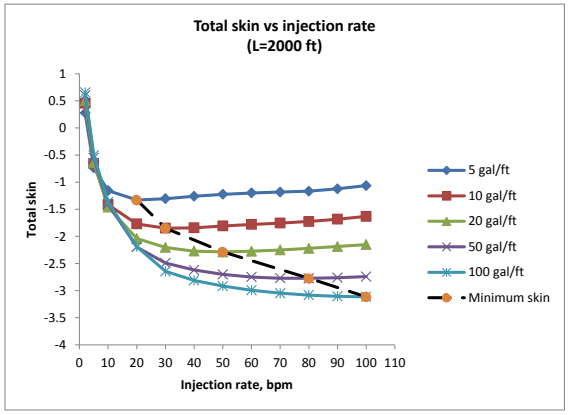

c) L = 2000 ft

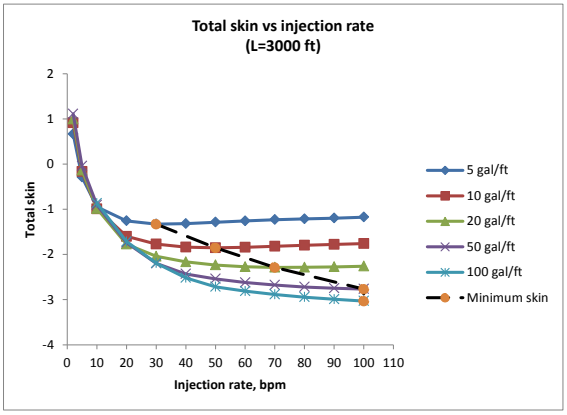

d) L = 3000 ft

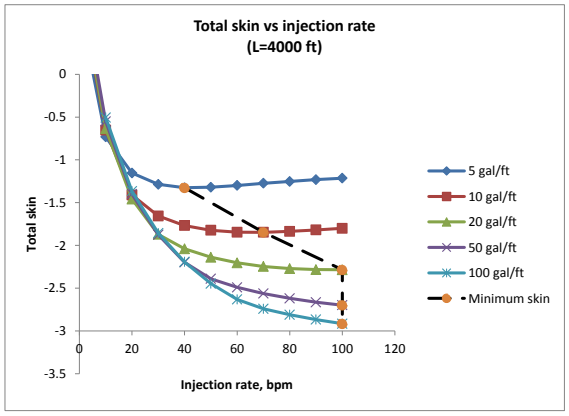

e) L = 4000 ft

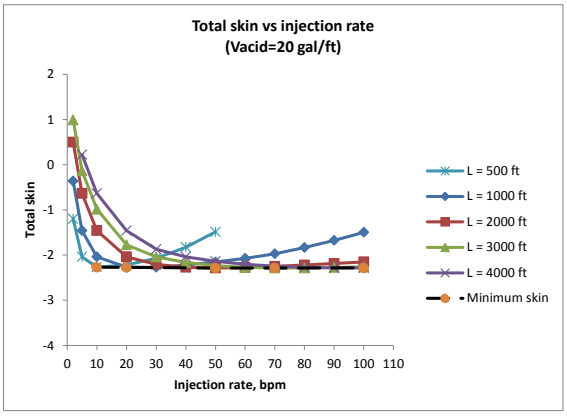

f) Vacid = 20gals/ ft

Fig. 4.2—Total skin factor for wellbore length from 500 to 4000 ft

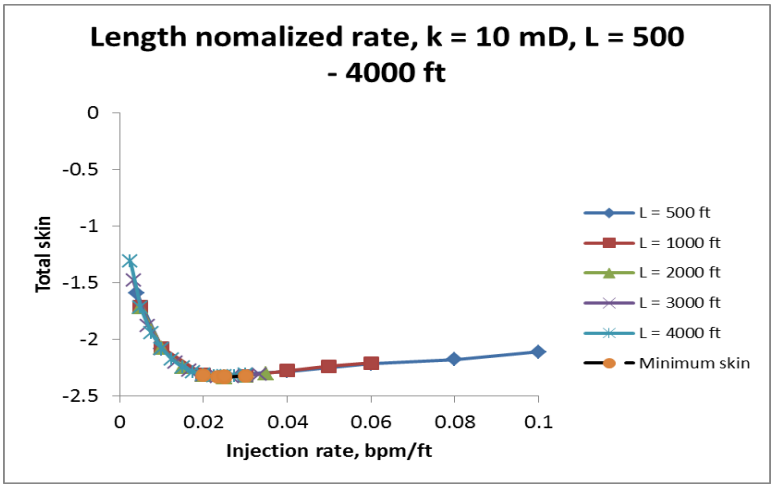

Fig. 4.3—Total skin vs length-normalized injection rate for 20 gal/ft of injected acid and wellbore length from 500 to 4000 ft

The conclusion for this section is that the optimum injection rate per unit length exists and is constant for a given reservoir, well, rock, and acid properties.

4.2.3 Effect of Acid Concentration

In this section, the effect of the acid concentration was studied for the case of 1000-ft wellbore length. To account for the acid concentration, the optimum pore volume to breakthrough and optimum interstitial velocity were taken from the experimental results for the same conditions. In the laboratory studies, the change in acid concentration was translated to the change in optimum pore volume to breakthrough and optimum interstitial velocity, or, the change in the optimum conditions in other words. The laboratory data used in this study was borrowed from the work of Furui et al. (2010) and taken from the plot of **Fig. 2.4** and re-numbered as **Fig. 4.4** here for convenience**.**

From **Fig. 4.4,** the three optimum conditions were used for 1”x6” core wt% 15 and wt% 28 HCl, 4”x20” core at the same temperature of 150 F.

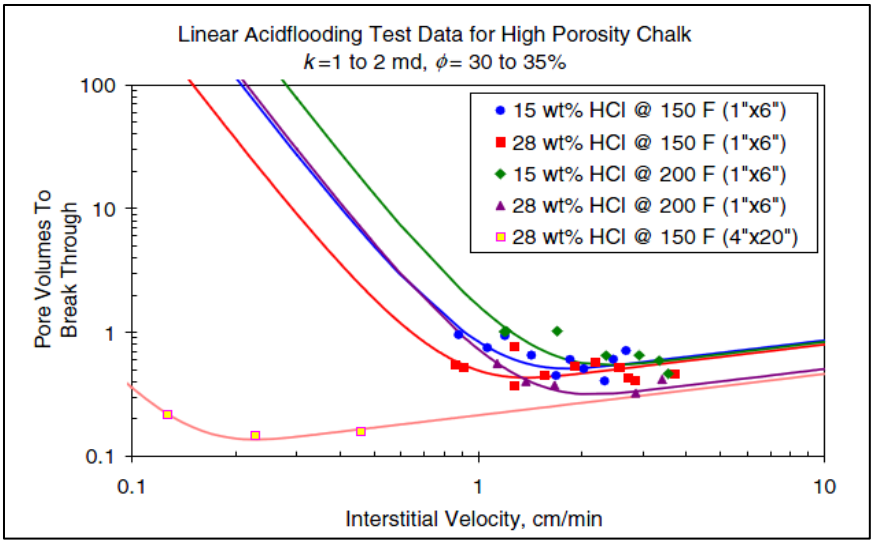

Fig. 4.4—Core-flood experiment results for high porosity outcrop chalk samples (from Furui et al., 2010)

The optimum condition data are presented in **Table 4.2**.

Table 4.2—Optimum parameters (experimental data at 150 F)

Acid concentration	wt% 15 HCl (1”x6” core)	wt% 28 HCl (1”x6” core)	wt% 28 HCl (4”x20” core)
Optimum pore volume to breakthrough ($PV_{bt,opt}$)	0.53	0.416	0.132
Optimum interstitial velocity (v_{iopt}), cm/min	1.75	1.4	0.23

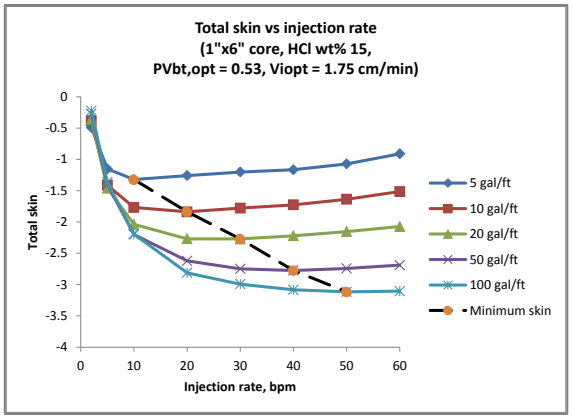

a) wt% 15 HCl (1"x6" core)

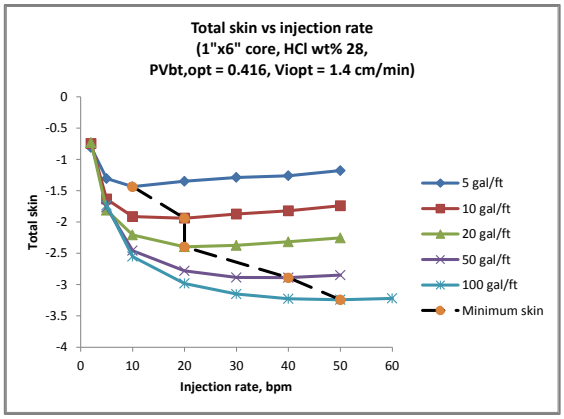

b) wt% 28 HCl (1"x6") core

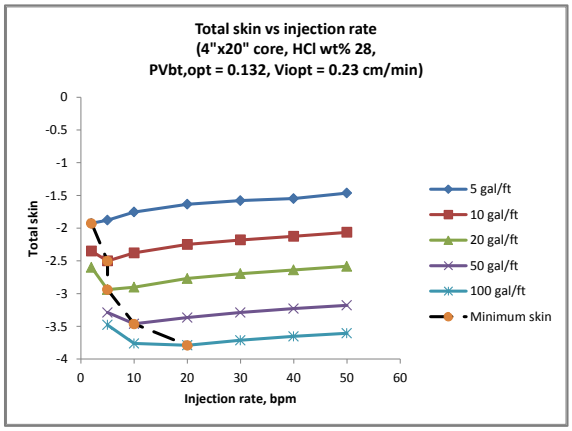

c) wt% 28 HCl (4"x20" core)

Fig. 4.5—Total skin factor for different acid concentrations

The results show that at low optimum interstitial velocity the optimum injection rate is much lower (**Fig. 4.5 c**) for all injected acid volumes compared to the higher optimum interstitial velocity (**Fig. 4.5 a, b**).

Buijse and Van Domelen (1998) showed that emulsified acid was effective for heterogeneous formations and was efficiently wormholing at low injection rates. Bazin (2001) showed that no optimum injection rate was found in core flooding experiments of

emulsified acid systems. The wormhole growth rate decreased slightly when injection rate increased; much lower acid volume is required to break through the core and it is not sensitive to the injection rate.

The important point can be made from the above discussion is that, to simulate emulsified acid treatments, the lower optimum pore volume to breakthrough and optimum interstitial velocity should be used. The emulsified acid systems are good candidate for longer horizontal wellbore, heterogeneous and severe damaged formations.

4.2.4 Effect of Reservoir Heterogeneity

To investigate the effect of reservoir heterogeneity on the optimum injection rate, we took one of the offshore wells in Middle East carbonate reservoirs as an example. This was a horizontal well with openhole completion. The production log after the treatment showed that there were 5 zones with significant contribution to the total well production. This was because those zones had higher permeability than others and the average permeability of the reservoir itself. In this example, we wanted to see how the permeability distribution affected the acid distribution and wormhole propagation along the wellbore, consequently, the acid treatment effectiveness. The input data are presented in **Table 4.3**.

Table 4.3—Input data for the effect of reservoir heterogeneity

Reservoir Data	
Initial reservoir pressure, psi	2800
Porosity	0.17
Total compressibility, 1/psi	3.50E-06
Formation thickness, ft	30
Reservoir fluid viscosity, cp	0.51
Permeability, md	1 - 20
Well Data	
Wellbore diameter, in	6.184
Pipe relative roughness	0.0001
Horizontal section length, ft	2160
Wellbore fluid density, lb/ft^3	62.42
Wellbore fluid viscosity, cp	0.51
Fluid Data	
15 wt% HCl volume, gal/ft	5 - 100
Viscosity, cp	0.51
Density, lb/ft^3	67.11
Rock Data	
Optimum pore volume to breakthrough ($PV_{bt,opt}$)	0.416 - 0.53*
Optimum interstitial velocity (ν_{iopt}), cm/min	1.4 - 1.75*

(*) Values are taken from Furui et al. (2010)

The results on **Fig. 4.6** show that, for heterogeneous permeability profile along the wellbore, the optimum injection rates still exist and the values are in the range of 20 to 60 bpm for the acid volume of 5 to 100 gal/ft.

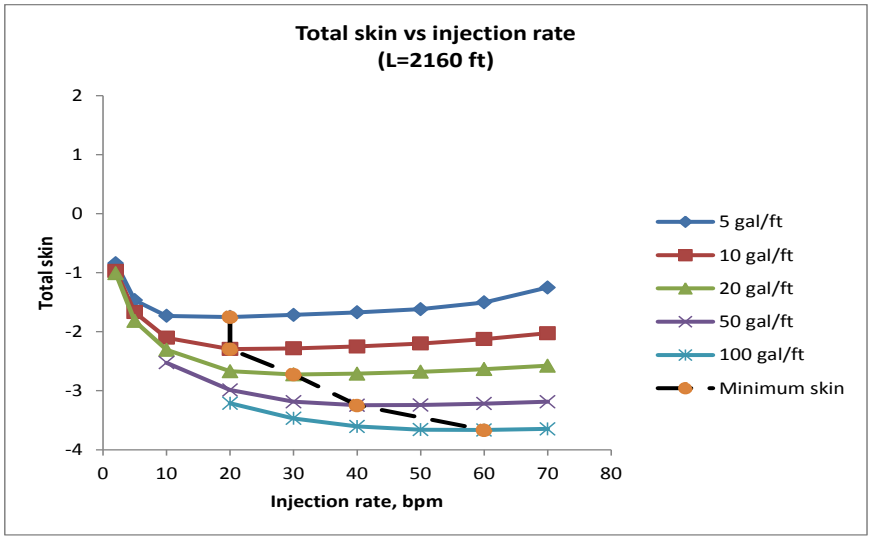

Fig. 4.6—Total skin for different injected acid volume for the same reservoir and well conditions

It is also important to note that, the permeability contrast for this well is relatively low and the ranges of optimum pore volume to breakthrough and interstitial velocity are narrow. However, for a higher permeability contrast reservoirs, the same procedure of numerical simulation can be run to determine the optimum injection rate for a given injected acid volume.

4.3 Matrix Acidizing Optimization

In this section, we study the optimum wormhole propagation conditions of matrix acidizing treatments in carbonate formations. As presented in **Section 3**, it is desired to maintain the interstitial velocity of acid at the tip of the wormhole at its optimum value to obtain the optimum wormhole propagation, in which the longest wormhole is achieved with the least amount of acid injected. To do this, the injection

rate needs to be increasing as more acid is injected into the formation. Using the procedure and equations for the increasing rate schedule, derived for different wormhole models in **Section 3,** we conduct an optimization study to compare acid distribution and wormhole penetration along the wellbore for the increasing rate injection to those of the constant optimum rate (determined in the parametric study) and constant maximum allowable rate below the fracture gradient of the formation. The numerical acidizing simulator developed in this work is used to this study.

4.3.1 Example of Volumetric Wormhole Model

As indicated in **Section 3,** to maintain the wormhole propagation at the optimum conditions, the acid injection is to be executed with an increasing rate schedule. This rate series can be calculated by **Eq. 3.7** for volumetric wormhole model. As also discussed in **Section 3.1**, it is notice that the wormhole penetration radius predicted by this wormhole model is a function of the injected acid volume, and does not depend on the injection rate for a given value of the optimum pore volume to breakthrough. As the result, the wormhole and the skin factor at the end of the acid treatment should have very similar values for any scenarios of the injection rate, again, for a given pore volume to breakthrough. In fact, however, as the injection rate changes the pore volume to breakthrough also changes. Therefore, in this example, the scenarios of different optimum conditions with different pair of optimum pore volume to breakthrough and optimum interstitial velocity are compared.

The input data for this case is presented in **Table 4.4**.

Table 4.4—Input data for volumetric model's example

Reservoir data	
Initial reservoir pressure, psi	2000
Porosity	0.2
Total compressibility, 1/psi	3.50E-06
Formation thickness, ft	50
Reservoir fluid viscosity, cp	0.5
Permeability, md	10
Well data	
Wellbore diameter, in	6.184
Pipe relative roughness	0.0001
Horizontal section length, ft	1000
Wellbore fluid density, lb/ft^3	63.58
Wellbore fluid viscosity, cp	0.5
Fluid Data	
15 wt% HCl volume, gal/ft	50
Viscosity, cp	0.5
Density, lb/ft^3	63.58
Rock Data	
Optimum porevolume to breakthrough, PV_{btopt}	0.416*
Optimum interstitial velocity (v_{iopt}), cm/min	1.4*

(*) Values are taken from Furui et al. (2010)

To start we calculate the wormhole radius and the injection rate schedule for given values of injected acid volume following the procedure and equation derived in **Section 3.1**.

The wormhole radius is calculated by **Eq. 3.5**,

$$r_{wh} = \sqrt{r_w^{\,2} + \frac{V}{\pi\phi LPV_{bt}}} = \sqrt{0.25^2 + \frac{\left(2\frac{gal}{ft}\right)\left(\frac{1bbl}{42gal}\right)\left(\frac{5.615\,ft^3}{1bbl}\right)}{(3.14)(0.2)(1000\,ft)(0.416)}} = 1.04\,ft \quad (4.1)$$

The injection rate is calculated by,

$$q = 2\pi\phi L v_{i,opt} r_{wh} =$$

$$= (2)(3.14)(0.2)(1000\,ft)\left(1.4\frac{cm}{\min}\frac{1in}{2.54cm}\frac{1\,ft}{12in}\right)(1.04\,ft)\left(\frac{1bbl}{5.615\,ft^3}\right) = 10.71bpm \qquad (4.2)$$

The calculation is continued for acid volume up to 20 gal/ft. The same procedure is followed for the other optimum condition. The result is presented in **Table 4.5**.

Table 4.5—Results for volumetric model's example

V_{acid}/L, gal/ft	$r_{wh,}$ ft	q, bpm PVbt = 0.416 Viopt = 1.4	q, bpm PVbt = 0.53 Viopt = 1.75
0.00	0.25	2.57	3.21
2.00	1.04	10.71	11.95
4.00	1.45	14.93	16.60
6.00	1.77	18.19	20.20
8.00	2.04	20.95	23.25
10.00	2.28	23.39	25.95
12.00	2.49	25.60	28.39
14.00	2.69	27.63	30.63
16.00	2.87	29.52	32.72
18.00	3.04	31.30	34.69
20.00	3.21	32.98	36.55

Fig. 4.7 plots the injection rate schedule for two optimum conditions with pore volume to breakthrough and interstitial velocity values (**Table 4.5**) taken from the work of Furui et al. (2010).

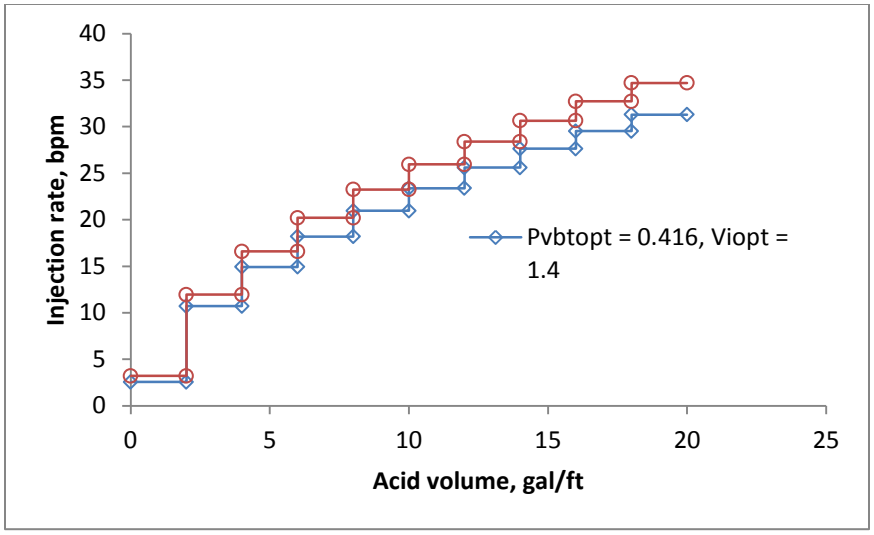

Fig. 4.7—Injection rate schedule (volumetric model's example)

Plots on **Fig. 4.8**, **Fig. 4.9**, and **Fig. 4.10** show the acid distribution, wormhole penetration, and skin factor profile along the horizontal wellbore. As expected, the acid distribution is identical for the two scenarios of the optimum conditions (**Fig. 4.8**).

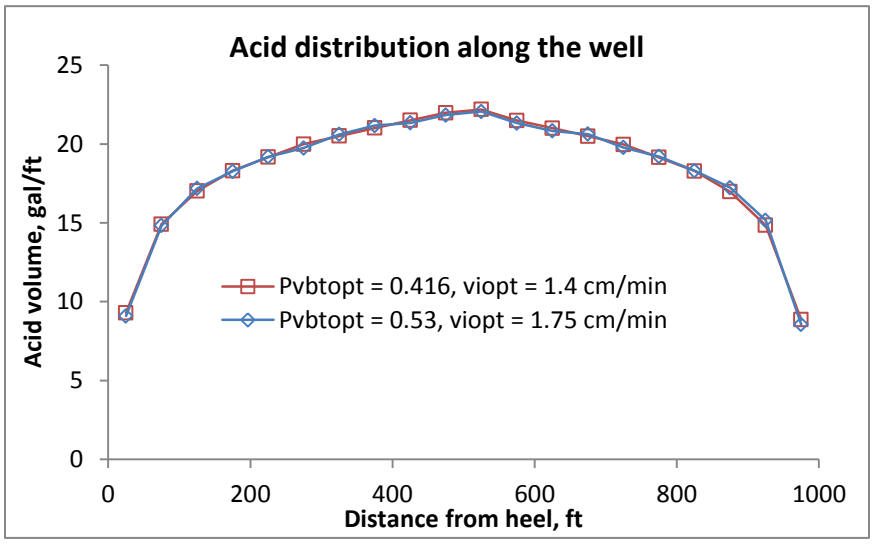

Fig. 4.8—Acid distribution along the horizontal wellbore (volumetric model's example)

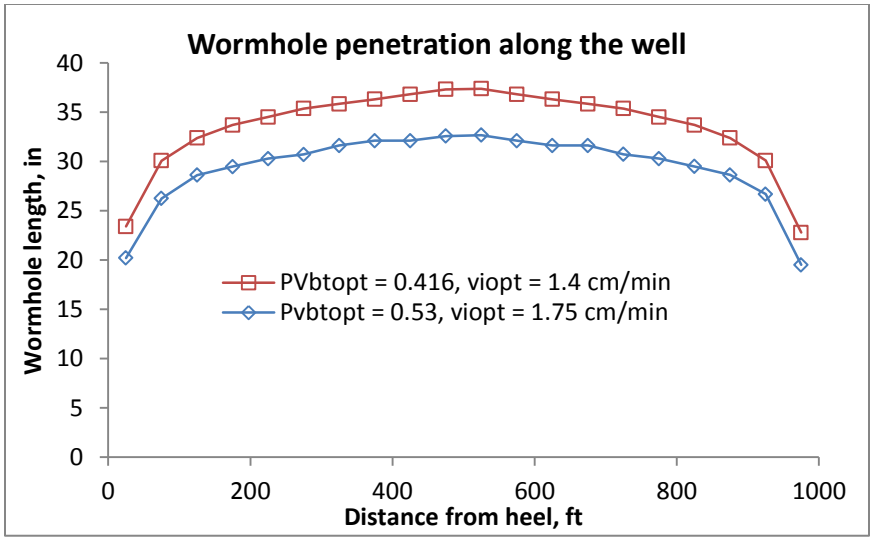

Fig. 4.9—Wormhole penetration along the horizontal wellbore (volumetric model's example)

The wormhole penetration is deeper (**Fig. 4.9)** and the skin factor is less negative (**Fig. 4.10**) for the case with lower optimum pore volume to breakthrough.

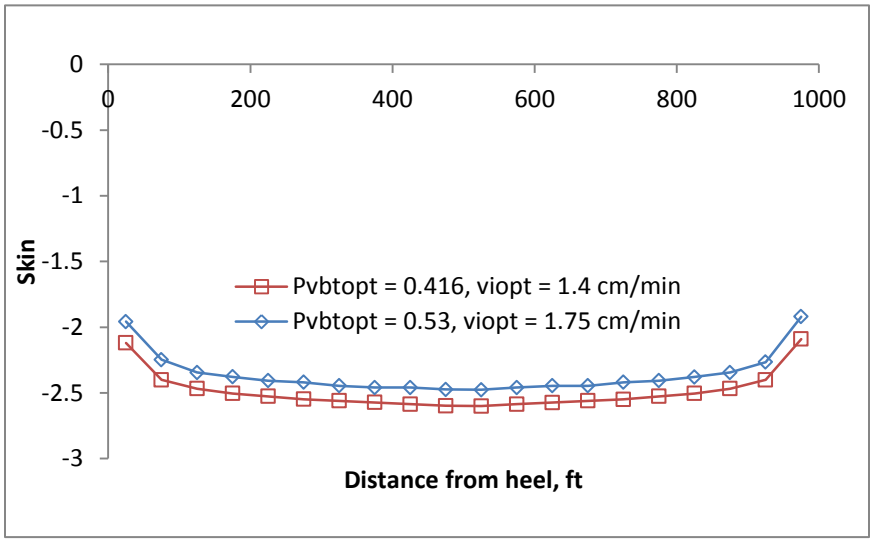

Fig. 4.10—Skin factor profile along the horizontal wellbore (volumetric model's example)

4.3.2 Example of Buijse and Glasbergen's Wormhole Model

In this section, an example of injection rate schedule calculation is presented for Buijse and Glasbergen's wormhole model following the equations derived in **Section 3.2**. After the injection rate schedule is obtain, a numerical simulation of acid treatments with different injection rate scenarios is conducted to compare the stimulation effectiveness. Input data for this example are presented in **Table 4.6**.

Table 4.6—Input data for Buijse – Glasbergen's example

Reservoir data	
Initial reservoir pressure, psi	2000
Porosity	0.2
Total compressibility, 1/psi	3.50E-06
Formation thickness, ft	50
Reservoir fluid siscosity, cp	0.5
Permeability, md	10
Well data	
Wellbore diameter, in	6.184
Pipe relative roughness	0.0001
Horizontal section length, ft	1000
Wellbore fluid density, lb/ft^3	63.58
Wellbore fluid viscosity, cp	0.5
Fluid data	
15 wt% HCl volume, gals/ft	30
Viscosity, cp	0.5
Density, lb/ft^3	63.58
Data for wormhole modeling	
Optimum pore volume to breakthrough, PV_{btopt}	0.416*
Optimum interstitial velocity (v_{iopt}), cm/min	1.4*

(*) *Values are taken from Furui et al. (2010)*

We start the calculation with wormhole growth rate by **Eq. 3.13**,

$$v_{wh}(r_{wh}) = 0.96 \times \left(\frac{v_{i,opt}}{PV_{bt,opt}} \right) = 0.96 \times \frac{1.4 \frac{cm}{\min}}{0.416} = 3.23 \frac{cm}{\min} \tag{4.3}$$

At the beginning of the acid injection, the wormhole is not created yet and its value is equal to the wellbore radius, 0.25 ft. The initial injection rate and acid volume are 2.57 bpm and 0.54 gal/ft respectively. Assuming a value of Δt = 5 min, during which the wormhole growth rate is constant. After the first time step, the wormhole radius is calculated by **Eq. 3.14**,

$$r_{wh}^{1} = r_{wh}^{0} + v_{wh} \Delta t = 0.25\, ft + \left(3.23 \frac{cm}{\min} \right) \times (5 \min) \left(\frac{1 in}{2.54 cm} \right) \left(\frac{1\, ft}{12 in} \right) = 0.78\, ft \tag{4.4}$$

From the wormhole penetration radius, the length-normalized injection rate is calculated by **Eq. 3.15**,

$$\left(\frac{q}{L} \right)^{1} = 2\pi\phi v_{i,opt} r_{wh}^{1} = 2(3.14)(0.2)(1.4)(0.78\, ft) = 0.00802 \frac{bpm}{ft} \tag{4.5}$$

Injection rate is calculated,

$$q^{1} = \left(\frac{q}{L} \right)^{1} \times L = (0.00802)(1000) = 8.02 bpm \tag{4.6}$$

The cumulative injected acid volume is calculated by **Eq. 3.16**,

$$\left(\frac{V}{L} \right)^{n+1} = \left(\frac{V}{L} \right)^{n} + \Delta t \left(\frac{q}{L} \right)^{n+1} = \left(0.54 \frac{gal}{ft} \right) + (5 \min) \left(0.00802 \frac{bpm}{ft} \right) \left(\frac{42 gal}{1 bbl} \right) = 1.68 \frac{gal}{ft} \tag{4.7}$$

The calculation is repeated until the desired injected acid volume is reached. In this example, a volume of about 20 gal/ft is assumed to be injected. The results for the next time steps are presented in **Table 4.7**.

. From the results, it is observed that the injection rate increases as more acid is injected and with increasing wormhole radius.

Table 4.7—Results for Buijse and Glasbergen's example

r_{wh}, ft	v_{wh}, cm/min	q, bpm	V_{acid}, gal/ft
0.25	3.23	2.57	0.54
0.78	3.23	8.02	1.68
1.31	3.23	13.47	4.51
1.84	3.23	18.91	8.48
2.37	3.23	24.36	13.60
2.90	3.23	29.81	19.86

The increasing rate schedule **Table 4.7** is used for a comparison study with an acid treatment which is based on the optimum injection rate. From the parametric study in **Section 4.2.1**, the normalized optimum injection rate for the same reservoir, well conditions, and acid volume of 20 gal/ft is 0.025bpm/ft, which is equal to 25 bpm for 1000-ft long horizontal well.

An example of acid treatments with three scenarios is presented for comparison of the stimulation benefits with different injection rate options. **Fig. 4.11** shows the plot of increasing rate, the optimum rate and maximum rate from **Table 4.7** to be used in the simulation. The injection location it at the middle of the horizontal well and the acidizing

treatment is executed at constant rate condition. The injection rate scenario is treatment with several intervals of constant rate as shown in **Fig. 4.11**.

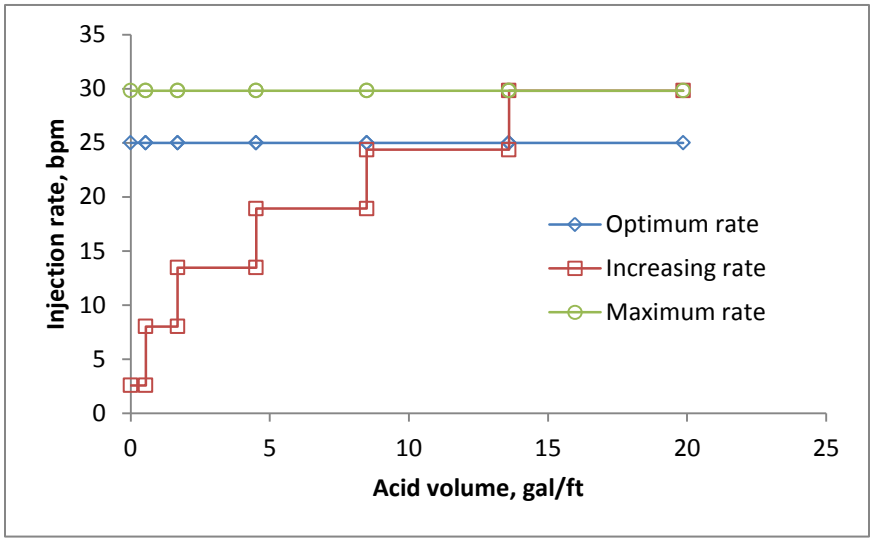

Fig. 4.11—Injection rate schedule (Buijse-Glasbergen's example)

The outputs of the simulation are the interstitial velocity, wormhole penetration at the injection location, the acid distribution and wormhole penetration along the horizontal well. The results are plotted on the same plot for all three scenarios to compare the wormhole growth efficiency and acid coverage along the wellbore.

As discussed, the goal of the matrix acidizing optimization is to maintain the wormhole propagation at the tip of the wormhole at its optimum conditions to achieve the best benefit. The acid flux at the tip of the wormhole is desired to be held around the optimum value by increasing the injection rate as more acid is injected into the formation. **Fig. 4.12** shows that the interstitial velocity of the increasing rate case is

maintained around its optimum value and is lower than that of the optimum constant rate and maximum rate cases.

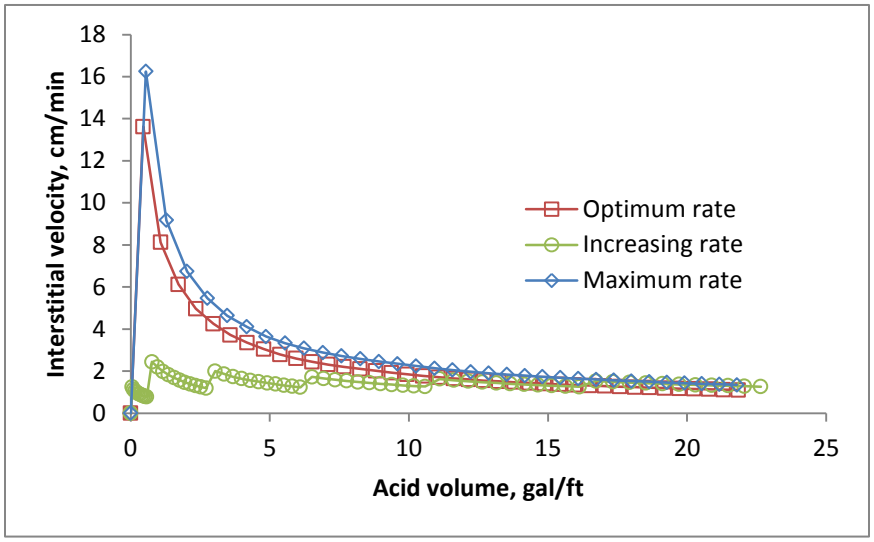

Fig. 4.12—Interstitial velocity at the injection location (Buijse-Glasbergen's example)

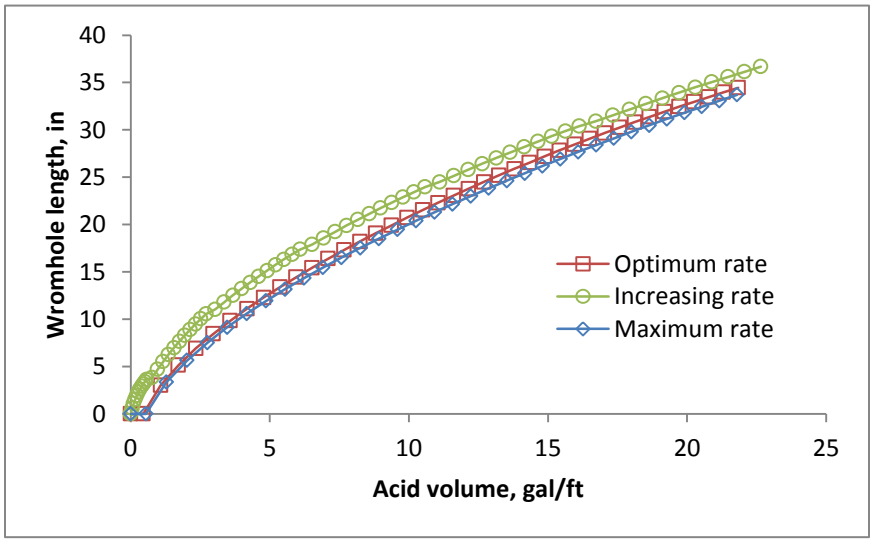

Fig. 4.13—Wormhole propagation at the injection location (Buijse-Glasbergen's example)

The wormhole at the injection location (**Fig. 4.13**) well penetrates deeper into the formation for the increasing rate injection. Therefore, the local skin factor at this location is lowering (less negative) compared to that of the other two scenarios (**Fig. 4.14**).

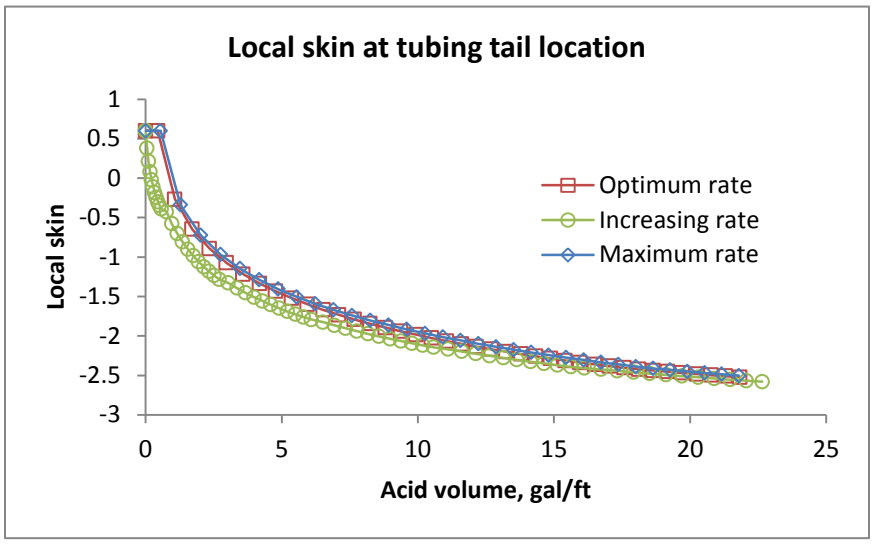

Fig. 4.14—Skin factor evolution at the injection location (Buijse-Glasbergen's example)

Fig. 4.15 and **Fig. 4.16** are the plots of acid distribution and wormhole penetration along the horizontal wellbore. From these plots it is observed that, although the acid distribution for all scenarios is not much different (**Fig. 4.15**), the wormhole along the horizontal wellbore for the increasing rate case penetrates deeper into the formation that that of the constant optimum and maximum rate cases (**Fig. 4.16**).

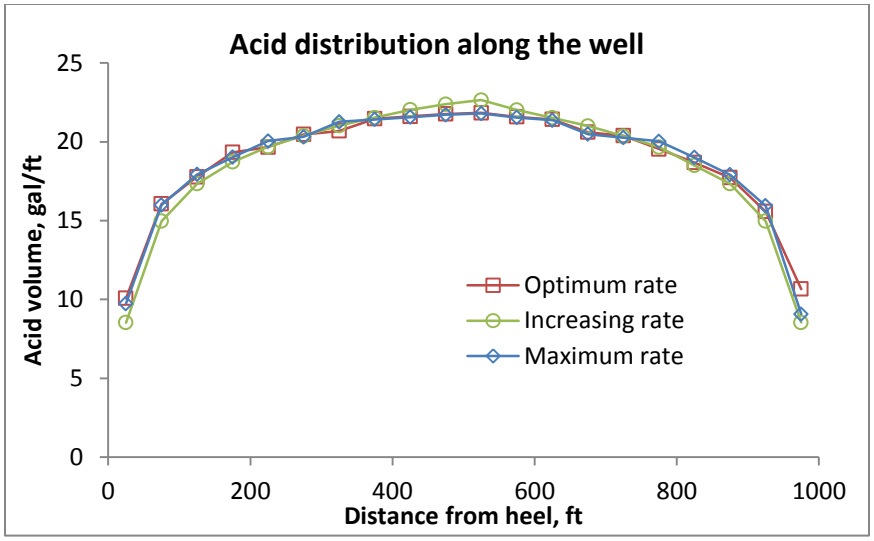

Fig. 4.15—Acid distribution along the horizontal wellbore (Buijse-Glasbergen's example)

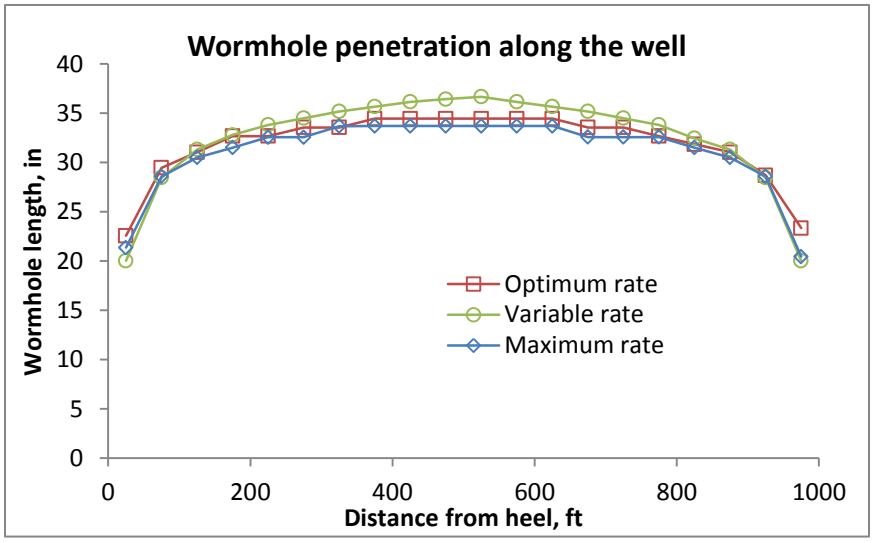

Fig. 4.16—Wormhole penetration along the horizontal wellbore (Buijse-Glasbergen's example)

Therefore, this example shows that in carbonate acidizing, executing acid treatments at an increasing rate schedule maintains the wormhole propagation at the tip of the wormholes at its optimum conditions. This gives better stimulation efficiency.

4.3.3 Example of Furui et al.'s Wormhole Model

In this example, a procedure similar to the example in **Section 4.3.2** is followed for analytical calculation and numerical simulation study. The injection rate schedule calculation is presented for Furui et al.'s wormhole model following the equations derived in **Section 3.3**. This example shares the common input data that are presented in **Table 4.6**. Additional input data for Furui et al.'s wormhole model are presented in **Table 4.8**.

Table 4.8—Input data for Furui et al.'s example

Data for Furui et al.'s wormhole model	
Core length, in	6
Core diameter**, in	1
Number of dominant wormholes	4
Effective wormhole diameter, cm	1.5*
Wormhole axial spacing coefficient, α_z	0.75

(*) *Values are taken from Furui et al. (2010)*
(**) Values are used in the acidizing simulator only

At the beginning of the acid injection, the wormhole is not created yet and its value is equal to the wellbore radius, 0.25 ft. We start the calculation with wormhole growth rate by **Eq. 3.24**,

$$v_{wh}(r_{wh}) = 0.96 \times \left(\frac{v_{i,opt}}{PV_{bt,opt}}\right)\left(\frac{r_{wh}}{L_{core}}\right)^{\frac{2}{3}} = 0.96 \times \frac{1.4\left(\frac{cm}{\min}\right)}{0.416}\left(\frac{0.25\,ft}{6in\left(\frac{1\,ft}{12in}\right)}\right)^{\frac{2}{3}} = 2.04\left(\frac{cm}{\min}\right) \tag{4.8}$$

The acid capacity number is calculated by **Eq. 3.20**,

$$N_{Ac} = \frac{\phi\beta C_0 \rho_{acid}}{(1-\phi)\rho_{rock}} = \frac{(0.2)(1.37)(0.15)\left(63.58\frac{lb}{ft^3}\right)}{(1-0.2)\left(2.71\frac{kg}{cm^3}\frac{62.4\frac{lb}{ft^3}}{\frac{kg}{cm^3}}\right)} = 0.0193 \tag{4.9}$$

The optimum interstitial velocity at the tip of the wormhole is calculated by **Eq. 3.22**,

$$v_{i,tip,opt} = \frac{v_{i,opt}}{PV_{bt,opt}N_{AC}}\frac{r_{wh}}{L_{core}} = \frac{\left(1.4\frac{cm}{\min}\right)}{(0.0193)}\frac{(0.25\,ft)}{\left(6\frac{1\,ft}{12in}\right)} = 87.11\frac{cm}{\min} \tag{4.10}$$

From the wormhole penetration radius, the length-normalized injection rate is calculated by **Eq. 3.26**,

$$\left(\frac{q}{L}\right)^1 = v_{i,tip,opt}\phi\sqrt{\pi m_{wh}}\frac{1}{\left[(1-\alpha_z)\frac{1}{\sqrt{d_{e,wh}r_{wh}^{n+1}}} + \alpha_z\left(\frac{1}{d_{e,wh}}\right)\right]} =$$

$$= \frac{1bbl}{5.615\,ft^3}\left(87.11\frac{cm}{\min}\frac{1in}{2.54cm}\frac{1\,ft}{12in}\right)(0.2)\sqrt{(3.14)(4)}\times \tag{4.11}$$

$$\left(\frac{q}{L}\right)^1 = \frac{1}{\left[(1-0.75)\frac{1}{\sqrt{(0.04\,ft)(0.25\,ft)}} + 0.75\left(\frac{1}{0.04\,ft}\right)\right]} = 0.0206\frac{bpm}{ft} \quad (4.12)$$

Injection rate is calculated,

$$q^1 = \left(\frac{q}{L}\right)^1 \times L = (0.0206)(1000) = 20.6bpm \quad (4.13)$$

The cumulative injected acid volume is calculated by **Eq. 3.16**,

$$\left(\frac{V}{L}\right)^1 = \left(\frac{V}{L}\right)^0 + \Delta t\left(\frac{q}{L}\right)^1 = \left(0\frac{gal}{ft}\right) + (0.65\min)\left(0.0206\frac{bpm}{ft}\right)\left(\frac{42gal}{1bbl}\right) = 1.68\frac{gal}{ft} \quad (4.14)$$

Assuming a value of Δt = 0.65 min, during which the wormhole growth rate is constant. After the first time step, the wormhole radius is calculated by **Eq. 3.14**,

$$r_{wh}^1 = r_{wh}^0 + v_{wh}\Delta t = 0.25\,ft + \left(2.04\frac{cm}{\min}\right) \times (0.65\min)\left(\frac{1in}{2.54cm}\right)\left(\frac{1\,ft}{12in}\right) = 0.29\,ft \quad (4.15)$$

The calculation is continued until the desired injected acid volume is reached. In this example, a volume of about 10 gal/ft is assumed to be injected. The results for the next time steps are presented in **Table 4.9**. From the results, it is observed that the injection rate increases as more acid is injected and with increasing wormhole radius.

Table 4.9—Results for Furui et al.'s example

r_{wh} ft	v_{wh} cm/min	$V_{i,tip,opt}$ cm/min	q/L bpm/ft	q bpm	V_{acid} gal/ft
0.25	2.04	87.11	0.021	20.63	0.56
0.29	2.26	102.24	0.024	24.45	1.23
0.34	2.51	119.06	0.029	28.73	2.02
0.40	2.76	137.69	0.033	33.49	2.93
0.45	3.03	158.21	0.039	38.75	3.99
0.52	3.31	180.73	0.045	44.55	5.20
0.59	3.60	205.33	0.051	50.91	6.59
0.67	3.91	232.11	0.058	57.85	8.17
0.75	4.23	261.18	0.065	65.41	9.96

Fig. 4.17 shows the injection rate schedule for constant optimum rate, constant maximum rate, and increasing rate for Furui et al.'s wormhole model. These injection rate scenarios are used to run the acidizing simulator for a comparison study. Data in **Table 4.6** and **Table 4.8** are used for simulation runs.

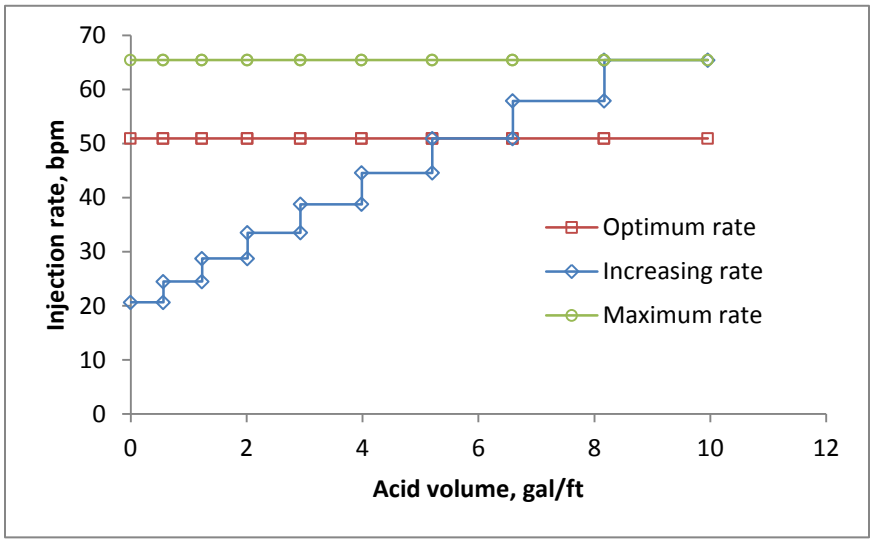

Fig. 4.17—Injection rate schedule (Furui et al.'s example)

It is noticed above that the acid flux at the tip of the wormhole is desired to be held around the optimum value by increasing the injection rate as more acid is injected into the formation. **Fig. 4.18** shows that the interstitial velocity of the increasing rate case is maintained around its optimum value and is lower than that of the optimum constant rate and maximum rate cases.

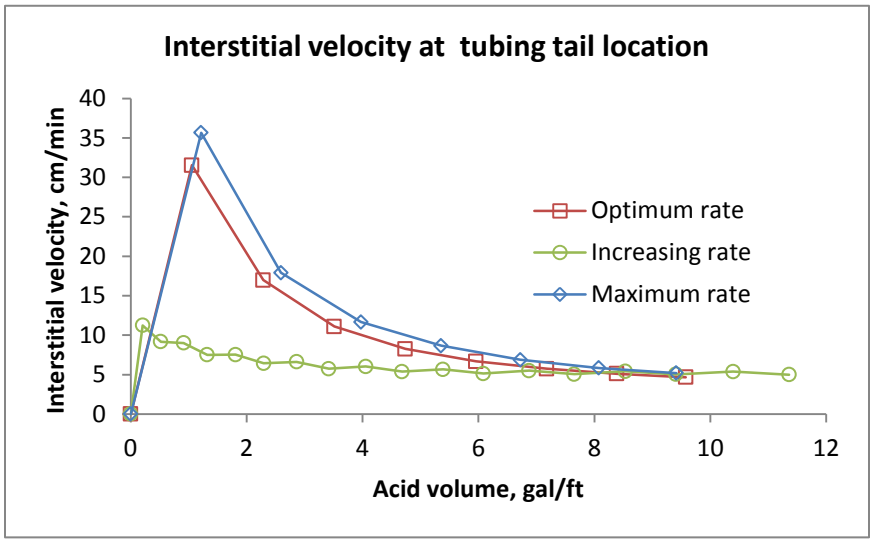

Fig. 4.18—Interstitial velocity at the injection location (Furui et al's example)

The wormhole at the injection location well penetrates deeper into the formation for the increasing rate injection compared to that of the constant rate cases (**Fig. 4.19**). Therefore, the local skin factor at this location is lowering (less negative) compared to that of the other two scenarios (**Fig. 4.20**).

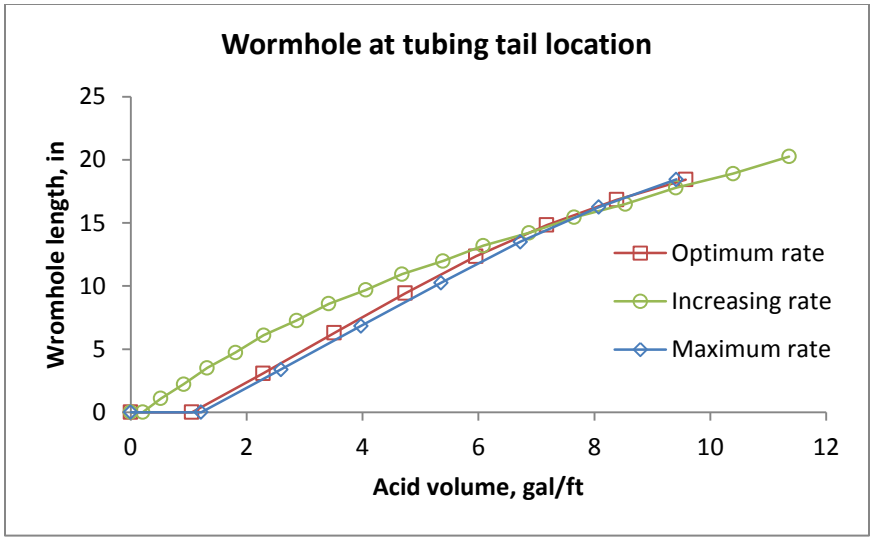

Fig. 4.19—Wormhole propagation at the injection location (Furui et al's example)

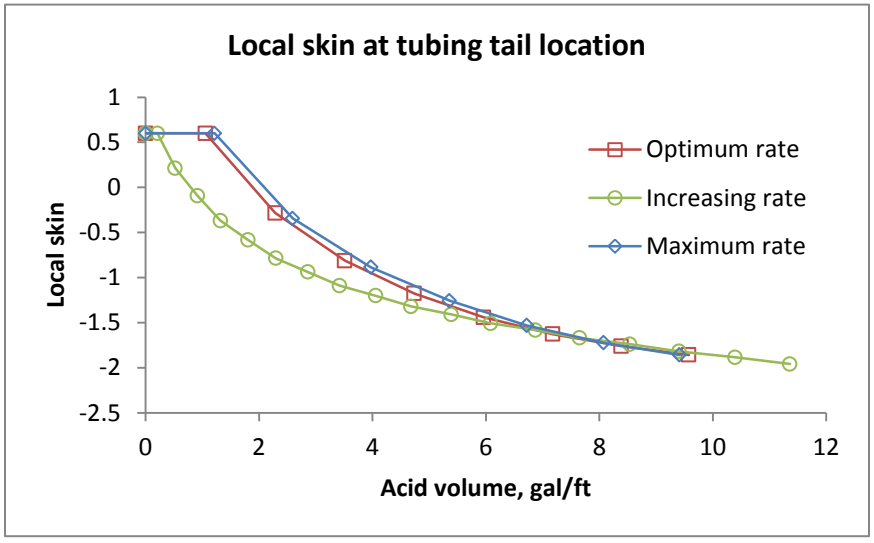

Fig. 4.20—Skin factor evolution at the injection location (Furui et al's example)

Fig. 4.21 and **Fig. 4.22** are the plots of acid distribution and wormhole penetration along the horizontal wellbore. From these plots it is observed that, the acid distribution of the increasing rate case is higher in the vicinity of the injection location. It

is because the tip velocity is high as predicted by Furui et al.'s wormhole model (**Fig. 4.21**).

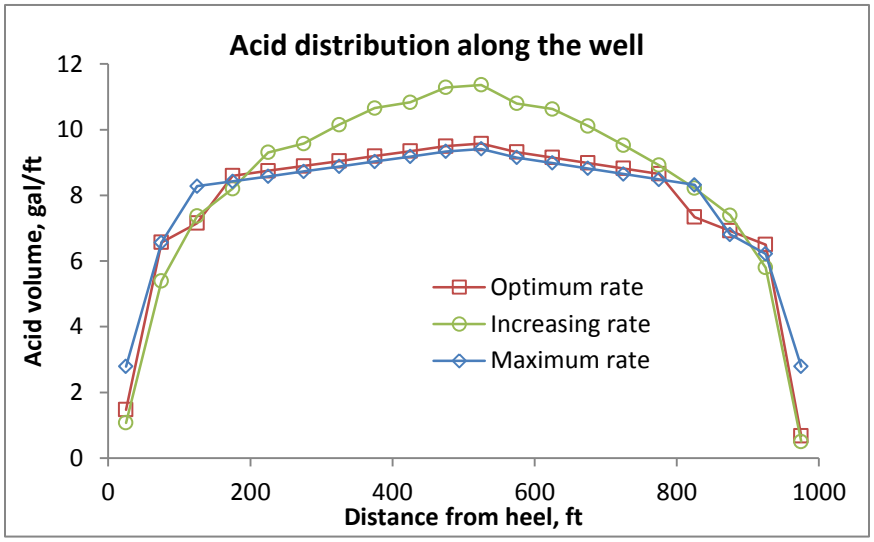

Fig. 4.21—Acid distribution along the horizontal wellbore (Furui et al's example)

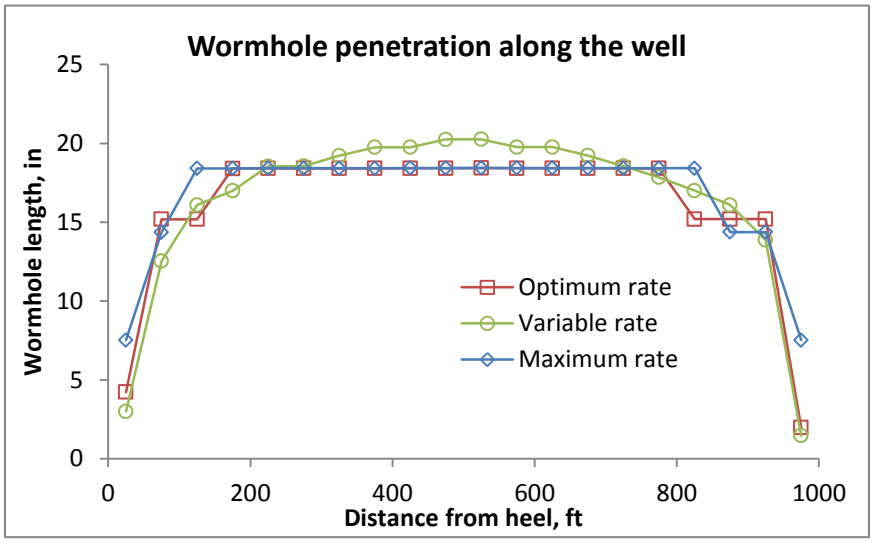

Fig. 4.22—Wormhole penetration along the horizontal wellbore (Furui et al's example)

The wormhole penetration along the horizontal wellbore for the increasing rate case has longer value around the injection location and is decreasing further away from it (**Fig. 4.22**).

The Furui et al.'s wormhole model takes into consideration the acid flux at the tip of the wormhole. Therefore, it predicts longer wormhole penetration in the region around the injection point along the wellbore as this region receives more acid with higher flux. To achieve better stimulation effectiveness in a heterogeneous formation, the injection point should be place at the lower permeability zones.

4.4 Field Cases

Field case study was conducted for treatment data of horizontal wells in onshore and offshore Middle East carbonate formations. Typical reservoir, well, and acids of the acidized horizontal wells had the following properties,

- permeability from 1 to 1000 md, with or without natural fractures,
- horizontal wellbore/lateral length from 610 to 4600 ft,
- openhole and cased perforated completions,
- acid systems used: regular HCl, carbonate emulsion acid (CEA), viscoelastic surfactant (VES), nitrified foam acid. The typical treatments and dosage were:
    - wt% 15 HCl: 5-20 gal/ft; for acid wash
    - wt% 22 CEA 100 gal/ft treatment
    - wt% 15 HCl 10-20 gal/ft and wt% 22 CEA 25-100 gal/ft

- wt% 15 HCl 20 gal/ft, VES 15 gal/ft and wt% 22 CEA 50 gal/ft,
- wt% 15 HCl 10 gal/ft and VES 5 gal/ft,
- wt% 15 HCl 15 – 20 gal/ft and foamed acid 2 – 5 gal/ft.

The study procedure was cconsists of two steps: first step is to perform the skin analysis using the skin monitoring method proposed by (Hill and Zhu, 1996). This skin analysis use measured pressure and rate data of the treatment to calculate the skin factor (Pandya 2012). The second step is to use the developed acidizing simulator to history match the pressure response of the treatment and the estimated skin factor by inputting the rate schedule.

All the treatments, from cases 7 to 10, have been executed through 2.00'' coiled tubing with two main stages: RIH with regular acid HCl and POH with nitrified foamed acid. The digital data provided in the reports include: pressure in the annulus, surface pumping pressure and liquid acid rate. For the treatment data analysis, the bottomhole pressure is calculated from the annular pressure. For the second stage (foamed acid) the total injection rate is calculated as the sum of liquid acid and nitrogen gas rates.

The nitrogen gas rate is estimated as following (**Eq. 4.16**),

$$q_g = q_l \times GLR \times B_g \tag{4.16}$$

with,

$$B_g = 0.0283 \times z \times \frac{T}{p} \tag{4.17}$$

where,

q_g – nitrogen gas injection rate, bpm

q_l – liquid acid rate, bpm

GLR – gas liquid ratio, scf/bbl

B_g – gas formation volume factor, cuft/scf

T – temperature at downhole condition, R

p – bottomhole pressure, psia

z – gas compressibility factor

Total injection rate is calculated by **Eq. 4.18**,

$$q_t = q_l + q_g \tag{4.18}$$

4.4.1 Case 1

4.4.1.1 Treatment Description

This well is a horizontal well with an open-hole lateral, as seen in **Fig. 4.23**. The actual acidizing treatment design comprised of treating the target interval with 15% hydrochloric acid (HCl) using coil-tubing.

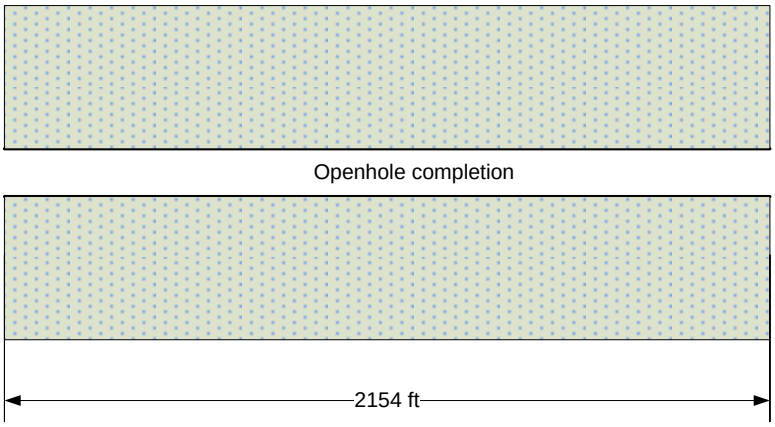

Fig. 4.23—Well diagram for Case 1

The data for the reservoir, the wellbore, and the acid injection is shown in **Table 4.10** and **Table 4.11**.

Table 4.10—Input data for Case 1

Reservoir Data	
Initial reservoir pressure, psi	2800
Porosity	0.17
Total compressibility, 1/psi	3.50E-06
Formation thickness, ft	30
Reservoir fluid viscosity, cp	0.51
Reservoir temperature, F	150
Permeability, md	5.5
Well Data	
Wellbore radius, in	3.500
Tubing diameter, in	1.68
Pipe relative roughness	0.0001
Horizontal section length, ft	2154
Wellbore fluid density, lbm/ft3	62.42
Wellbore fluid viscosity, cp	0.51

Table 4.11—Injection schedule for Case 1

Fluid Name	Volume Used, gal	Density, lb/ft3	Viscosity, cp
HCl	73118	67.11	0.51
Water	1991	62.42	0.51

4.4.1.2 Skin Monitoring Results

The surface pressure and injection rate data was measured on-site during the acid job. **Fig. 4.24** plots the measured injection rate, and the measured surface pressure recorded during the acidizing treatment.

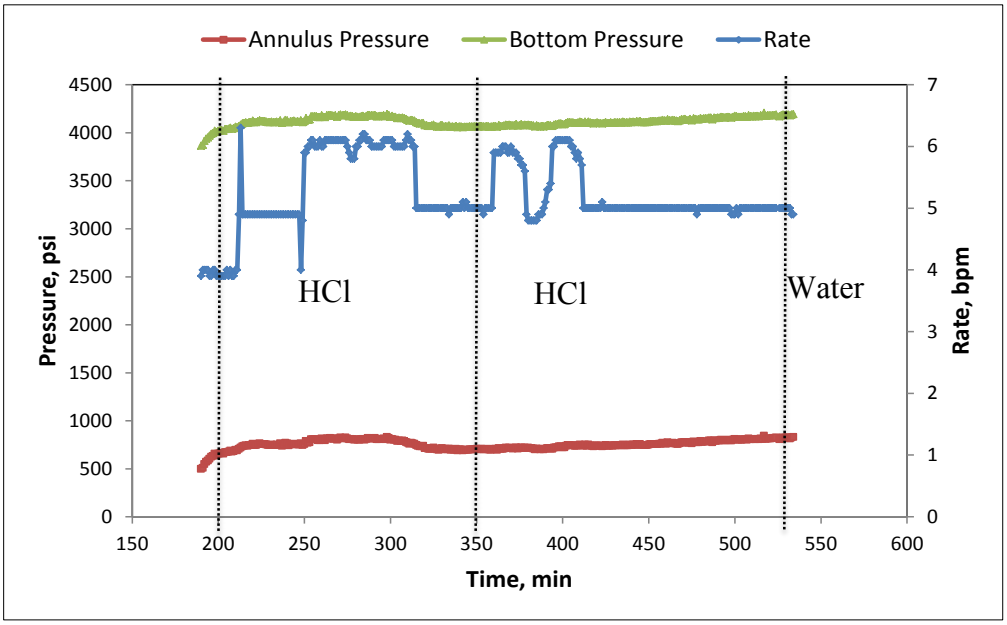

Fig. 4.24—Treatment data for Case 1

In **Fig. 4.24**, the bottomhole pressure was calculated from the annulus pressure. From the calculated bottomhole pressure and measured injection rate, the skin was calculated at each time step. The skin evolution during the acid job is shown in **Fig. 4.25.**

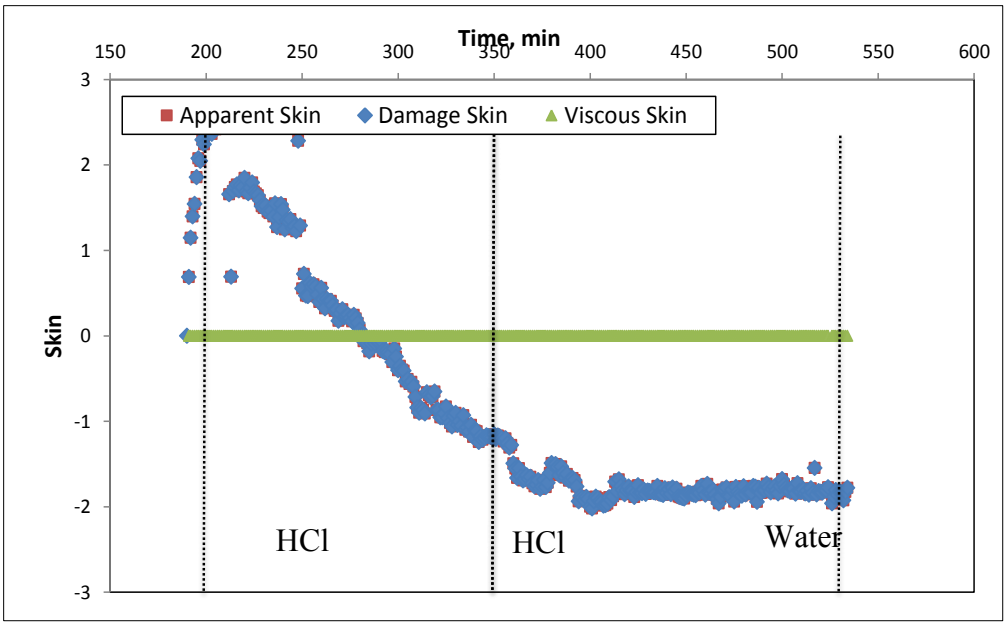

Fig. 4.25—Skin evolution for Case 1

4.4.1.3 History Matching Results

Fig. 4.26 shows the post-treatment production log of the horizontal well. This log shows that significant amount of the total production is from 5 intervals. Production from other intervals is small.

Buijse and Glasbergen's wormhole model is used to propagate wormholes. Optimum pore volume to breakthrough and interstitial velocity are the input. An initial guess of reservoir properties along the wellbore is obtained with the help of the production log. The zone has higher production will have higher permeability and more severe damage. Based on this reasoning, the permeability, damage properties, optimum pore volume to breakthrough and interstitial velocity are presented in **Table 4.12**.

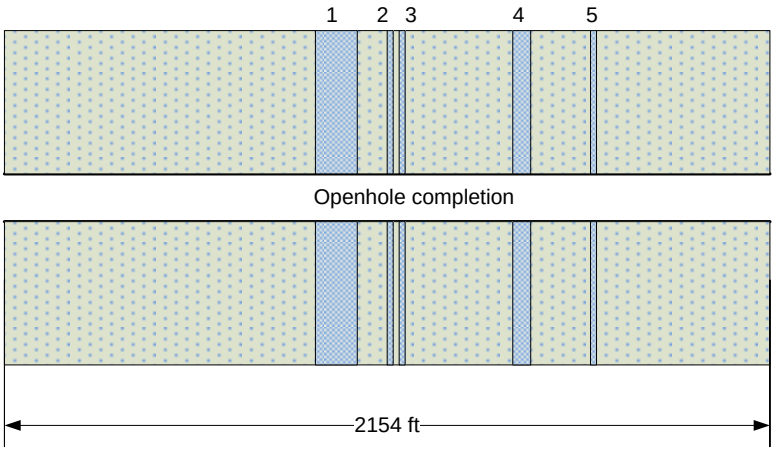

Fig. 4.26—Post-treatment production log for Case 1

Table 4.12—Zone properties for Case 1

Zone data					
Zone	Horizontal permeability, md	Impairment ratio	Damage penetration, ft	PV_{bt-opt}	V_{i-opt}, cm/min
1	25	0.9	0.5	0.85	1
2	30	0.9	0.5	0.85	1
3	15	0.9	0.5	0.85	1
4	15	0.9	0.5	0.85	1
5	10	0.9	0.5	0.85	1
6	20	0.9	0.5	0.85	1
Others	1-5	0.9	0.5	1	2

Fig. 4.27 and **Fig. 4.28** show the results of history matching of the pressure, rate and skin factor of the treatment. The obtained history matched results are in good agreement with the ones approximated by skin analysis.

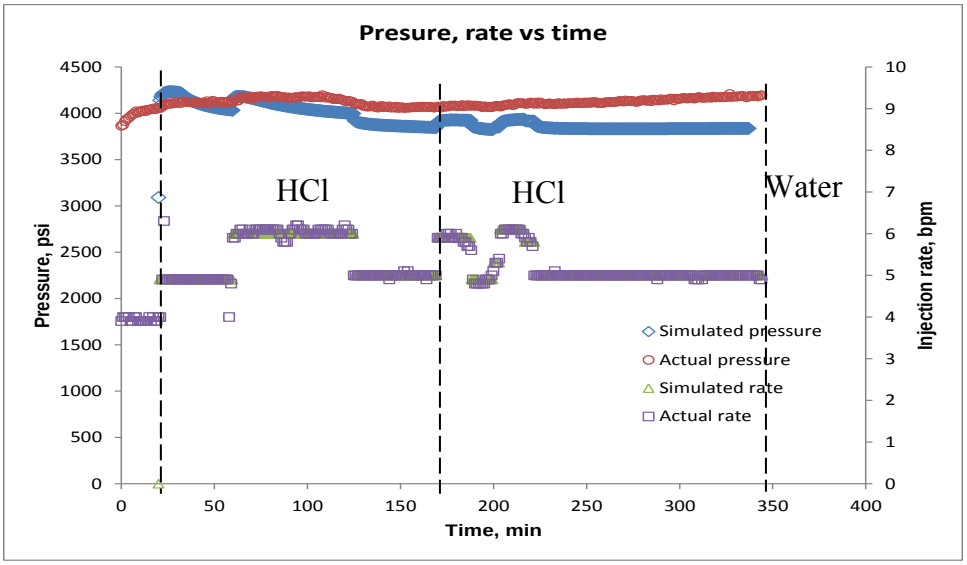

Fig. 4.27—Pressure and rate history matched results for Case 1

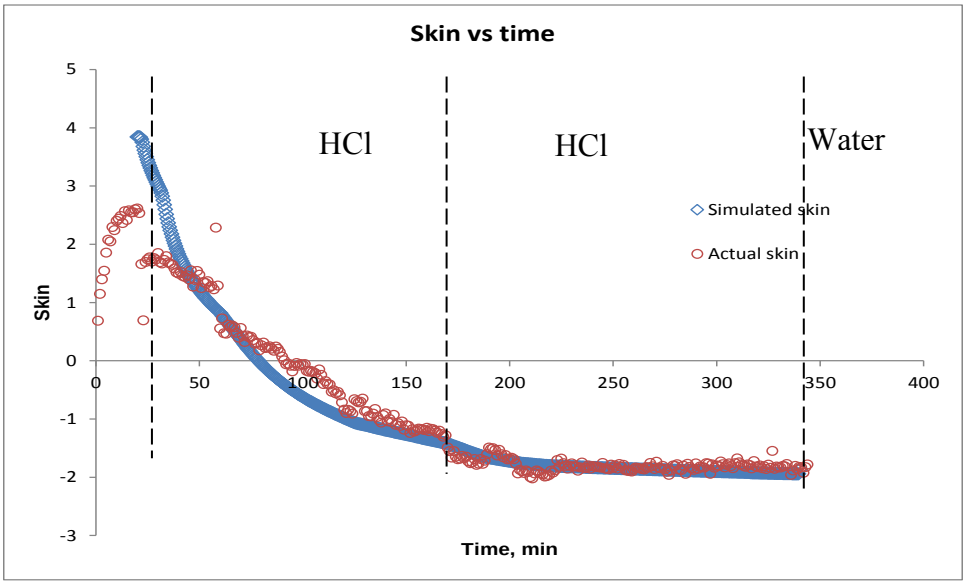

Fig. 4.28—Skin evolution history matched results for Case 1

4.4.2 Case 2

4.4.2.1 Treatment Description

This well is a horizontal well with a cased and perforated completion, as shown in **Fig. 4.29**. The actual acidizing treatment design comprised of bullheading 22% carbonate emulsion acid (CEA). The perforated interval was completed towards the end of the horizontal wellbore.

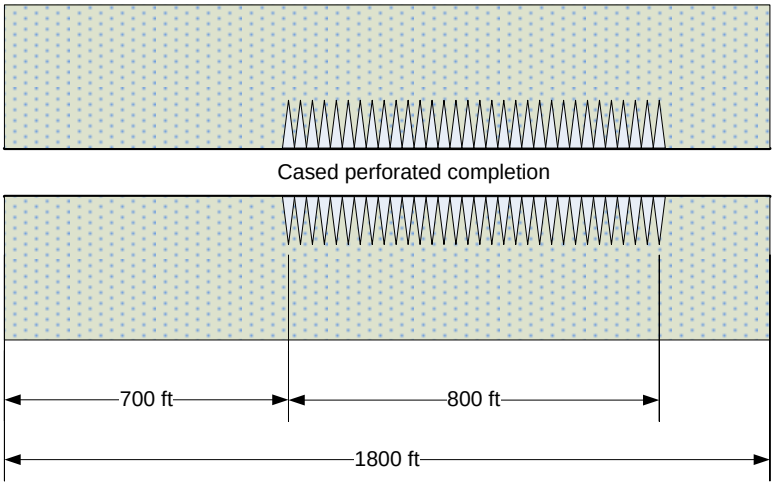

Fig. 4.29—Well diagram for Case 2.

The input data are presented in **Table 4.13** and **Table 4.14**.

Table 4.13—Input data for Case 2

Reservoir Data	
Initial reservoir pressure, psi	2500
Porosity	0.2
Total compressibility, 1/psi	3.50E-06
Formation thickness, ft	307
Reservoir fluid viscosity, cp	0.46
Reservoir temperature, F	150
Permeability, md	10
Well Data	
Wellbore diameter, in	6.184
Pipe relative roughness	0.0001
Horizontal section length, ft	1800
Wellbore fluid density, lbm/ft3	63.58
Wellbore fluid viscosity, cp	0.46

Table 4.14—Injection schedule for Case 2

Fluid Name	Volume Used, gal	Density, lb/ft3	Viscosity, cp	Friction Reducer
CEA	27007	63.58	0.46	1

4.4.2.2 Skin Monitoring Results

The surface pressure and injection rate data was measured on-site during the acid job. **Fig. 4.30** plots the measured injection rate, and the measured surface pressure recorded during the acidizing treatment.

In **Fig. 4.30**, the bottomhole pressure was calculated from the surface pressure. From the calculated bottomhole pressure and measured injection rate, the skin was calculated at each time step. The skin evolution during the acid job is shown in **Fig. 4.31.**

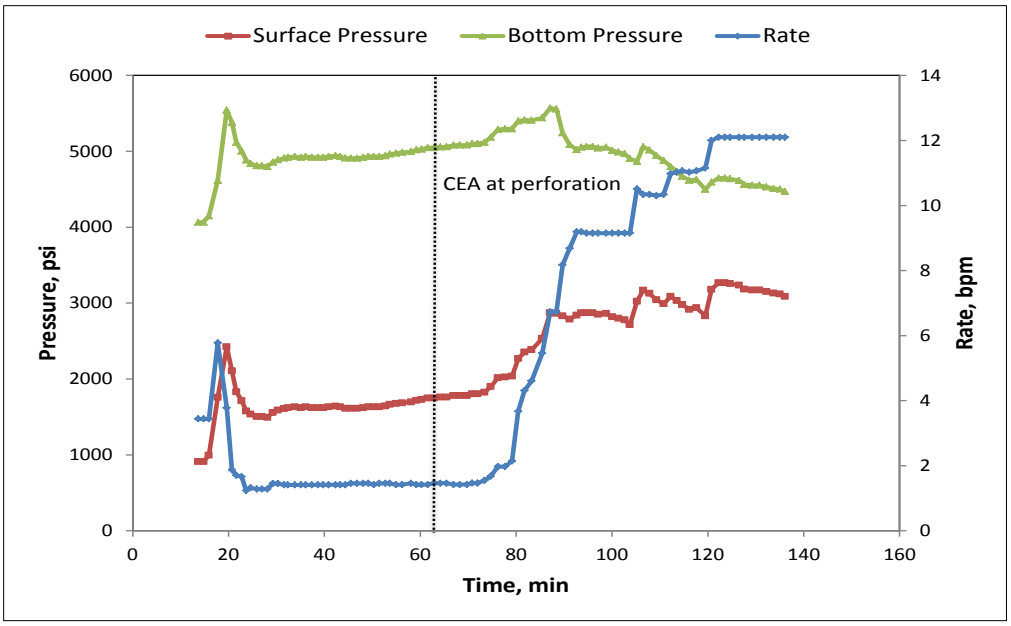

Fig. 4.30—Treatment data for Case 2

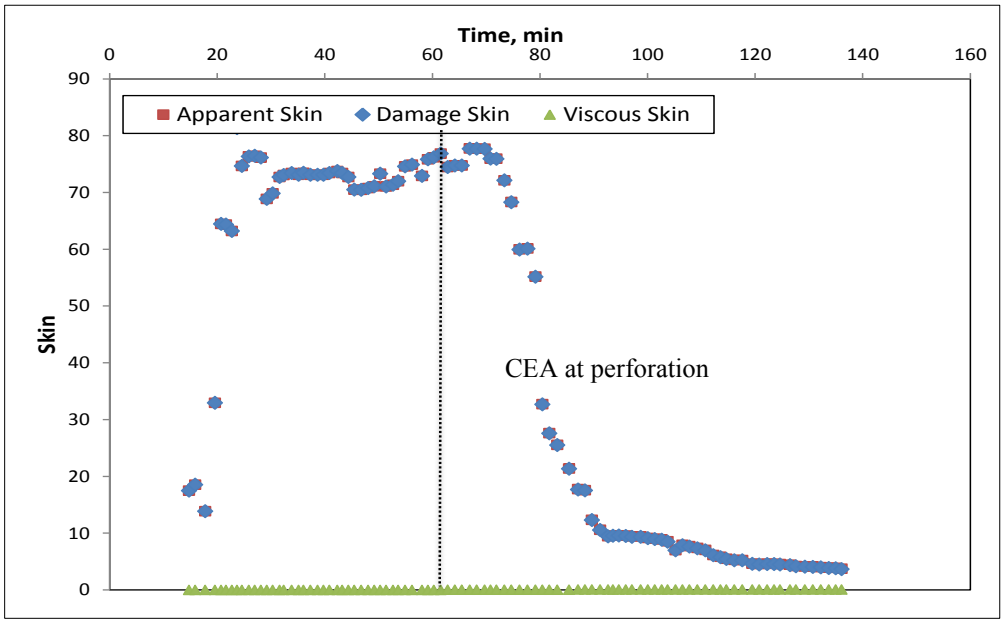

Fig. 4.31—Skin evolution for Case 2

4.4.2.3 History Matching Results

Fig. 4.32 shows the post-treatment production log of this horizontal well. This log shows that a large amount of the total production (about 70%) is from a small interval (zone 5) at about 9400 – 9410 ft with 4 other intervals contributing production. Based on the observation from the production log, the reservoir properties profile is presented in **Table 4.12**.

The objective of the history matching of treatment data is to estimate the permeability and damage of the 5 zones along the horizontal wellbore that give the best match with the actual pressure and skin assuming the perforated completion properties.

The Buijse and Glasbergen's wormhole model is used. Optimum pore volume to breakthrough and interstitial velocity are the input. We assume lower value of optimum pore volume to breakthrough and interstitial velocity in the higher permeability zones (zones 3, 4 and 5 in **Fig. 4.32**).

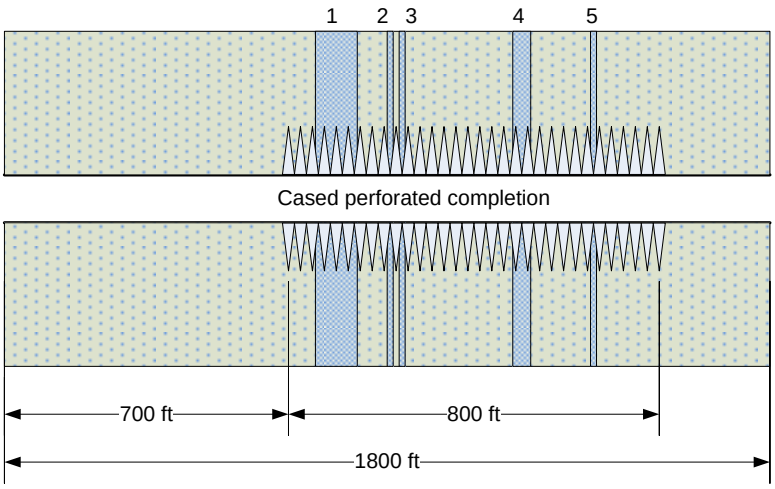

Fig. 4.32—Post-treatment production log for Case 2

From the post-treatment production log (**Fig. 4.32**), we observe that after the treatment the well had production from 5 zones (numbered from 1 to 5 in **Fig. 4.32**). This observation implies that those 5 zones were stimulated during the acid treatment. Among the treated zones, the production from zones 3, 4, 5 has contributed approximately 5, 20 and 70%, respectively, to the total well production. The production from the other two zones has accounted for the remaining 5% of the total production. The production log should give us the hint that zone 5 has the highest permeability; zones 3 and 4 have lower permeability; zones 1 and 2 has the lowest permeability but higher than the base permeability of the reservoir. Zone data for history matching are presented in **Table 4.15**. Skin evolution in **Fig. 4.31** shows that stimulation occurs once acid reaches the top of perforations and skin factor starts to decrease. In about 20 minutes, a rapid decrease of skin from about 70 to 10 is observed. This abrupt change in skin indicates the wormholes breaks through the damage in the higher permeability zones.

Table 4.15—Zone properties for Case 2

Zone data					
Zone	Permeability, md	k_d/k_H	Damage penetration, ft	$PV_{bt\text{-}opt}$	$V_{i\text{-}opt}$, cm/min
1	15	0.2	3	0.85	1.75
2	15	0.2	3	0.85	1.75
3	30	0.2	3	0.85	1.75
4	80	0.1	3	0.85	1.75
5	180	0.1	3	0.53	1.75

Fig. 4.33 and **Fig. 4.34** show the results of history matching of the pressure, rate and skin factor of the treatment. In **Fig. 4.33** the simulated pressure is in good agreement with the actual pressure although higher values are observed for the first about 30 minutes. This is possibly because of the severe, deep damage and transient effect. In **Fig. 4.34**, the simulated skin curve shows that in about the first 13 minutes the well has not yet been stimulated. Skin factor decreases rapidly from 70 to 3 in about 20 minutes which indicates that all the zones are being stimulated, from which significant effect has been contributed by high permeability zone.

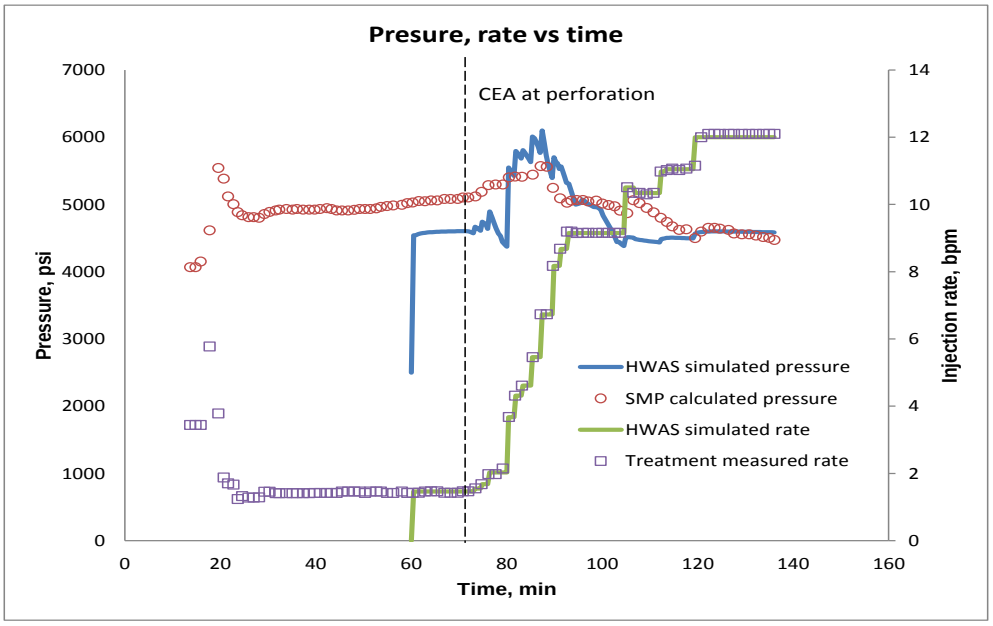

Fig. 4.33—Pressure and rate history matched results for Case 2

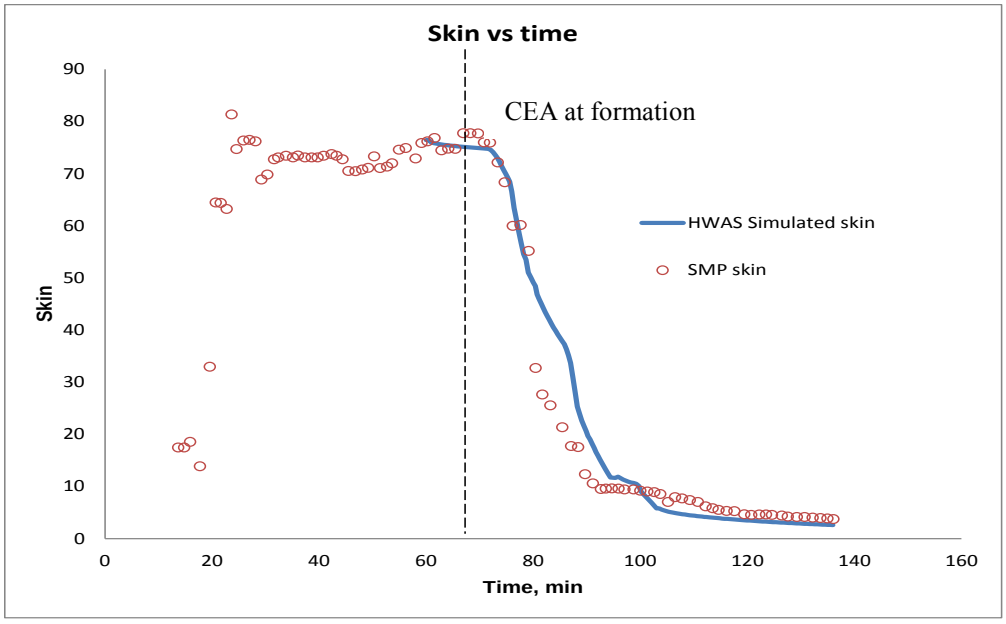

Fig. 4.34—Skin evolution history matched results for Case 2

Well pressure and stimulation response is dominant by higher permeability zones that appear to have deep damage. When wormholes begin to extend beyond the damage the skin factor drops rapidly. Other zones with lower permeability are also stimulated, but contribute considerable less to the total production.

5 CONCLUSIONS AND RECOMMENDATIONS

5.1 Conclusions

A horizontal well acidizing simulator was developed that implemented the coupled reservoir and wellbore flow to model the acid treatments in horizontal wells in carbonate formations. This numerical simulator is capable of modeling the openhole, cased and perforated, and slotted liners completions; production tubing and coiled tubing acid injections. It is also capable of modeling the injection of straight hydrochloric as well as viscosified acids and fluids.

The developed horizontal well acidizing simulator was validated against the field treatment data by history matching the bottomhole response and skin evolution of acid treatments. Post-treatment production logs helped in resolving the non-uniqueness of the history matching problem.

The numerical acidizing simulator was used to conduct parametric studies to investigate the effects of varying acid volume, wellbore length, acid concentration, and reservoir heterogeneity on the single optimum injection rate. The study showed that the optimum injection rate increases with increasing injected acid volume, wellbore length and acid concentration. However, the optimum injection rate per unit length does not change significantly with changing wellbore length for a given injected acid volume.

The equations to calculate the increasing injection rate series were derived for volumetric, Buijse and Glasbergen, and Furui et al.'s wormhole models. This increasing rate schedule is a series of injection rates designed to maintain the wormhole

propagation at the tip of the wormholes at its optimum conditions, therefore, to achieve the best stimulation effectiveness.

The comparison study of the increasing injection rate, the constant optimum injection rate, and the maximum allowable rate was conducted. The results showed that the acid treatment with increasing injection rate delivered longer wormhole penetration depth, and therefore, less negative skin factor for a given injected acid volume.

5.2 Recommendations

The developed numerical acidizing simulator is a portable and reliable tool and can be used for design, optimization and history matching of acid treatment data.

The increasing rate schedule treatment works well for a homogeneous formation, which is not normally the case for actual acid treatments. Therefore, to optimize an acid treatment design, different scenarios are recommended run to determine the single optimum injection rate for a given amount of acid to be injected. This single optimum injection rate acid treatment should then be compared to the increasing injection rate acid treatment to estimate the stimulation benefit. For highly heterogeneous reservoirs where the optimum injection rate does deliver a good acid coverage, alternative acid systems, for example the emulsified and gelled acid, should be investigated in addition to the treatment with straight hydrochloric acid at the optimum injection rate.

Post-treatment production logs are recommended to be performed for acid treatments to facilitate the stimulation evaluation

REFERENCES

Bazin, B. 2001. From Matrix Acidizing to Acid Fracturing: A Laboratory Evaluation of Acid/Rock Interactions. *SPE Prod & Oper* **16** (1): 22-29. 00066566. http://dx.doi.org/10.2118/66566-pa.

Buijse, M.A. 1997. Understanding Wormholing Mechanisms Can Improve Acid Treatments in Carbonate Formations. Paper 38166-MS presented at the SPE European Formation Damage Conference, The Hague, Netherlands.

Buijse, M.A. 2000. Understanding Wormholing Mechanisms Can Improve Acid Treatments in Carbonate Formations. *SPE Prod & Oper* **15** (3). 65068. http://dx.doi.org/10.2118/65068-pa.

Buijse, M.A. and Glasbergen, G. 2005. A Semi-Empirical Model to Calculate Wormhole Growth in Carbonate Acidizing. Paper 96892-MS presented at the SPE Annual Technical Conference and Exhibition, Dallas, Texas.

Chen, N.H. 1979. An Explicit Equation for Friction Factor in Pipe. *Industrial & Engineering Chemistry Fundamentals* **18** (3): 296-297. http://dx.doi.org/10.1021/i160071a019.

Daccord, G., Touboul, E., and Lenormand, R. 1989. Carbonate Acidizing: Toward a Quantitative Model of the Wormholing Phenomenon. *SPE Prod Eng* **4** (1): 63-68. 00016887. http://dx.doi.org/10.2118/16887-pa.

Eckerfield, L.D., Zhu, D., Hill, A.D. et al. 1998. Fluid Placement Model for Horizontal Well Stimulation. Paper 00048861 presented at the SPE International Oil and Gas Conference and Exhibition in China, Beijing, China. 2-6 November 1998. http://dx.doi.org/10.2118/48861-ms.

Economides, M.J., Hill, A.D., and Ehlig-Economides, C. 1994. *Petroleum Production Systems*. Englewood Cliffs, N.J.: PTR Prentice Hall.

Fredd, C.N. 2000. Dynamic Model of Wormhole Formation Demonstrates Conditions for Effective Skin Reduction During Carbonate Matrix Acidizing. Paper 59537-MS presented at the SPE Permian Basin Oil and Gas Recovery Conference, Midland, Texas.

Fredd, C.N. and Fogler, H.S. 1998a. Alternative Stimulation Fluids and Their Impact on Carbonate Acidizing. *SPE J.* **3** (1): 34-41. 00031074. http://dx.doi.org/10.2118/31074-pa.

Fredd, C.N. and Fogler, H.S. 1998b. Influence of Transport and Reaction on Wormhole Formation in Porous Media. *AIChE Journal* **44** (9): 1933-1949. http://dx.doi.org/10.1002/aic.690440902.

Fredd, C.N., Tjia, R., and Fogler, H.S. 1997. The Existence of an Optimum Damkohler Number for Matrix Stimulation of Carbonate Formations. Paper 00038167 presented at the SPE European Formation Damage Conference, The Hague, Netherlands. 2-3 June 1997. http://dx.doi.org/10.2118/38167-ms.

Frick, T.P., Mostofizadeh, B., and Economides, M.J. 1994. Analysis of Radial Core Experiments for Hydrochloric Acid Interaction with Limestones. Paper 00027402 presented at the SPE Formation Damage Control Symposium, Lafayette, Louisiana. 7-10 February 1994. http://dx.doi.org/10.2118/27402-ms.

Furui, K., Burton, R.C., Burkhead, D.W. et al. 2010. A Comprehensive Model of High-Rate Matrix Acid Stimulation for Long Horizontal Wells in Carbonate Reservoirs. Paper 134265-MS presented at the SPE Annual Technical Conference and Exhibition, Florence, Italy.

Furui, K., Zhu, D., and Hill, A.D. 2003. A Rigorous Formation Damage Skin Factor and Reservoir Inflow Model for a Horizontal Well (Includes Associated Papers 88817 and 88818). *SPE Prod & Oper* (08). 84964. http://dx.doi.org/10.2118/84964-pa.

Gdanski, R. 1999. A Fundamentally New Model of Acid Wormholing in Carbonates. Paper 54719-MS presented at the SPE European Formation Damage Conference, The Hague, Netherlands.

Glasbergen, G., Kalia, N., and Talbot, M.S. 2009. The Optimum Injection Rate for Wormhole Propagation: Myth or Reality? Paper 121464-MS presented at the 8th European Formation Damage Conference, Scheveningen, The Netherlands.

Hill, A.D. and Rossen, W.R. 1994. Fluid Placement and Diversion in Matrix Acidizing. Paper 27982-MS presented at the University of Tulsa Centennial Petroleum Engineering Symposium, Tulsa, Oklahoma.

Hill, A.D. and Zhu, D. 1996. Real-Time Monitoring of Matrix Acidizing Including the Effects of Diverting Agents. *SPE Prod & Oper* **11** (2). 28548. http://dx.doi.org/10.2118/28548-pa.

Hoefner, M.L. and Fogler, H.S. 1987. Role of Acid Diffusion in Matrix Acidizing of Carbonates. *SPE J. of Pet Tech* **39** (2): 203-208. 00013564. http://dx.doi.org/10.2118/13564-pa.

Hoefner, M.L. and Fogler, H.S. 1988. Pore Evolution and Channel Formation During Flow and Reaction in Porous Media. *AIChE Journal* **34** (1): 45-54. http://dx.doi.org/10.1002/aic.690340107.

Hoefner, M.L. and Fogler, H.S. 1989. Fluid-Velocity and Reaction-Rate Effects During Carbonate Acidizing: Application of Network Model. *SPE Prod Eng* **4** (1): 56-62. 00015573. http://dx.doi.org/10.2118/15573-pa.

Huang, T., Hill, A.D., and Schechter, R.S. 2000. Reaction Rate and Fluid Loss: The Keys to Wormhole Initiation and Propagation in Carbonate Acidizing. *SPE J.* **5** (3). 65400. http://dx.doi.org/10.2118/65400-pa.

Huang, T., Zhu, D., and Hill, A.D. 1999. Prediction of Wormhole Population Density in Carbonate Matrix Acidizing. Paper 54723-MS presented at the SPE European Formation Damage Conference, The Hague, Netherlands.

Hung, K.M., Hill, A.D., and Sepehrnoori, K. 1989. A Mechanistic Model of Wormhole Growth in Carbonate Matrix Acidizing and Acid Fracturing. *SPE J. of Pet Tech* **41** (1). 16886. http://dx.doi.org/10.2118/16886-pa.

Lee, J., Rollins, J.B., Spivey, J.P. et al. 2003. *Pressure Transient Testing*. Richardson, Tex.: Society of Petroleum Engineers.

McDuff, D., Jackson, S., Shuchart, C. et al. 2010. Understanding Wormholes in Carbonates: Unprecedented Experimental Scale and 3d Visualization. *SPE J. of Pet Tech* **62** (10). 129329-MS.

Mishra, V., Zhu, D., Hill, A.D. et al. 2007. An Acid Placement Model for Long Horizontal Wells in Carbonate Reservoirs. Paper 107780-MS presented at the European Formation Damage Conference, Scheveningen, The Netherlands.

Mostofizadeh, B. and Economides, M.J. 1994. Optimum Injection Rate from Radial Acidizing Experiments. Paper 00028547 presented at the SPE Annual Technical Conference and Exhibition, New Orleans, Louisiana. 25-28 September 1994. http://dx.doi.org/10.2118/28547-ms.

Nozaki, M. and Hill, A.D. 2009. A Placement Model for Matrix Acidizing of Vertically Extensive, Heterogeneous Gas Reservoirs. Paper 124881-MS presented at the SPE Annual Technical Conference and Exhibition, New Orleans, Louisiana.

Wang, Y., Hill, A.D., and Schechter, R.S. 1993. The Optimum Injection Rate for Matrix Acidizing of Carbonate Formations. Paper 26578 presented at the SPE Annual Technical Conference and Exhibition, Houston, Texas. 01/01/1993.

Williams, B.B., Gidley, J.L., and Schechter, R.S. 1979. *Acidizing Fundamentals*: Society of Petroleum Engineers.

APPENDIX A

MATRIX ACIDIZING SIMULATOR

A1. Equations

From **Section 2.1**, in oil field units the wellbore pressure drop equation is written in differential form as,

$$\frac{\partial p_w}{\partial x} = -1.525 f_f \frac{\rho q_w^{\ 2}}{d^5} \text{sgn}(q_w) \tag{A.1}$$

The above equation is non-linear. To linearize the equation, q_w can be separated as,

$$\frac{\partial P_w}{\partial x} = \left(-1.525 f_f \frac{\rho q_w}{d^5} \text{sgn}(q_w) \right) q_w \tag{A.2}$$

It can also be written as,

$$\frac{\partial P_w}{\partial x} = -\xi q_w \tag{A.3}$$

where,

$$\xi = 1.525 f_f \frac{\rho q_w}{d^5} \text{sgn}(q_w) \tag{A.4}$$

Eq. A.4 implies that the coefficient ξ is dependent on the f_f and q_w. In addition, f_f also depends on q_w as the friction factor is flow regime dependent. In our simulator, **Eq. A.4** can be used as if the value of coefficient ξ is calculated at the previous time step, the nature of this equation becomes linear and it can be solved with high accuracy.

This equation will be coupled with the reservoir flow **Eq. A.5** while solving for the wellbore pressure and flow rate during the simulation of the matrix acidizing process.

$$\frac{\partial q_w}{\partial x} = -q_{sR} \tag{A.5}$$

$$q_{sR}^n = -a_{Jx}\left(p_i - p_w^n\right) - b_{Jx} \tag{A.6}$$

and,

$$a_{Jx} = \frac{4.91816\times10^{-6}k}{\mu[p_D(t_D^n - t_D^{n-1}) + s^n]} \tag{A.7}$$

$$b_{Jx} = \frac{\sum_{j=1}^{n-1}\Delta q_{sR}^j p_D(t_D^n - t_D^{j-1}) - q_{sR}^{n-1} p_D(t_D^n - t_D^{n-1})}{p_D(t_D^n - t_D^{n-1}) + s^n} \tag{A.8}$$

where, k is in md, μ - cP, and q_{sR} - bpm/ft

A2. Discretization and Solution

From Eqs. A.1 and A.5, the following systems of ODEs are to be solved:

$$\begin{cases} \dfrac{\partial q_w}{\partial x} = -q_{sR} \\ \dfrac{\partial p_w}{\partial x} = -\xi q_w \end{cases} \tag{A.9}$$

The system **Eq. A.9** can be re-written as,

$$\begin{cases} \dfrac{\partial q_w(x,t)}{\partial x} = a_{Jx}[p_i - p_w(x,t)] + b_{Jx} \\ \dfrac{\partial p_w(x,t)}{\partial x} = -\xi q_w(x,t) \end{cases} \tag{A.10}$$

where,

$$a_{Jx} = \frac{4.91816\times10^{-6}k}{\mu[p_D(t_D^n - t_D^{n-1}) + s^n]} \tag{A.11}$$

$$b_{Jx} = \frac{\sum_{j=1}^{n-1}(q_{sR}^{j} - q_{sR}^{j-1})p_D(t_D^n - t_D^{j-1}) - q_{sR}^{n-1}p_D(t_D^n - t_D^{n-1})}{p_D(t_D^n - t_D^{n-1}) + s^n} \tag{A.12}$$

Initial and boundary conditions are required to solve the above systems of ODEs:

$$q_w(x,0) = 0\,,\ p_w(x,0) = p_i \tag{A.14}$$

$$q_w(0,t) = 0\,,\ q_w(x \geq L,t) = 0 \tag{A.15}$$

$$Q_w(x_{tubing},t) \text{ or } p_w(x_{tubing},t) \text{ is to be specified} \tag{A.16}$$

where L is the length of the horizontal wellbore, and Q_w is the total injected acid volumetric flow rate. In a discretized form, **Eq. A.10** is expressed as

$$\begin{cases} q_{w,i+1/2} - q_{w,i-1/2} = \Delta x_i[a_{Jx,i}(p_i - p_{w,i}) + b_{Jx,i}] \\ p_{w,i+1} - p_{w,i} = -\dfrac{\Delta x_i + \Delta x_{i+1}}{2}\xi_i q_{w,i+1/2} \end{cases} \tag{A.17}$$

where i is defined in **Fig. A.1**. p_i represents the initial reservoir pressure.

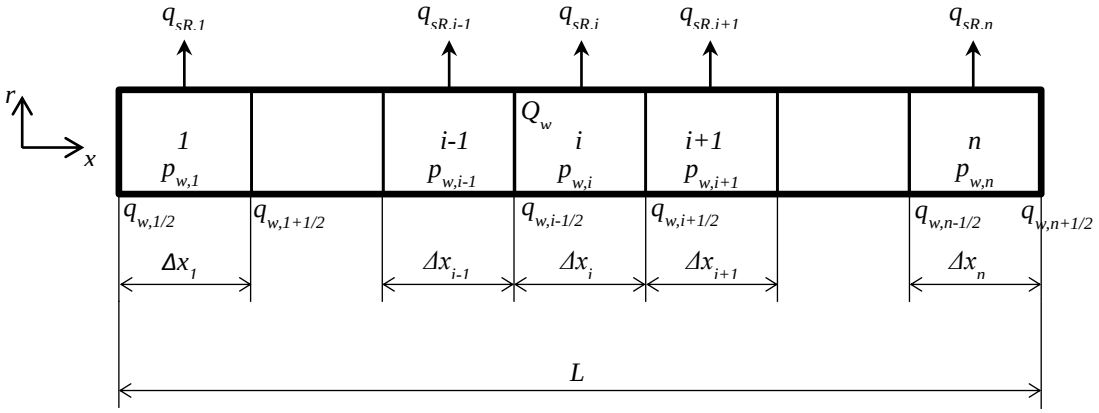

Fig. A.1—A schematic of segmented wellbore

Assuming the tubing tail is place at i-th grid block we have,

$$q_{w,i+1/2} - q_{w,i-1/2} = \Delta x_i[a_{Jx,i}(p_i - p_{w,i}) + b_{Jx,i}] + Q_w \text{ for i = 1, 2, …, n .....}$$

$$p_{w,i+1} - p_{w,i} = -\frac{\Delta x_i + \Delta x_{i+1}}{2} \xi_i q_{w,i+1/2} \text{ for i = 1, 2, …, n-1} \tag{A.18}$$

with,

$$A_i = \Delta x_i a_{Jx,i} \tag{A.19}$$

$$B_i = \Delta x_i b_{Jx,i} \tag{A.20}$$

$$C_i = \frac{1}{2}(\Delta x_i + \Delta x_{i+1})\xi_i \tag{A.21}$$

When the total injection rate is specified ($Q_w = \hat{Q}_w(t)$) at i-th grid block, the system of equations **Eq. A.18** can be rearranged to have the form

$$\begin{cases} -q_{w,1-1/2} + A_1 p_{w,1} + q_{w,1+1/2} = A_1 p_i + B_1 \\ -p_{w,1} - C_1 q_{w,1+1/2} + p_{w,2} = 0 \\ \vdots \\ -q_{w,i-1/2} + A_i p_{w,i} + q_{w,i+1/2} = A_i p_i + B_i + \hat{Q}_w \\ -p_{w,i} - C_i q_{w,i+1/2} + p_{w,i+1} = 0 \\ \vdots \\ -q_{w,n-1/2} + A_n (p_i - p_{w,n}) + q_{w,n+1/2} = A_n (p_i - p_{w,n}) + B_n \\ -p_{w,n-1} - C_{n-1} q_{w,n-1/2} + p_{w,n} = 0 \end{cases} \tag{A.22}$$

It is noticed that $q_{w,n+1/2}$ (x = L) and $q_{w,1-1/2}$ (x = 0) from the boundary conditions and $C_i = C_i(q)$ is a function of the wellbore flow rate. We obtain the system of equations in matrix form.

$$\begin{pmatrix} A_1 & 1 & 0 & \cdots & \cdots & \cdots & \cdots & \cdots & \cdots & 0 \\ -1 & C_1(q) & 1 & 0 & \cdots & \cdots & \cdots & \cdots & \cdots & 0 \\ 0 & -1 & A_2 & 1 & 0 & \cdots & \cdots & \cdots & \cdots & 0 \\ \vdots & & \ddots & \ddots & \ddots & & & & & \vdots \\ 0 & \cdots & \cdots & -1 & A_i & 1 & \cdots & \cdots & \cdots & 0 \\ 0 & \cdots & \cdots & \cdots & -1 & C_i(q) & 1 & \cdots & \cdots & 0 \\ \vdots & & & & & \ddots & \ddots & \ddots & & \vdots \\ 0 & \cdots & \cdots & \cdots & \cdots & 0 & -1 & A_{n-1} & 1 & 0 \\ 0 & \cdots & \cdots & \cdots & \cdots & \cdots & 0 & -1 & C_{n-1}(q) & 1 \\ 0 & \cdots & \cdots & \cdots & \cdots & \cdots & \cdots & 0 & -1 & A_n \end{pmatrix} \begin{pmatrix} p_{w,1} \\ q_{w,1+1/2} \\ p_{w,2} \\ \vdots \\ p_{w,i} \\ q_{w,i+1/2} \\ \vdots \\ p_{w,n-1} \\ q_{w,n-1/2} \\ p_{w,n} \end{pmatrix} = \begin{pmatrix} A_1 p_i + B_1 \\ 0 \\ A_{J,2} p_{i,2} + B_{J,2} \\ \vdots \\ A_i p_i + B_i + Q_w \\ 0 \\ \vdots \\ A_{n-1} p_{i,n-1} + B_{n-1} \\ 0 \\ A_n p_i + B_n \end{pmatrix} \quad \text{(A.23)}$$

APPENDIX B

FIELD CASES

B1. Well 1

B1.1 Treatment Description

This well is a horizontal well with a cased and perforated completion, as seen below in **Fig. B1.** The actual acidizing treatment design comprised of 15% HCl treatment followed by two stages of 2% viscoelastic surfactant (VES), and 22% carbonate emulsion acid (CEA) each.

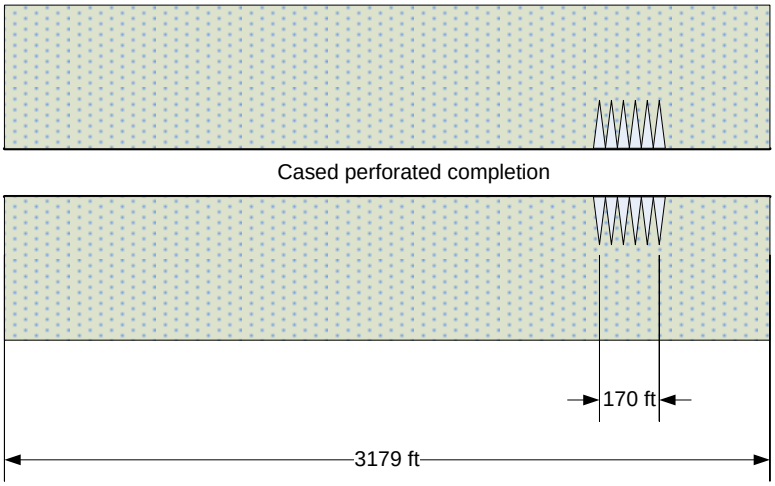

Fig. B1—Well diagram for Well 1

The data for the reservoir, the wellbore, and the acid injection is shown in Table B1 and Table B2**.**

Table B1—Input data for Well 1

Reservoir Data	
Initial reservoir pressure, psi	3500
Porosity	0.22
Total compressibility, 1/psi	3.50E-06
Formation thickness, ft	50
Reservoir fluid viscosity, cp	0.51
Reservoir temperature, F	150
Permeability, md	1
Well Data	
Casing OD, in	9.625
Casing ID, in	8.681
Liner OD, in	7.000
Liner ID, in	6.184
Wellbore radius, in	3.500
Tubing diameter, in	2
Pipe relative roughness	0.0001
Horizontal section length, ft	3180
Wellbore fluid density, lbm/ft3	59.84
Wellbore fluid viscosity, cp	0.51

The treatment schedule of this well was conducted with multiple injection fluids: regular hydrochloric acid, viscoelastic surfactant and carbonate emulsion acids. The viscoelastic surfactant was used for diversion purpose. In addition, viscoelastic surfactant and the carbonate emulsion acid stages were alternated by a water stage because of their chemical compatibility. The viscosity of viscoelastic surfactant and carbonate emulsion acids had the value of 3 cp as used in the skin monitoring analysis of the treatment data.

Table B2—Injection schedule for Well 1

Stage	Fluid Name	Volume Used, gal	Density, lb/ft3	Viscosity, cp	Friction Reducer
1	HCl	4416	65.82	1	0.1
2	VES	1598	63.58	1	0.1
3	Water	127	63.58	1	0.1
4	CEA	3244	63.58	3	0.1
5	Water	126	62.83	1	0.1
6	VES	810	63.58	1	0.1
7	Water	127	62.98	1	0.1
8	CEA	5198	63.58	3	0.1
9	Water	4201	62.83	1	0.1

B1.2 Skin Monitoring Results

Fig. B2 plots the measured injection rate, and the measured surface pressure recorded during the acidizing treatment. The bottomhole pressure was calculated from the surface pressure. The treatment was conducted for about 200 minutes with 9 stages. The maximum bottomhole hole injection pressure was about 7000 psi.

From the calculated bottomhole pressure and measured injection rate, the skin was calculated at each time step. The numbered flags indicate the time when the corresponding stage fluids hit the formation. The skin evolution during the acid job is shown in **Fig. B3.**

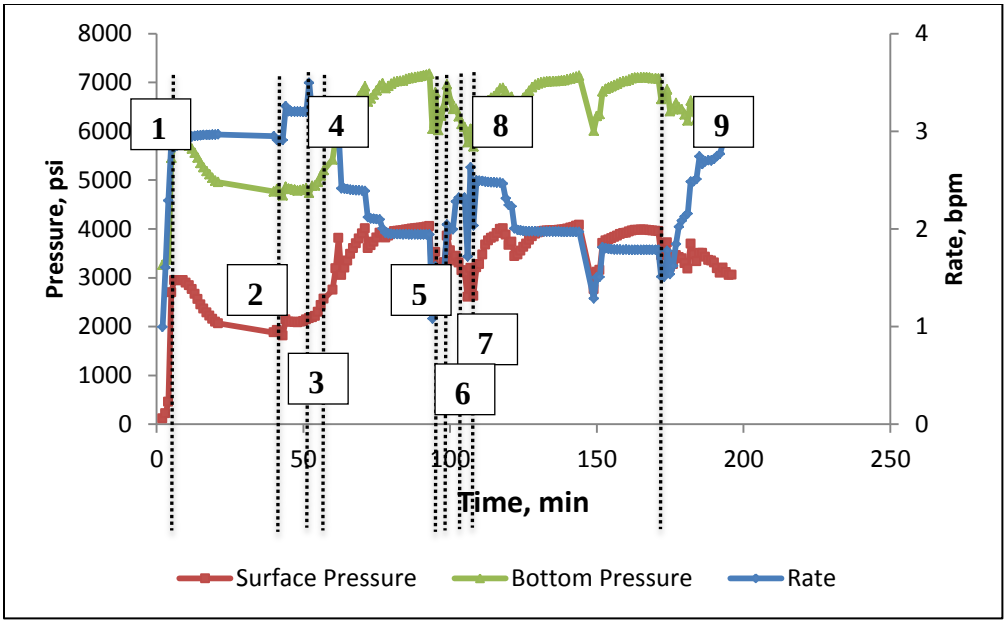

Fig. B2—Treatment data for Well 1

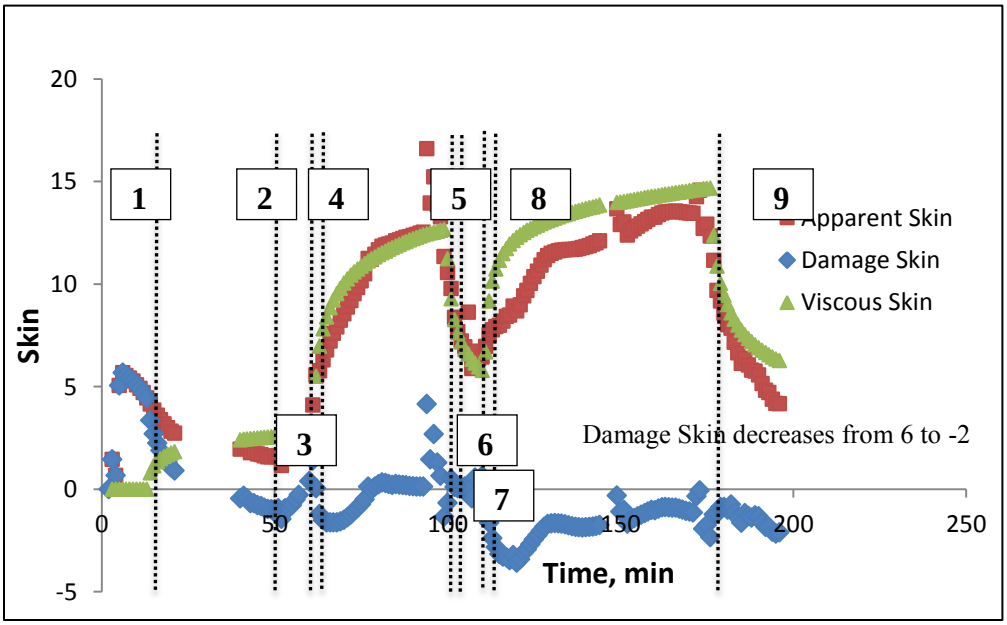

Fig. B3—Skin evolution for Well 1

The apparent skin factor had the maximum value of about 15 because of the viscous effect. The final stimulation skin factor came down to about -2 at the end of the acid treatment.

B1.3 History Matching Results

The input for reservoir and wellbore data are presented in **Table B1** and **Table B2**. The damage penetration is assumed to be 2 ft and permeability reduction 10%. This well has about 170 ft perforated interval, of which the last 30 ft has average permeability 100 mdmd) compared to base permeability of 7 md (obtained from the well formation top). Thus we can assume that the high permeability zone has lower pore volume to breakthrough, consequently, more wormholing efficiency.

Fig. B4 and **Fig. B5** show that the bottmhole pressure and skin factor predicted by the acidizing simulator have similar trend compared to the values estimated by the skin monitoring program. In the history matching for this treatment, the viscous diversion model is used. The viscosity of CEA and VES has to have very high value, in the range of 250 to 300 cp, to match the increasing skin evolution trend. The high viscosity is seen, as the matched model shows, indicates that there exists the competing trend of the wormholing effect and the viscous effect. Once dominant wormholes are initiated and extended beyond the damage zone, they will have significant contribution to the stimulation effect. To overcome this wormhole stimulation to block the high permeability zone, higher viscosity of diverting fluid should be used.

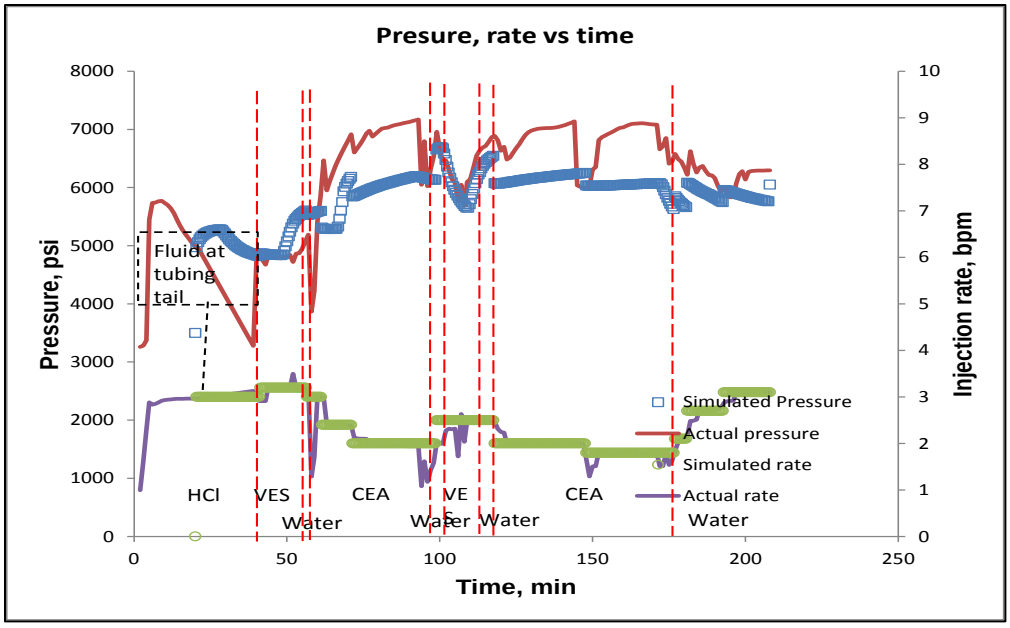

Fig. B4—Pressure and rate history matched results for Well 1

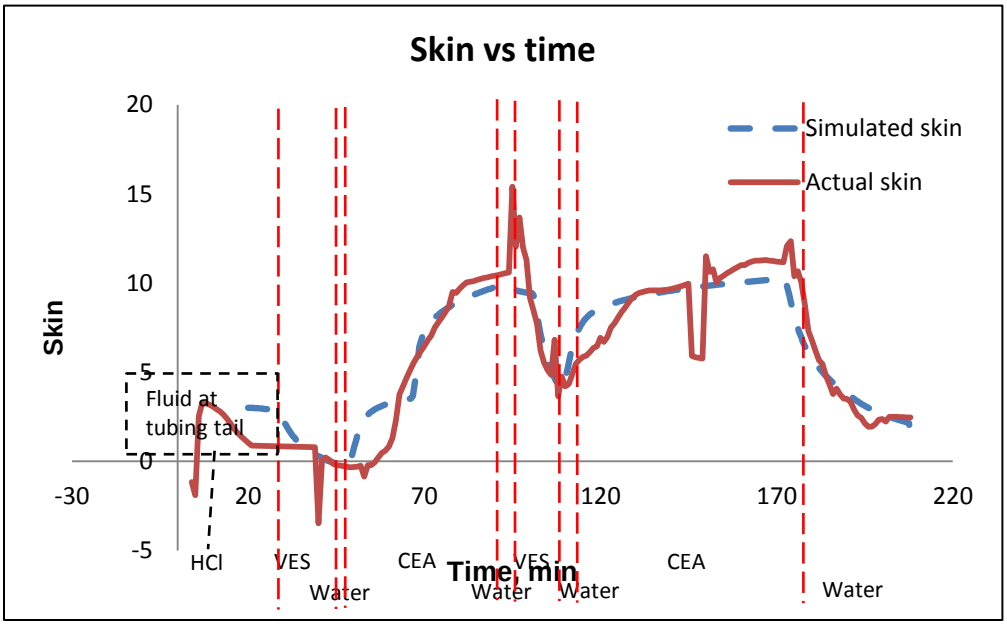

Fig. B5—Skin evolution history matched result for Well 1

Fig. B6 shows the final skin factor of the treatment without viscous effect. The skin at the end of treatment has the value of -2.8. This value of skin factor has confirmed the increase in production rate after the treatment.

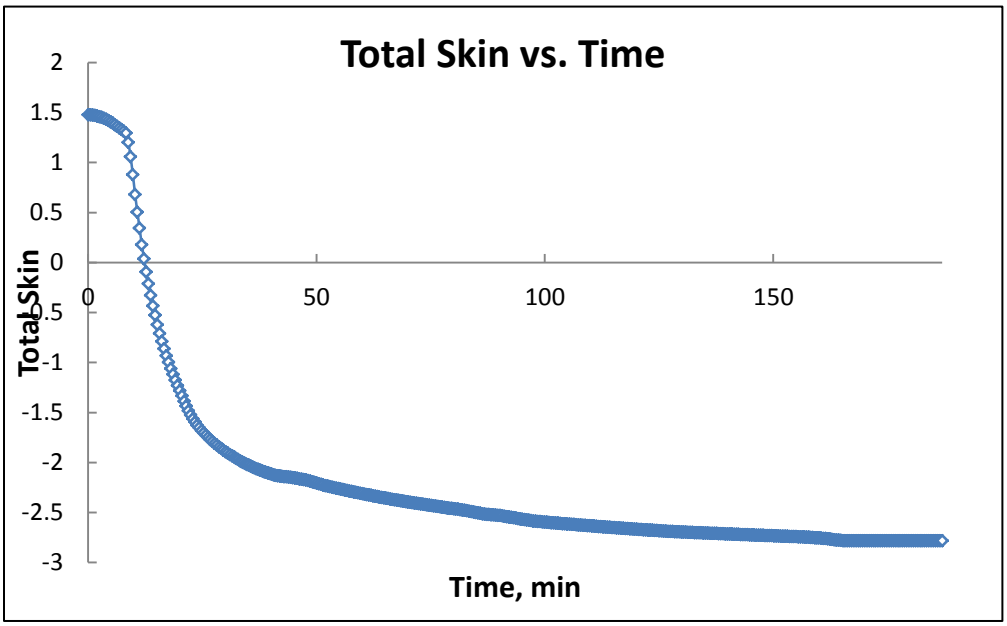

Fig. B6—Final skin for Well 1 (without viscous effect)

B2. Well 2

B2.1 Treatment Description

This well is a horizontal well with an open-hole lateral, as seen in the well diagram below. The actual acidizing treatment design comprised of treating the target interval with 22% carbonate emulsion acid (CEA) using coil-tubing.

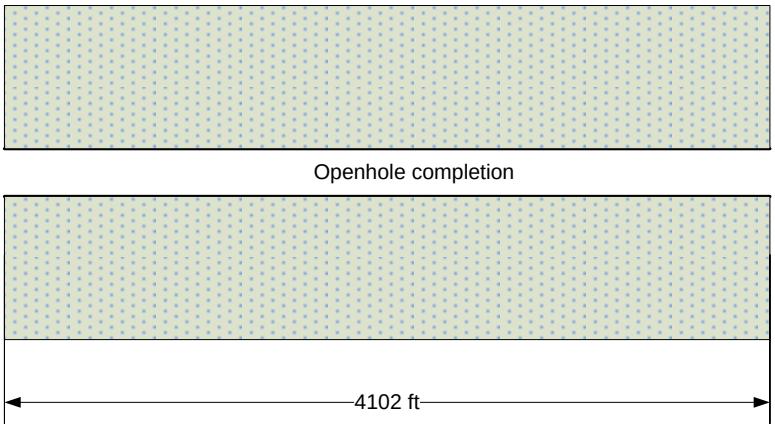

Fig. B7—Well diagram for Well 2.

The data for the reservoir, the wellbore, and the acid injection is shown in the **Table B3** and **Table B4**.

Table B3—Input data for Well 2

Reservoir data	
Initial reservoir pressure, psi	2500
Porosity	0.21
Total compressibility, 1/psi	3.50E-06
Formation thickness, ft	40
Reservoir fluid viscosity, cp	0.51
Reservoir temperature, F	150
Permeability, md	10
Well ata	
Wellbore radius, in	4.25
Tubing diameter, in	1.68
Pipe relative roughness	0.0001
Horizontal section length, ft	4102
Wellbore fluid density, lbm/ft3	64.3
Wellbore fluid viscosity, cp	0.51

Table B4—Injection schedule for Well 2

Fluid Name	Volume Used, gal	Density, lb/ft3	Viscosity, cp	Friction Reducer
Flush	414	63.3	0.51	1
CEA	20510	64.3	0.51	1
Flush	2964	62.3	0.51	1

B2.2 Skin Monitoring Results

The surface pressure and injection rate data was measure on-site during the acid job. **Fig. B8** plots the measured injection rate, and the measured surface pressure recorded during the acidizing treatment.

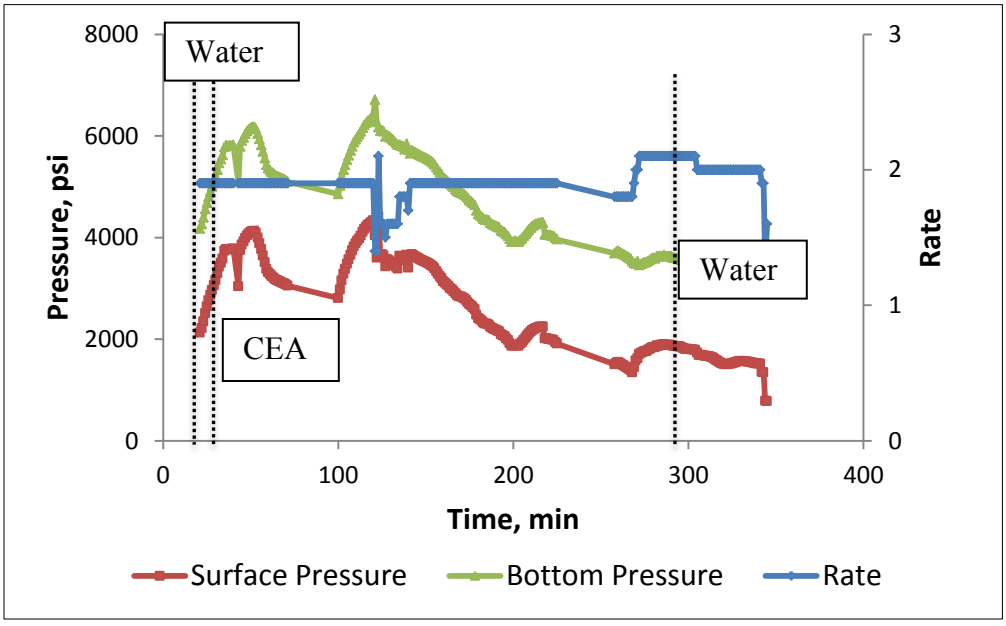

Fig. B8—Treatment data for Well 2

In **Fig. B8**, the bottomhole pressure was calculated from the surface pressure. From the calculated bottomhole pressure and measured injection rate, the skin was calculated at each time step. The skin evolution during the acid job is shown in the **Fig. B9**.

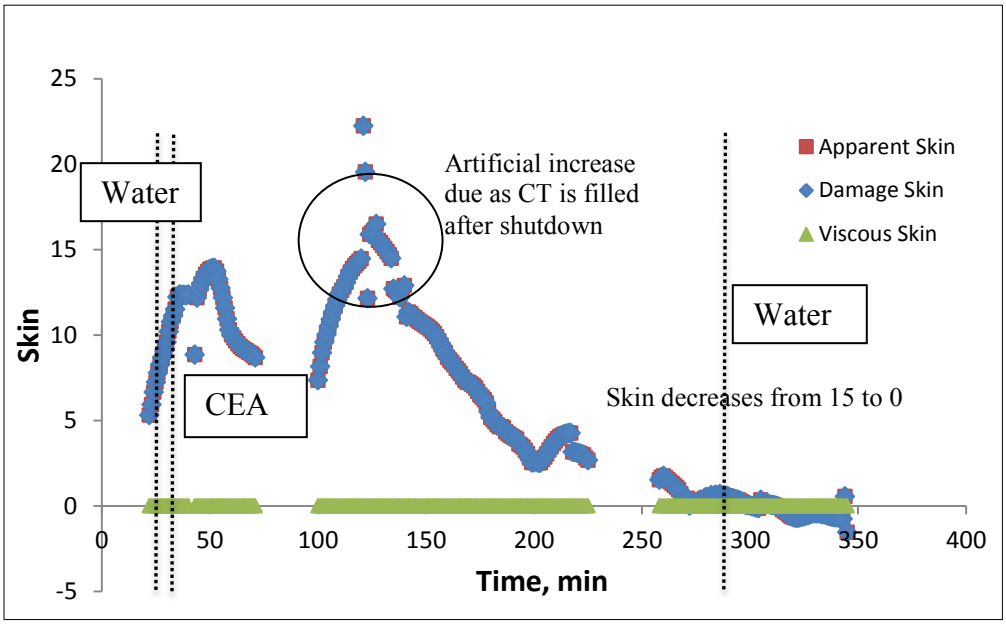

Fig. B9—Skin response for Well 2

B2.3 History Matching Results

In **Fig. B10**, the skin begins to decrease when the acid front enters the formation, and the skin value decreases from 15 to 0 by the end of acid injection. It is noticed that the volume of acid injected was sufficient as the skin continues to decrease until the end of the injection. Also, the skin trend flattens during the water injection.

The history matched results showed a close trend of pressure response and skin evolution from the time 124 minutes.

Fig. B10 and **Fig. B11** show the history matched results of this CEA treatment. The history matched model predicted similar trend with the skin analysis results. This well is completed in dolomite/dolomite-limestone formation; the wormhole propagation is not efficient compared to the limestone wells. In addition, the production after treatment showed that the flow rate decreased from 1400 barrels/day to 400 barrels/day within 12 hours of production. The formation damage reported was due to the presence of bitumen (tar) in the formation. Although, the treatment was initially successful in increasing production, the bitumen present in the reservoir returned to lower the productivity of this well.

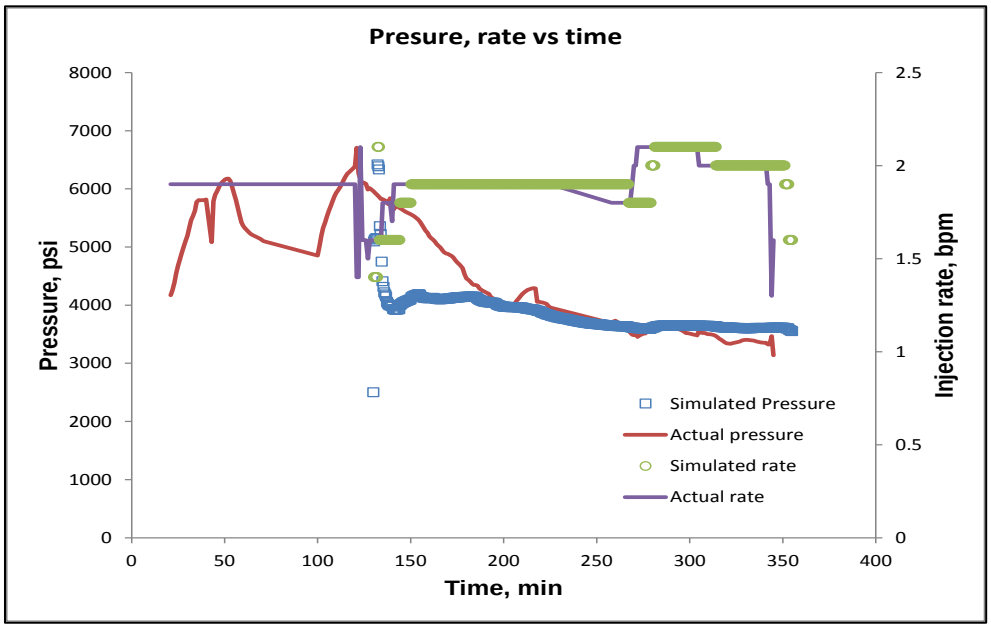

Fig. B10—Pressure and rate history matched results for Well 2

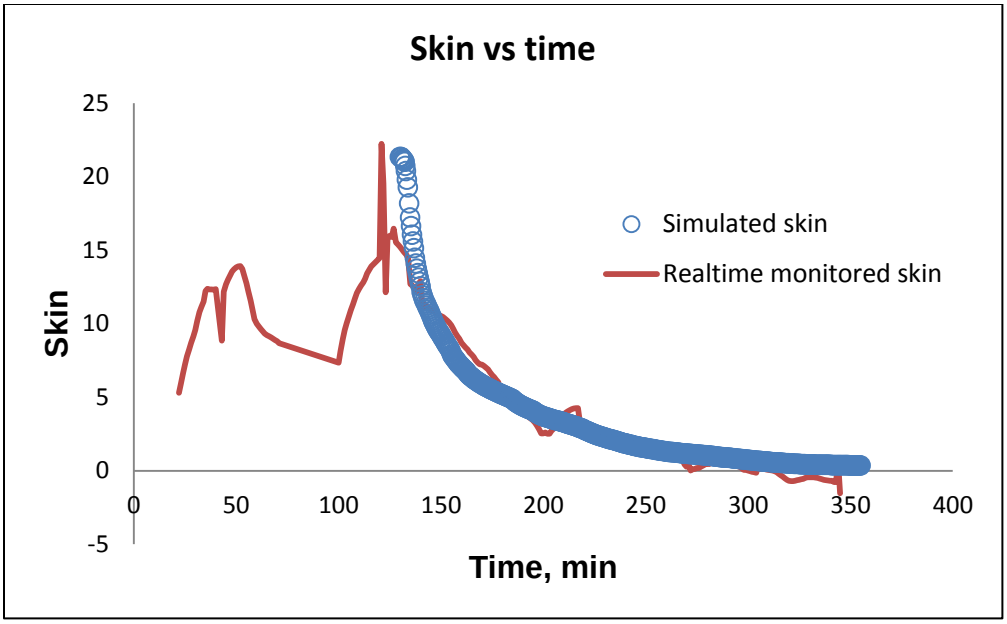

Fig. B11—Skin evolution history matched results for Well 2

B3. Well 3

B3.1 Treatment Description

This well is a horizontal well with an open-hole lateral, as seen in the well diagram below. The actual acidizing treatment design comprised of treating the target interval with 15% hydrochloric acid (HCl) using coil-tubing.

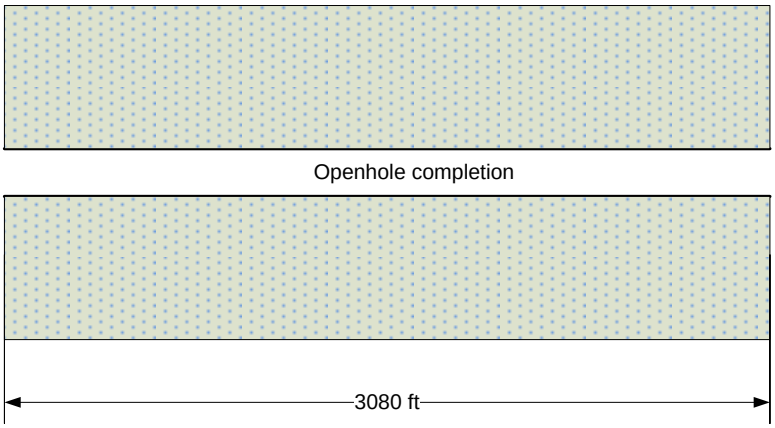

Fig. B12—Well diagram for Well 3

The data for the reservoir, the wellbore, and the acid injection is shown in **Table B.5** and **Table B.6**.

Table B.5—Input data for Well 3

Reservoir data	
Initial reservoir pressure, psi	2500
Porosity	0.21
Total compressibility, 1/psi	3.50E-06
Formation thickness, ft	40
Reservoir fluid viscosity, cp	0.51
Reservoir temperature, F	150
Permeability, md	1
Well data	
Wellbore radius, in	4.25
Tubing diameter, in	1.68
Pipe relative roughness	0.0001
Horizontal section length, ft	3080
Wellbore fluid density, lbm/ft3	64.3
Wellbore fluid viscosity, cp	0.51

Table B.6—Injection schedule for Well 3

Fluid Name	Volume Used, gal	Density, lb/ft3	Viscosity, cp	Friction Reducer
Flush	414	63.3	0.51	1
CEA	20510	64.3	0.51	1
Flush	2964	62.3	0.51	1

B3.2 Skin Monitoring Results

The surface pressure and injection rate data was measure on-site during the acid job. **Fig. B13** below plots the measured injection rate, and the measured surface pressure recorded during the acidizing treatment.

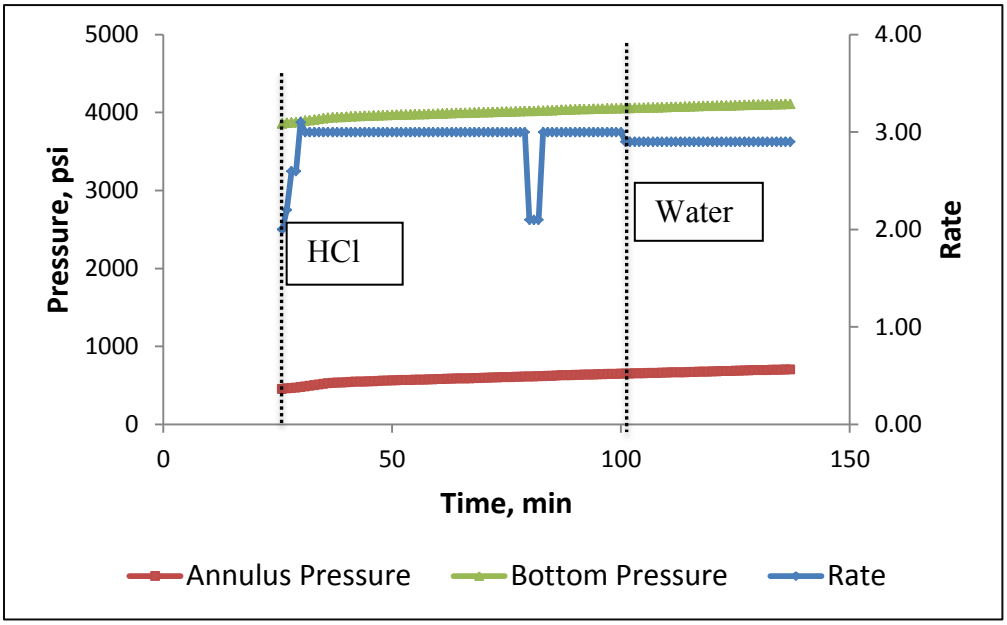

Fig. B13—Treatment data for Well 3

In **Fig. B13**, the bottomhole pressure was calculated from the annulus pressure. From the calculated bottomhole pressure and measured injection rate, the skin was calculated at each time step. The skin evolution during the acid job is shown in the figure below.

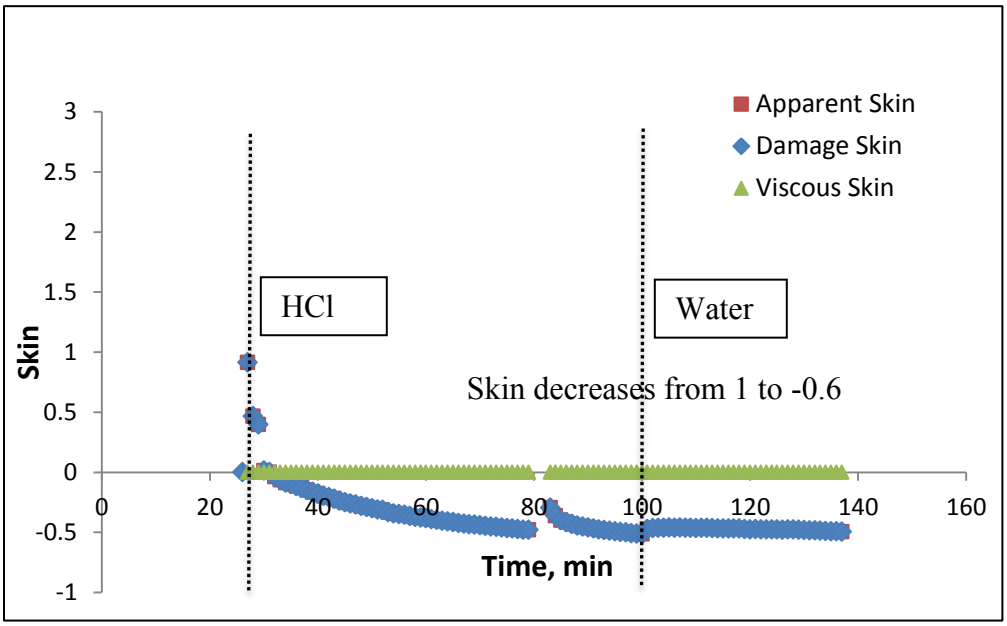

Fig. B14—Skin response for well 3

B3.3 History Matching Results

The damage penetration is assumed to be 1 ft and permeability reduction 5%. According to the production log, there are seven producing zones and have different inflow rates. Thus we assume permeability profile with higher permeability for higher rate zones. The pore volume to breakthrough is assumed 1.5 because the formation rock is dolomite/dolomite limestone.

The production log (**Fig. B15**) helps guest initial reservoir properties along the wellbore. There are only seven zones with production after the treatment. Zone 5 alone has 60 % of the total production of the well.

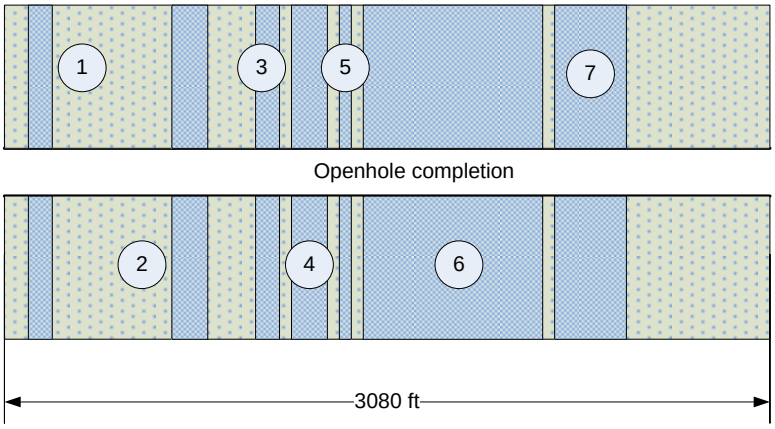

Fig. B15—Production log for Well 3

The properties of the seven producing zones (**Fig. B15)** are presented in **Table B7.**

Table B7—Zone properties for Well 3

Zone	Length, ft	Horizontal permeability, md	Impairment ratio	Damage penetration, ft	PV_{bt-opt}	V_{i-opt}, cm/min
1	100	1	0.95	0.5	1	2
2	150	0.5	0.95	0.5	1	2
3	100	1	0.95	0.5	1	2
4	150	0.1	0.95	0.5	0.85	2
5	50	0.5	0.95	0.5	1	2
6	750	3	0.8	1	1	1.75
7	300	1	0.95	0.5	1	2

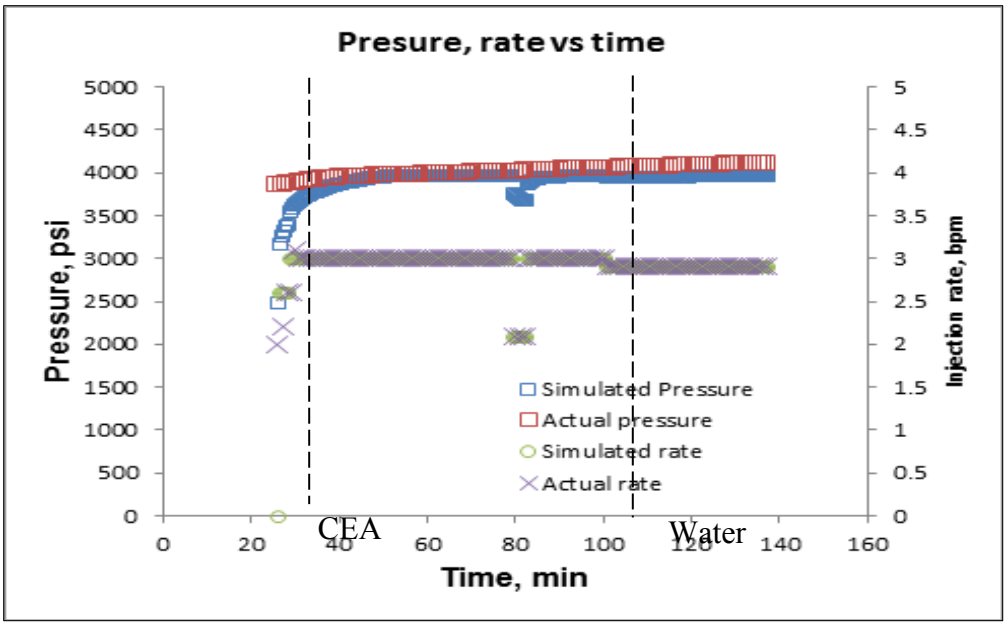

Fig. B16—Pressure and rate history matched results for Well 3

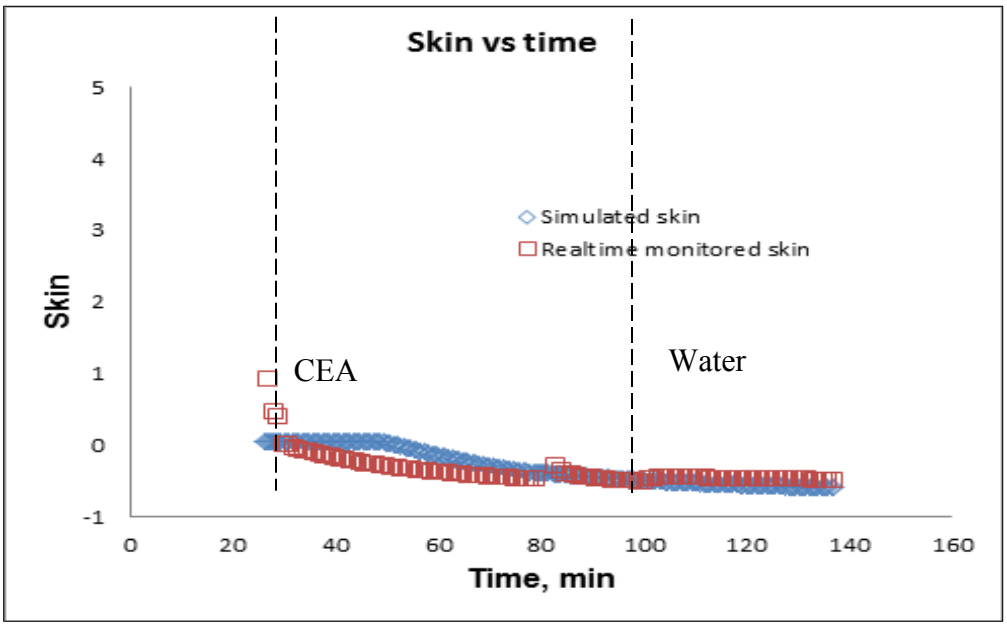

Fig. B17—Skin evolution history matched results for Well 3

Fig. B16 shows the actual and simulated injection rate and bottomhole pressure matched results of the treatment. In **Fig. B17**, the skin begins to decrease when the acid front enters the formation, and the skin value decreases from 1 to -0.6 by the end of acid injection. It is noticed that the designed acid coverage was not sufficient as the skin begins to flatten towards the end of acid injection.

The skin trend was validated using the production test from before and after the stimulation process. In this case, the production rate of liquids from this well after stimulation increased from 2653 barrels/day to 2757 barrels/day. Therefore, the production test confirms the decreasing skin trend.

B4. Well 4

B4.1 Treatment Description

This well is a horizontal well with a cased and perforated completion, as seen in the well diagram below. The actual acidizing treatment design was divided into two parts: 1) injection of 15% hydrochloric acid (HCl); and 2) injection of 22% carbonate emulsion acid (CEA). Each of the two parts of the treatments comprised of the acid stage followed by the fresh water displacement stage.

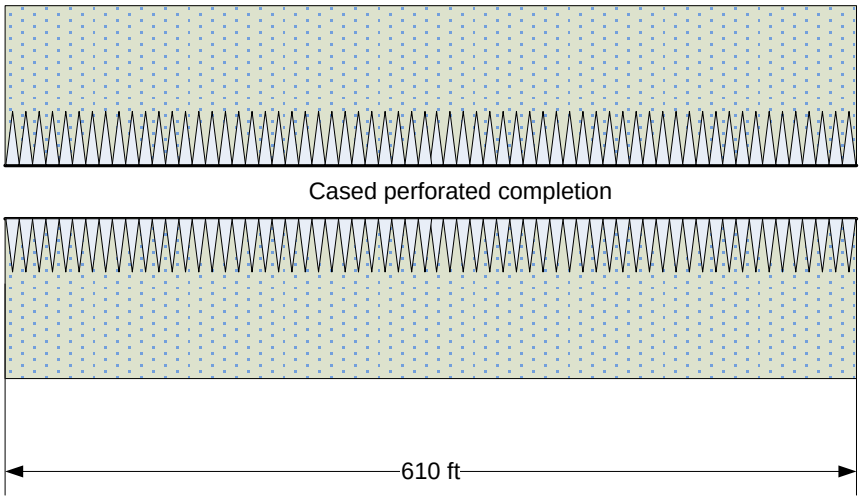

Fig. B18—Well diagram for Well 4

The data for the reservoir, the wellbore, and the acid injection is shown in the **Table B8** and **Table B9**.

Table B8—Input data for Well 4

Reservoir data	
Initial reservoir pressure, psi	2500
Porosity	0.17
Total compressibility, 1/psi	3.50E-06
Formation thickness, ft	161
Reservoir fluid viscosity, cp	0.51
Reservoir temperature, F	150
Permeability, md	3
Well data	
Wellbore radius, in	3
Tubing diameter, in	2.227
Pipe relative roughness	0.0001
Horizontal section length, ft	610
Wellbore fluid density, lbm/ft3	63.58
Wellbore fluid viscosity, cp	0.51

Table B9—Injection schedule for Well 4

Fluid Name	Volume Used, gal	Density, lb/ft3	Viscosity, cp	Friction Reducer
15% HCl	7318	67.3	0.51	0.1
Fresh water	880	63.6	0.51	0.1
22% CEA	18219	64.48	0.51	0.1
Fresh water	7707	63.21	0.51	0.1

B4.2 Skin Monitoring Results

Fig. B19 plots the measured injection rate, and the measured surface pressure recorded during the acidizing treatment.

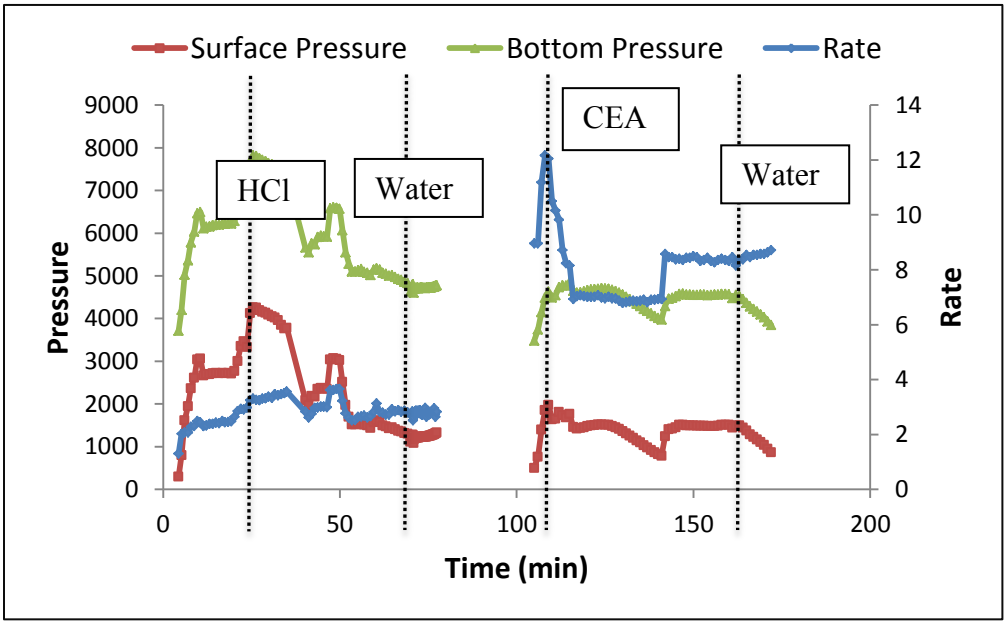

Fig. B19—Treatment data for Well 4

In **Fig. B19**, the bottomhole pressure was calculated from the surface pressure. From the calculated bottomhole pressure and measured injection rate, the skin was calculated at each time step. The skin evolution during the acid job is shown in the figure below.

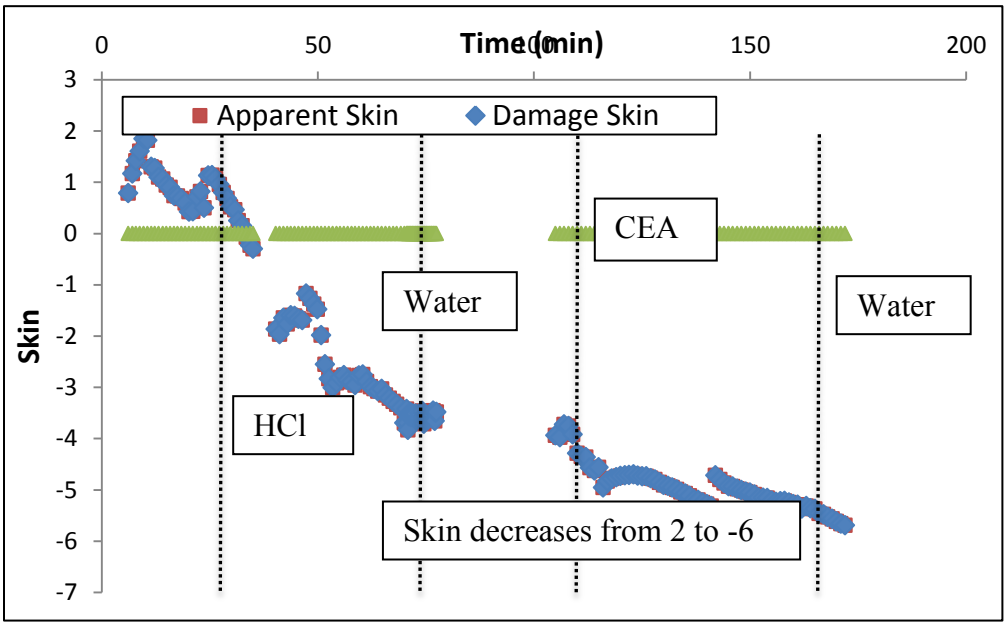

Fig. B20—Skin response for Well 4

B4.3 History Matching Results

From **Fig. B21**, it is observed that there are 7 zones of production, of which one zone has about 70 % of the total. To history match, the initial guess of the reservoir properties such as permeability and damage can be estimated for the beginning of the history matching process.

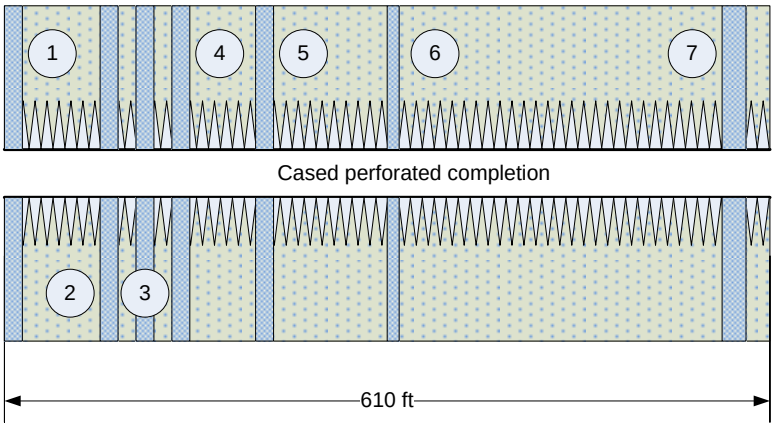

Fig. B21—Production log for Well 4

Table B10—Zone properties for Well 4

Zone	Length, ft	Horizontal permeability, md	Impairment ratio	Damage penetration, ft	PV_{bt-opt}	V_{i-opt}, cm/min
1	3	50	0.8	1	0.85	1.75
2	3	15	0.9	0.5	1	1.75
3	3	10	0.9	0.5	1	1.75
4	3	25	0.8	1	0.85	1.75
5	3	5	0.9	0.5	1	1.75
6	2	3	0.9	0.5	1	1.75
7	4	1	0.9	0.5	1	1.75

Since there was a stop in between the treatment, the data was missing. The history matching is divided into two stages HCl and CEA as shows in figures below.

The pressure response and skin factor predicted by the acidizing simulator for this well, which was stimulated by CT acid washed, are in good agreement with the skin analysis results.

For the acid treatment of this case, although the predicted the pressure response and skin evolution have a very similar trend, a slightly difference between the simulated values and skin monitoring program results was observed with lower pressure for HCl stage and higher pressure for CEA stage. An abrupt decrease in skin factor is observed at about 45 minute of the HCl stage. It is because the acid breaks through the damage in the high permeability zone.

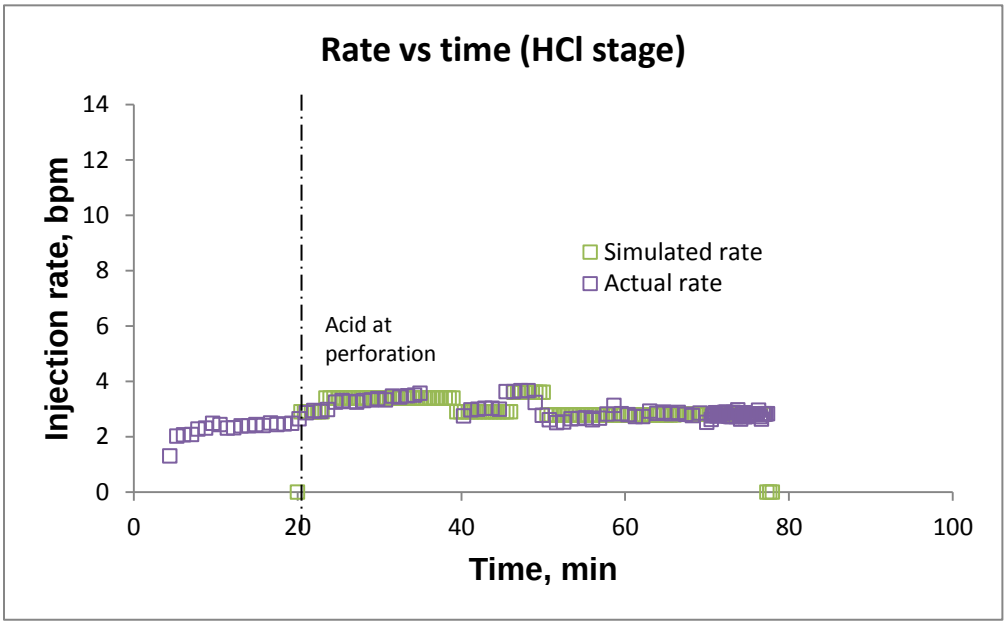

Fig. B22—Injection rate versus time for HCl stage for Well 4

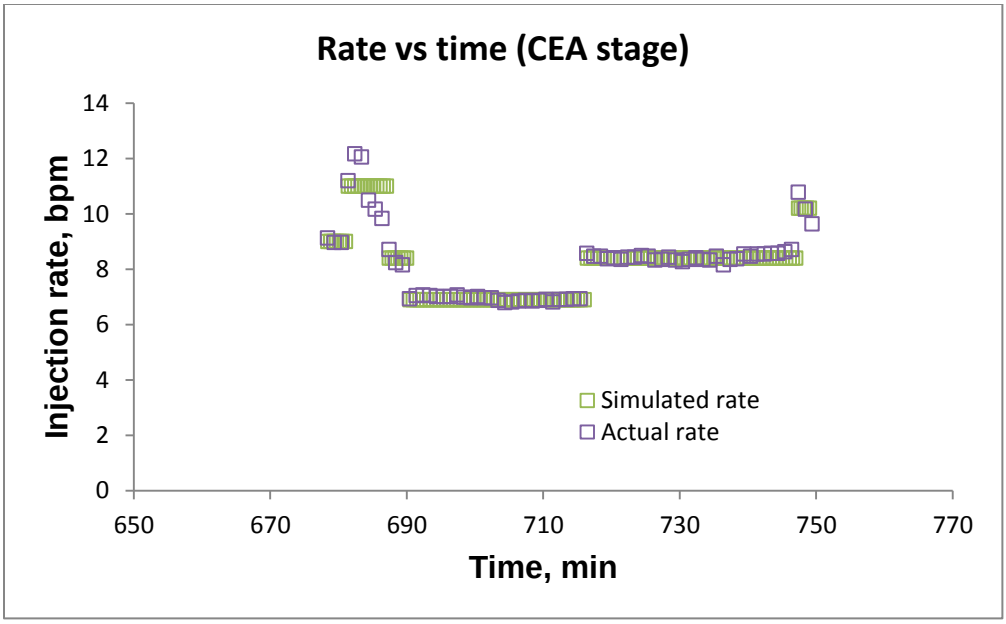

Fig. B23—Injection rate versus time for CEA stage for Well 4

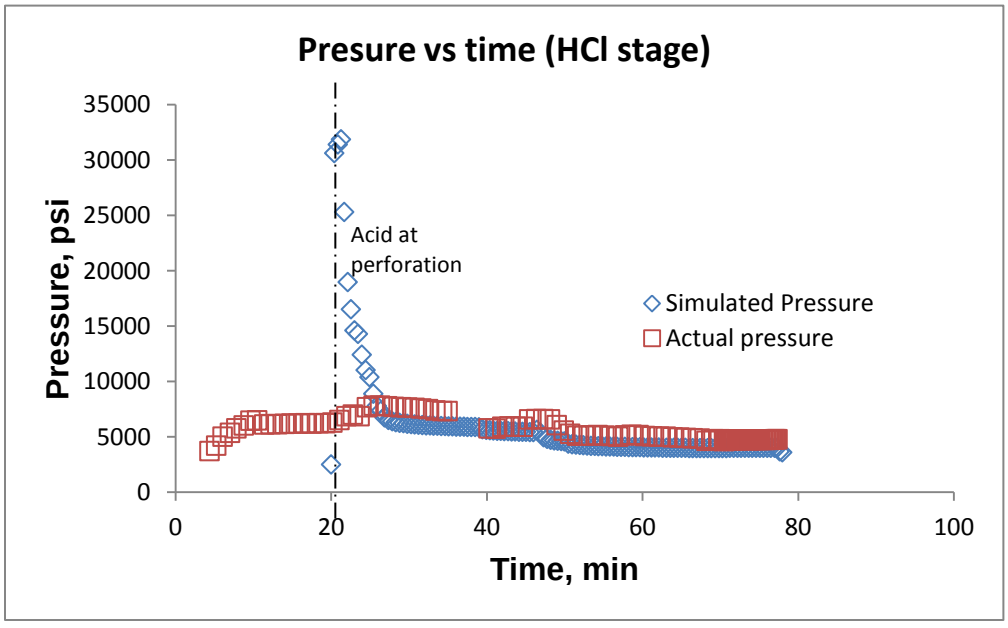

Fig. B24—Pressure versus time for HCl stage for Well 4

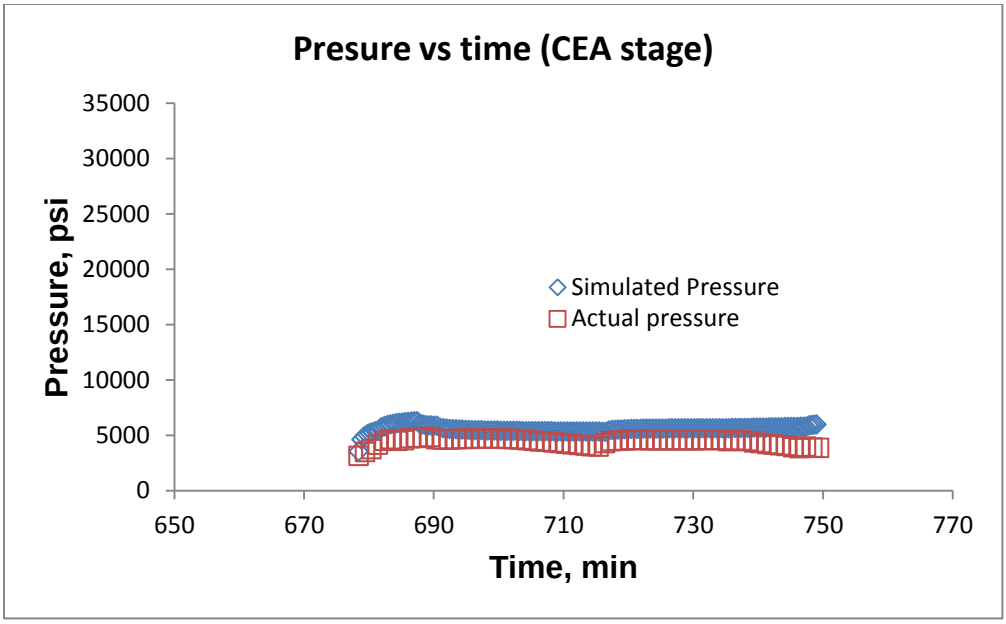

Fig. B25—Pressure versus time for CEA stage for Well 4

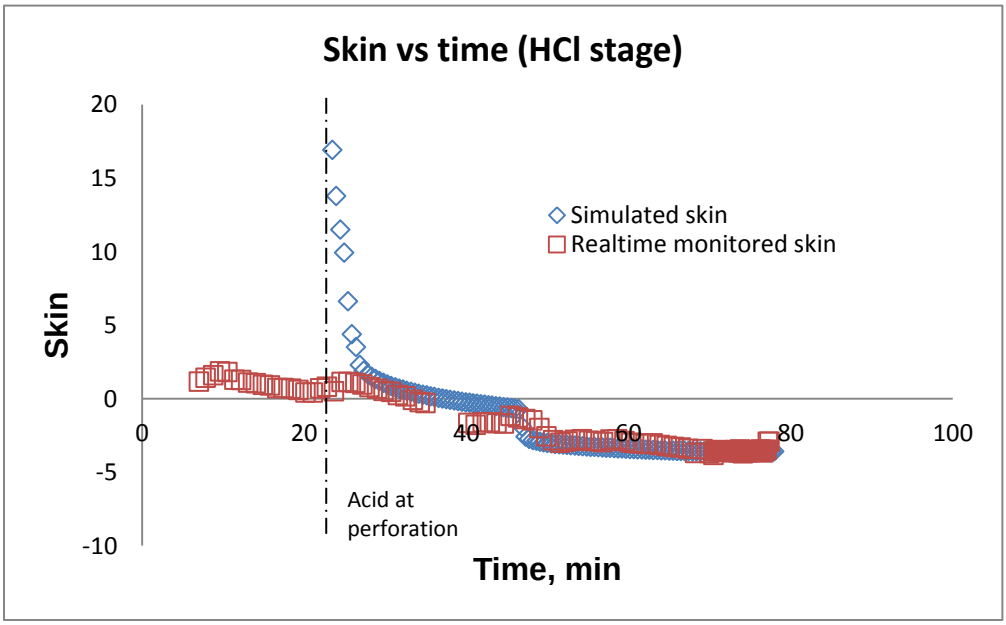

Fig. B26—Skin versus time for HCl stage for Well 4

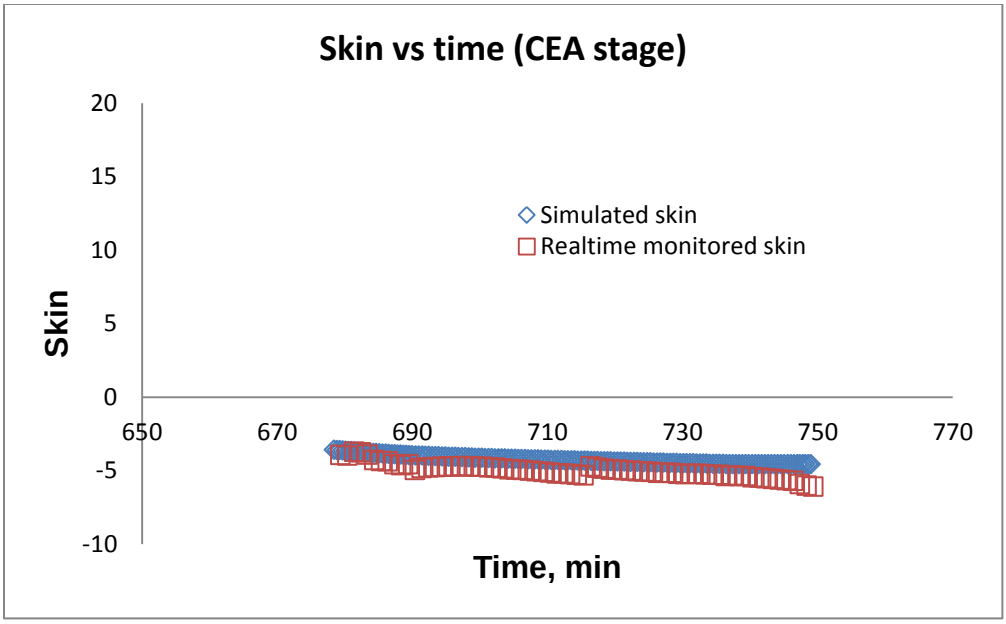

Fig. B27—Skin versus time for CEA stage for Well 4

In the figure above, the skin begins to decrease from 1 to -4 during HCl injection and from -4 to -6 during CEA injection. It is noticed that CEA system did not contribute significantly to the stimulation process as most of the decline in skin resulted during the HCl injection. The emulsified acid did not show any evidence of viscous diversion because no increasing trend in the skin is noticed.

The skin trend was validated using the production test from before and after the stimulation process. In this case, the production rate of liquids from this well after stimulation increased to 8462 barrels/day.

B5. Well 5

B5.1 Treatment Description

This well is a horizontal well with an open-hole lateral, as seen in **Fig. B28**. The actual acidizing treatment design comprised of treating the target interval in two stages: first stage with 15% hydrochloric acid (HCl) and second stage with nitrified foam acid using coil-tubing.

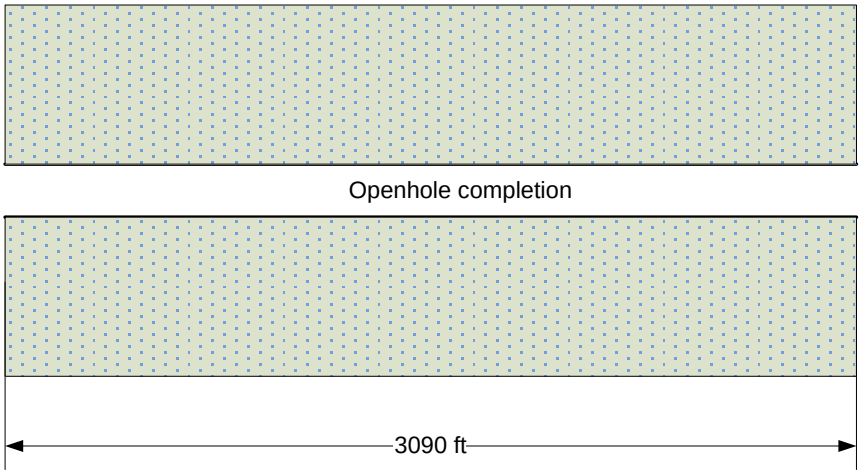

Fig. B28—Well diagram for Well 5

The data for the reservoir, the wellbore, and the acid injection is shown in the **Table B11** and **Table B12**.

Table B11—Input data for Well 5

Reservoir data	
Initial reservoir pressure, psi	2200
Porosity	0.08
Total compressibility, 1/psi	3.50E-06
Formation thickness, ft	25
Reservoir fluid viscosity, cp	0.46
Reservoir temperature, F	100
Permeability, md	2.5
Well ata	
Casing OD, in	9.625
Casing ID, in	8.681
Liner OD, in	7.000
Liner ID, in	6.184
Tubing OD, in	3.500
Tubing ID, in	2.992
Pipe relative roughness	0.0001
Horizontal section length, ft	3090
Wellbore fluid density, lbm/ft3	63.58
Wellbore fluid viscosity, cp	1.0

Table B12—Injection schedule for Well 5

Fluid Name	Volume Used, gal	Density, lb/ft3	Viscosity, cp	Friction Reducer
HCl	63798	63.58	0.51	0
Foam acid	15960	50.00	0.51	0

B5.2 Skin Monitoring Results

Fig. B29, Fig. B30 and **Fig. B31** show the measured annular pressure, bottomhole pressure, injection rate, and skin evolution of the treatment.

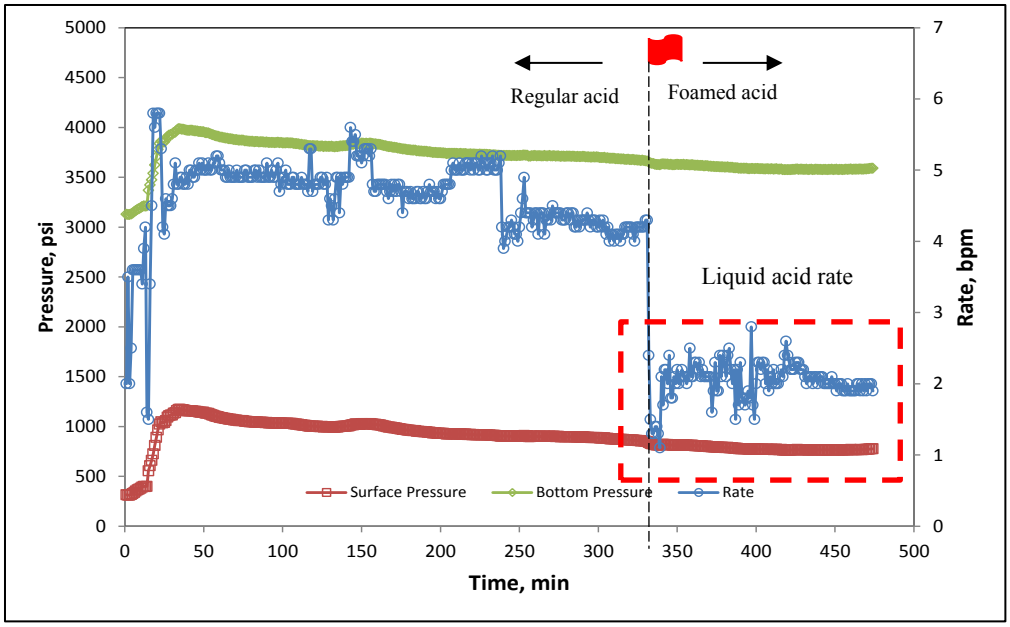

Fig. B29—Treatment data for Well 5

In **Fig. B29** the injection rate of the foamed acid stage is the liquid acid rate only. The injection rate of foamed acid in **Fig. B30** is the total acid injection rate which is the sum of liquid and nitrogen gas rates calculated from **Eqs. 4.1** and **4.2**.

The bottomhole pressure response indicates the stimulation effect of the acid treatment and the skin factor of this well decreases from about zero to -2 (**Fig. B31**). The production test after the acid job shows that the production rate of this well has doubled compared to the one before the test.

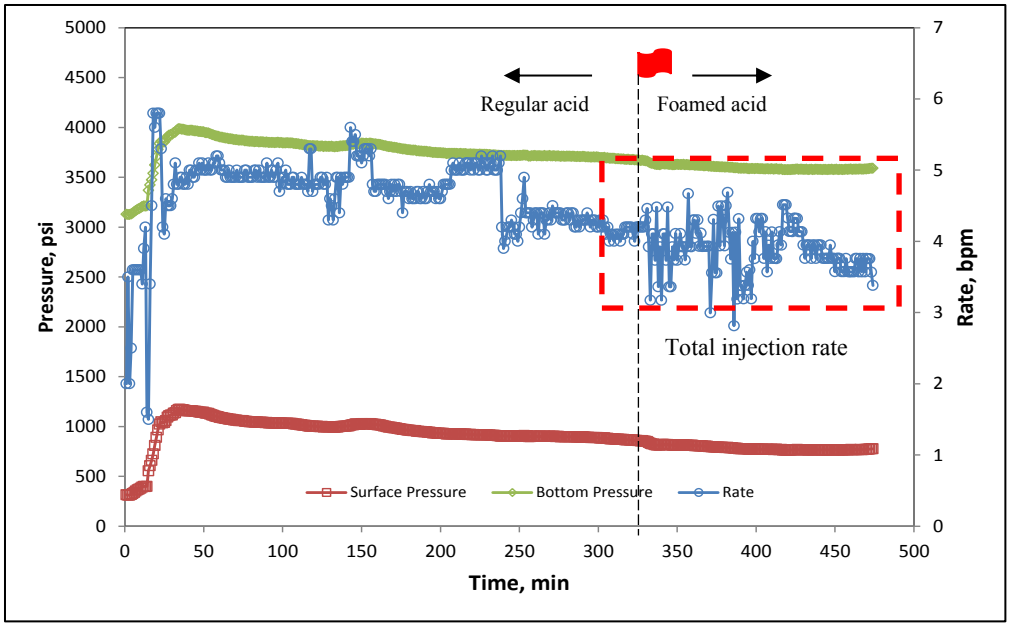

Fig. B30—Treatment data with adjusted total injection rate for Well 5

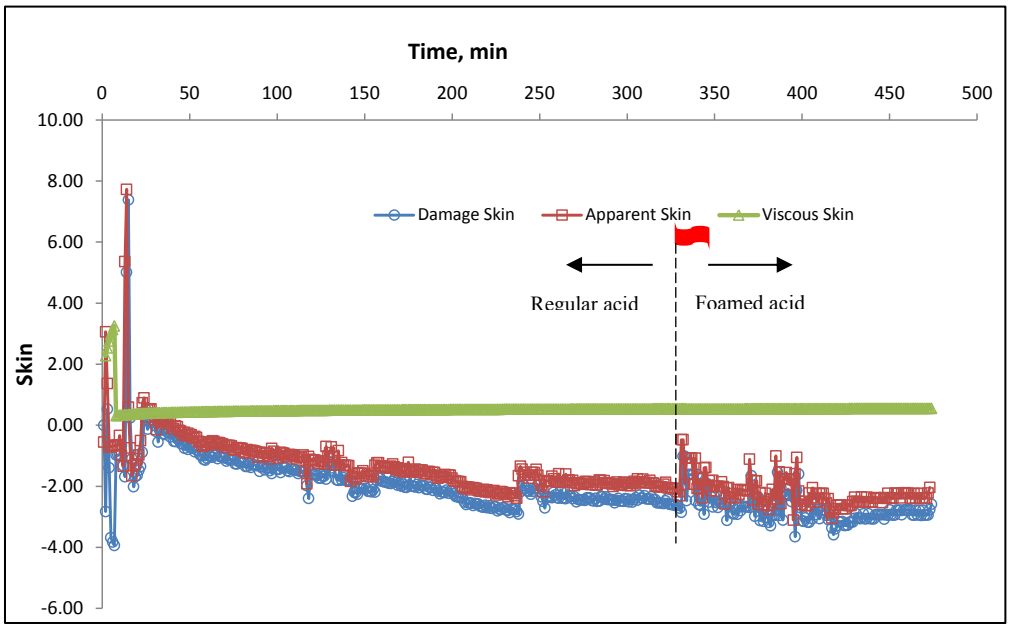

Fig. B31—Skin response for Well 5

B5.3 History Matching Results

This horizontal well penetrated dolomite and limestone layers in the reservoir. The zone properties input for history matching by the acidizing simulator is presented in **Table B13**.

Table B13—Zone properties for Well 5

Zone data							
Zone	Rock type	Porosity	Perm, md	Impairment ratio	Damage penetration, ft	PV_{bt-opt}	V_{i-opt}, cm/min
1	Dolomite	0.07	5	0.2	2	1	1
2	Limestone	0.08	0	0.2	2	1	1
3	Limestone	0.08	2	0.1	2	0.23	0.41
5	Limestone	0.08	1	0.5	2	0.85	1

Fig. B32 and **Fig. B33** show the results of history matching the bottomhole pressure and skin factor. The bottomhole pressure and skin factor obtained from running the acidizing simulator have good agreement with the actual values estimated from the skin analysis results.

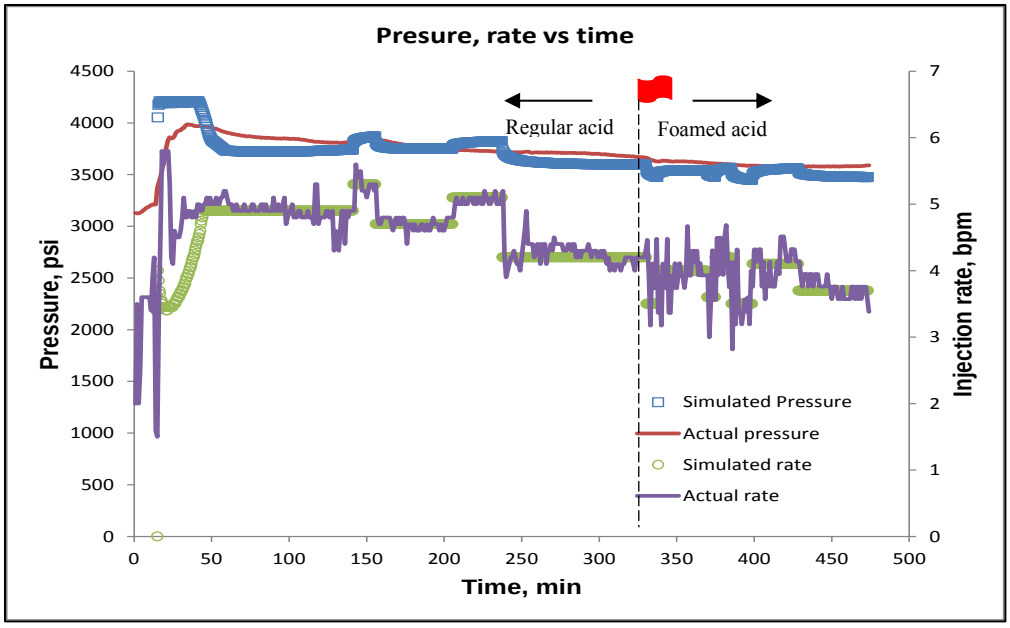

Fig. B32—Pressure and rate history matched results for Well 5

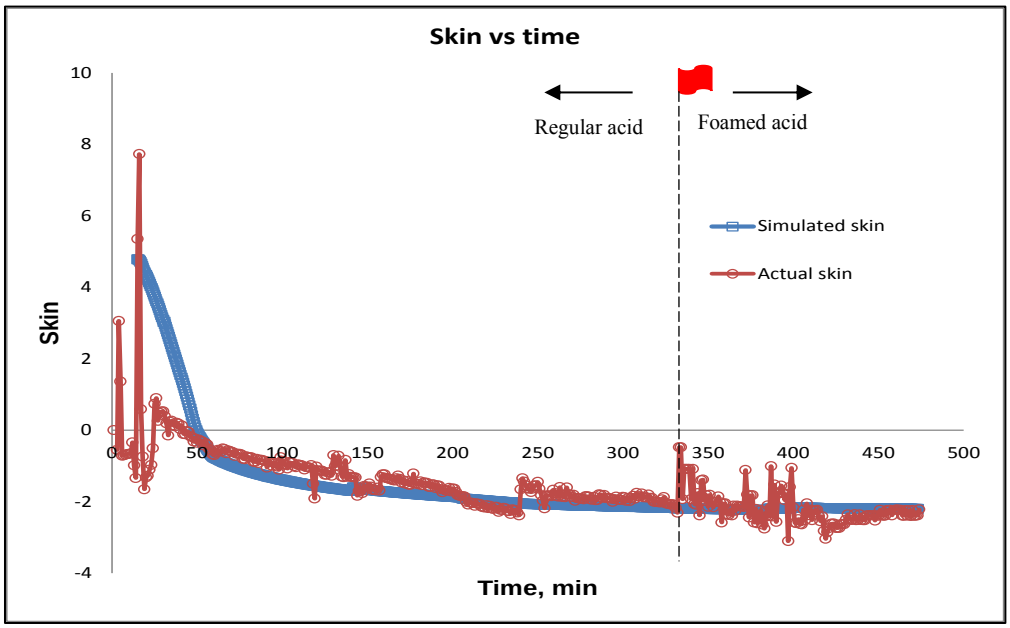

Fig. B33—Skin evolution history matched result for Well 5

B6. Well 6

B6.1 Treatment Description

This well is a horizontal well with an open-hole lateral, as seen in **Fig. B34**. The actual acidizing treatment design comprised of treating the target interval in two stages: first stage with 15% hydrochloric acid (HCl) and second stage with nitrified foam acid using coil-tubing.

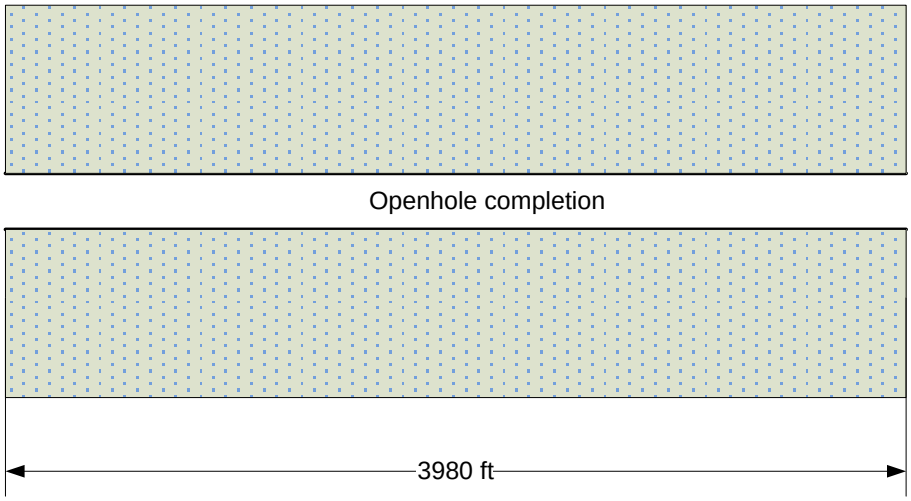

Fig. B34—Well diagram for Well 6

The data for the reservoir, the wellbore, and the acid injection is shown in the **Table B.14** and **Table B.15**.

Table B.14—Input data for Well 6

Reservoir data	
Initial reservoir pressure, psi	2500
Porosity	0.15
Total compressibility, 1/psi	3.50E-06
Formation thickness, ft	70
Reservoir fluid viscosity, cp	0.46
Reservoir temperature, F	100
Permeability, md	6
Well data	
Casing OD, in	9.625
Casing ID, in	8.681
Liner OD, in	7.000
Liner ID, in	6.184
Tubing OD, in	3.500
Tubing ID, in	2.992
Pipe relative roughness	0.0001
Horizontal section length, ft	3980
Wellbore fluid density, lbm/ft3	63.58
Wellbore fluid viscosity, cp	1.0

Table B.15—Injection schedule for Well 6

Fluid Name	Volume Used, gal	Density, lb/ft3	Viscosity, cp	Friction Reducer
HCl	79590	63.58	0.51	0
Foam acid	19908	50.00	0.51	0

B6.2 Skin Monitoring Results

Fig. B35, Fig. B 36 and **Fig. B37** show the measured annular pressure, bottomhole pressure, injection rate, and skin evolution of the treatment.

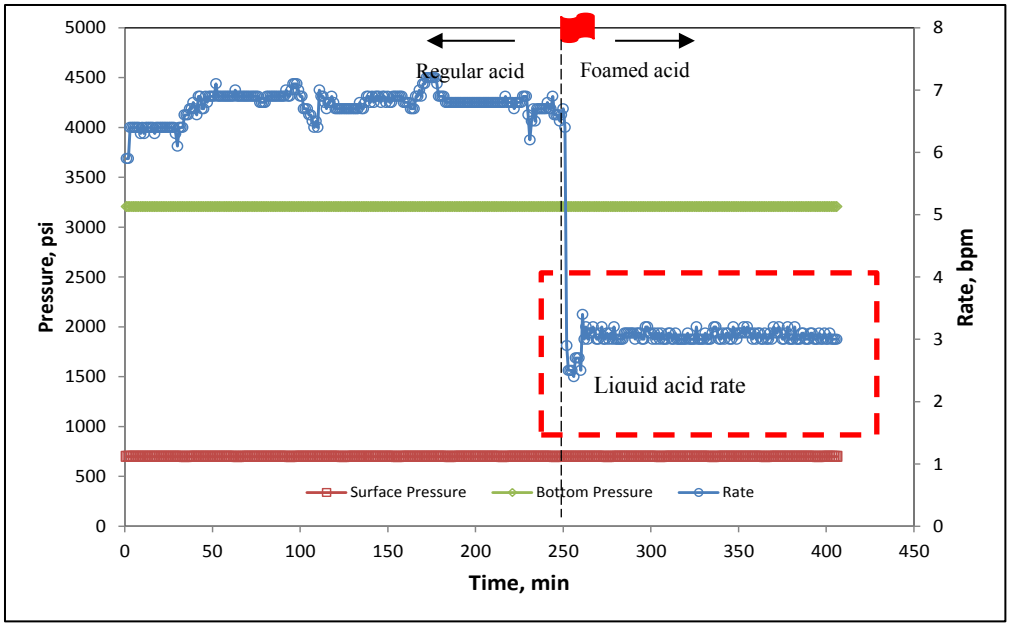

Fig. B35—Treatment data for Well 6

In **Fig. B35** the injection rate of the foamed acid stage is the liquid acid rate only. The injection rate of foamed acid in **Fig. B 36** is the total acid injection rate which is the sum of liquid and nitrogen gas rates.

The annular pressure is almost constant for the treatment of this well then is the bottomhole pressure. The production test after the acid job shows that the production rate of this well has increased about 15% (from 2981 to 3431 BOPD). The result of the skin analysis (**Fig. B37**) shows that the stimulation effect of the treatment is not significant.

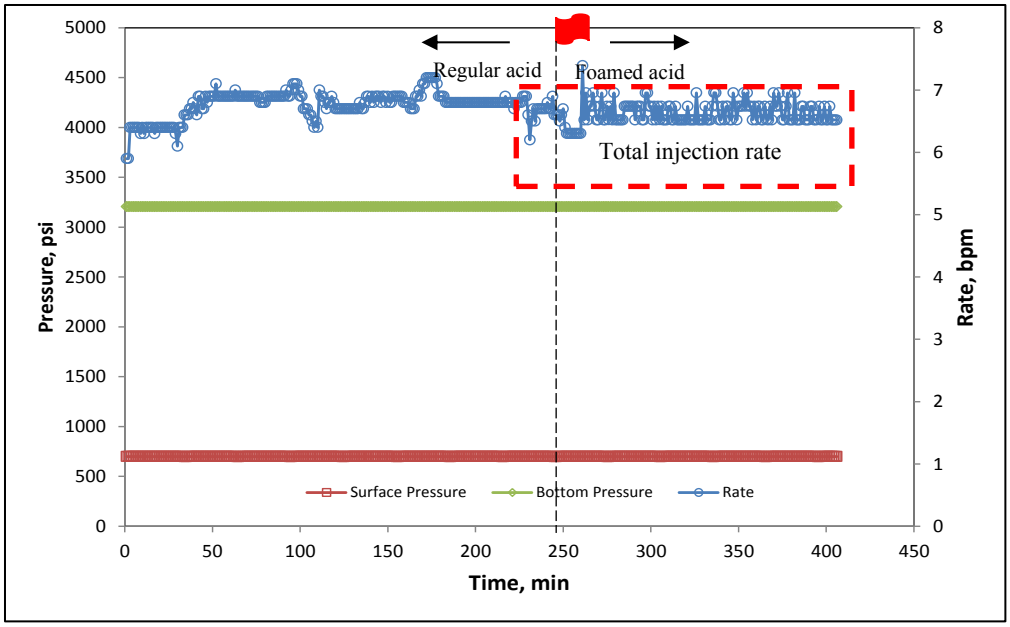

Fig. B 36—Treatment data with adjusted total injection rate for Well 6

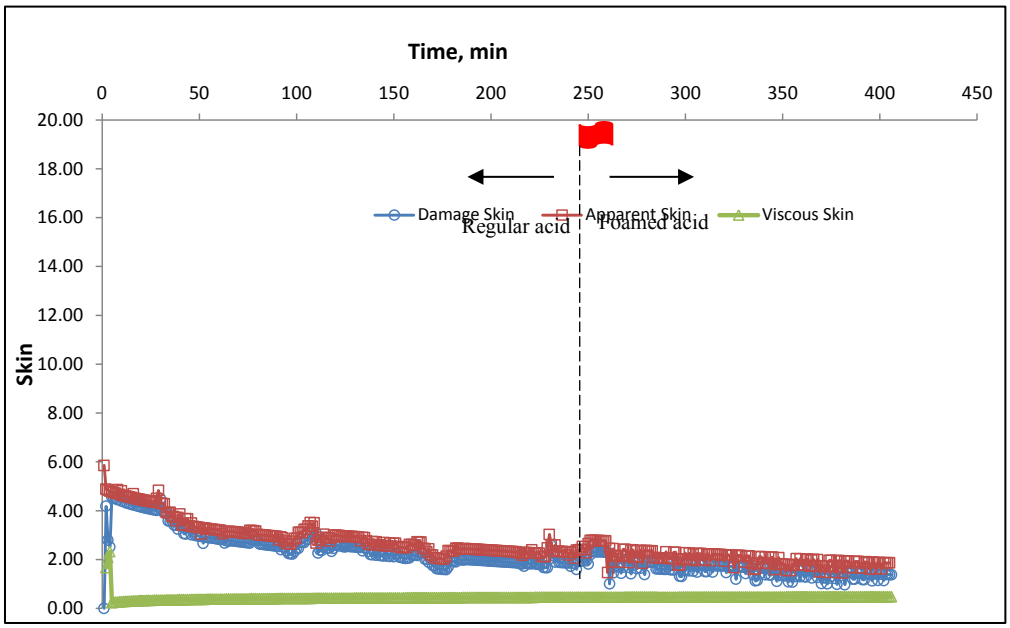

Fig. B37—Skin response for Well 6

B6.3 History Matching Results

Fig. B38 and **Fig. B39** show the results of history matching the bottomhole pressure and skin factor.

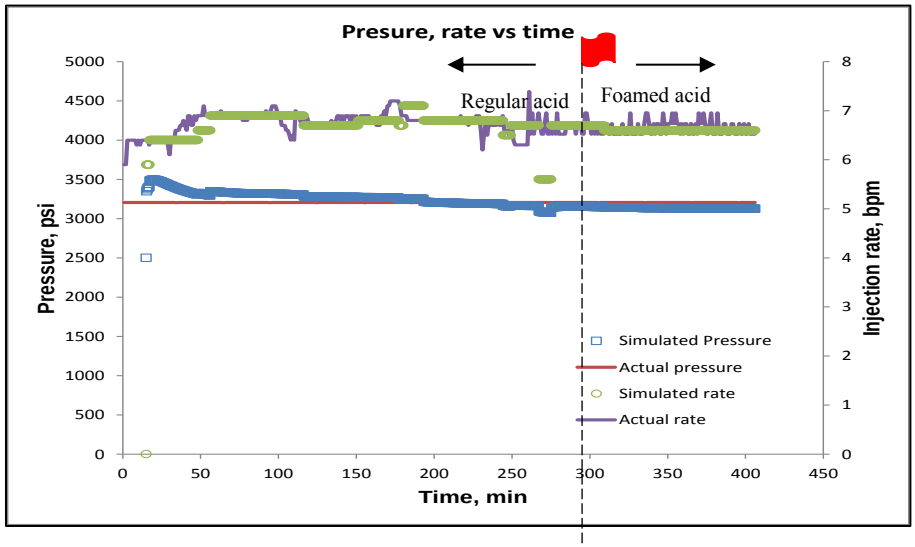

Fig. B38—Pressure and rate history matched results for Well 6

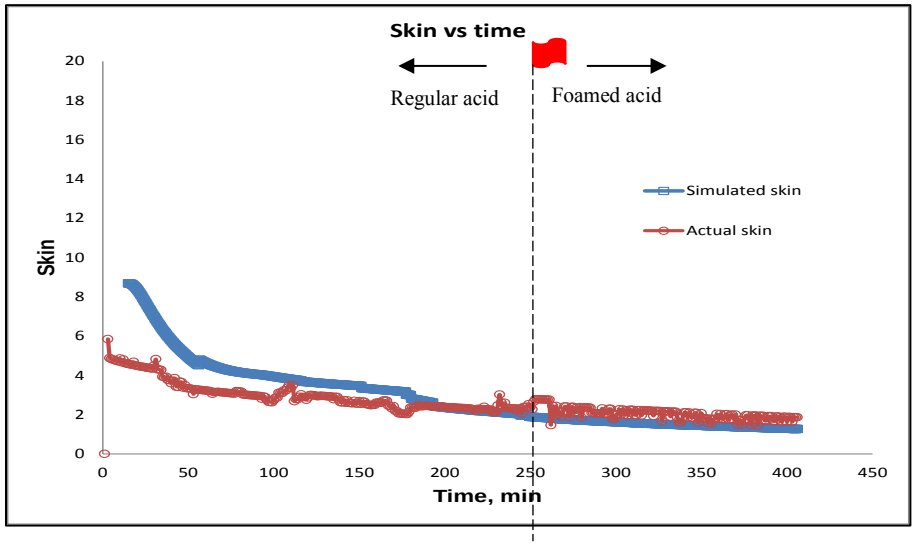

Fig. B39—Skin evolution history matched result for Well 6

B7. Well 7

B7.1 Treatment Description

This well is a horizontal well with an open-hole lateral, as seen in **Fig. B40**. The actual acidizing treatment design comprised of treating the target interval in two stages: first stage with 15% hydrochloric acid (HCl) and second stage with nitrified foam acid using coil-tubing.

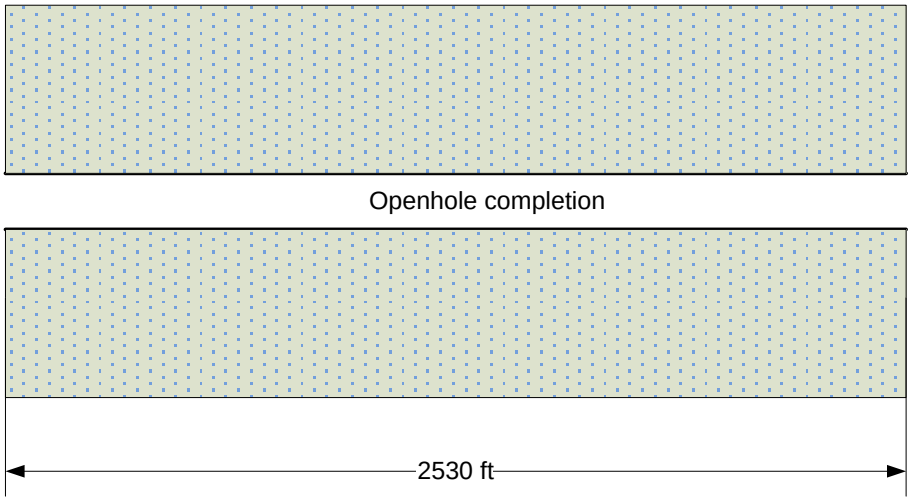

Fig. B40—Well diagram for Well 7

The data for the reservoir, the wellbore, and the acid injection is shown in the **Table B16** and **Table B17**.

Table B16—Input data for Well 7

Reservoir data	
Initial reservoir pressure, psi	2500
Porosity	0.20
Total compressibility, 1/psi	3.50E-06
Formation thickness, ft	16
Reservoir fluid viscosity, cp	0.46
Reservoir temperature, F	100
Permeability, md	15
Well data	
Casing OD, in	9.625
Casing ID, in	8.681
Liner OD, in	7.000
Liner ID, in	6.184
Tubing OD, in	3.500
Tubing ID, in	2.992
Pipe relative roughness	0.0001
Horizontal section length, ft	2530
Wellbore fluid density, lbm/ft3	63.58
Wellbore fluid viscosity, cp	1.0

Table B17—Injection schedule for Well 7

Fluid Name	Volume Used, gal	Density, lb/ft3	Viscosity, cp	Friction Reducer
HCl	25242	63.58	0.51	0
Foam acid	27502	50.00	0.51	0

B7.2 Skin Monitoring Results

Fig. B41, **Fig. B42** and **Fig. B43** show the measured annular pressure, bottomhole pressure, injection rate, and skin evolution of the treatment.

The production test after the acid job shows that the production rate of this well has increased about 2% or almost no stimulation effect has occurred. The annular pressure for the treatment of this well slightly increases, so does the bottomhole pressure (**Fig. B42**). The estimated apparent skin has the same trend as that of the bottomhole pressure (**Fig. B43**). The increasing trend does not mean that the well has been damaged during the treatment. This is possibly caused by the increasing of the viscosity of the nitrified foamed acid and that viscosity changes overtime during the treatment. The damage skin does not change during the treatment.

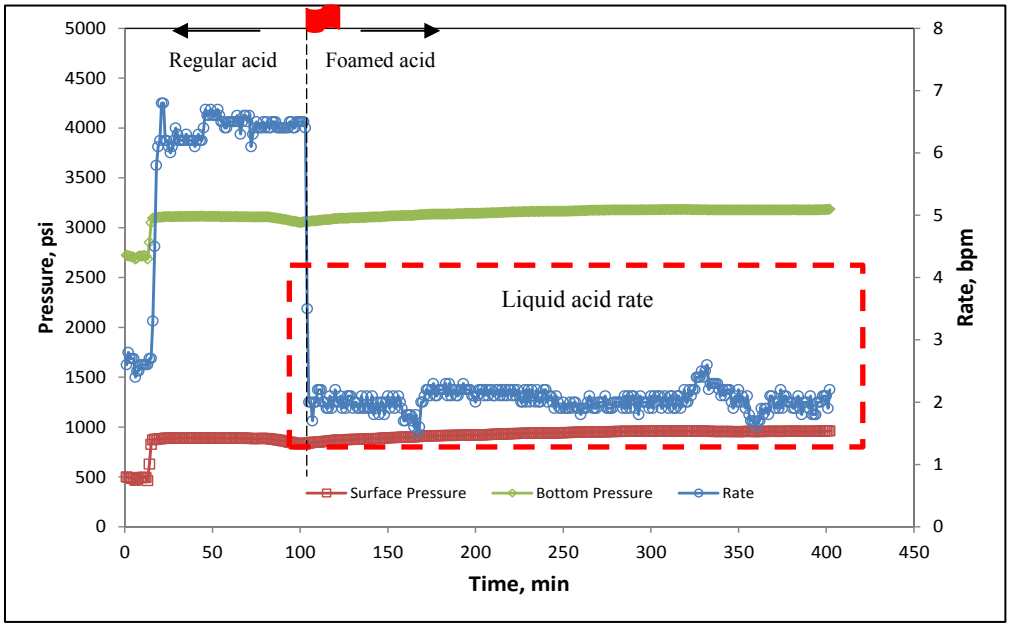

Fig. B41—Treatment data for Well 7

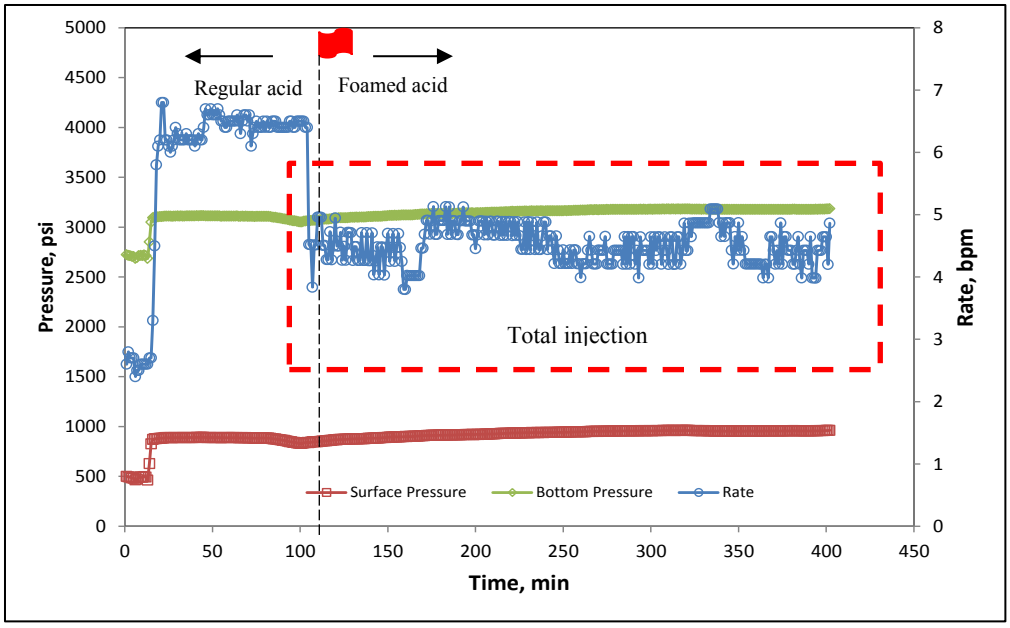

Fig. B42— Treatment data with adjusted total injection rate for Well 7

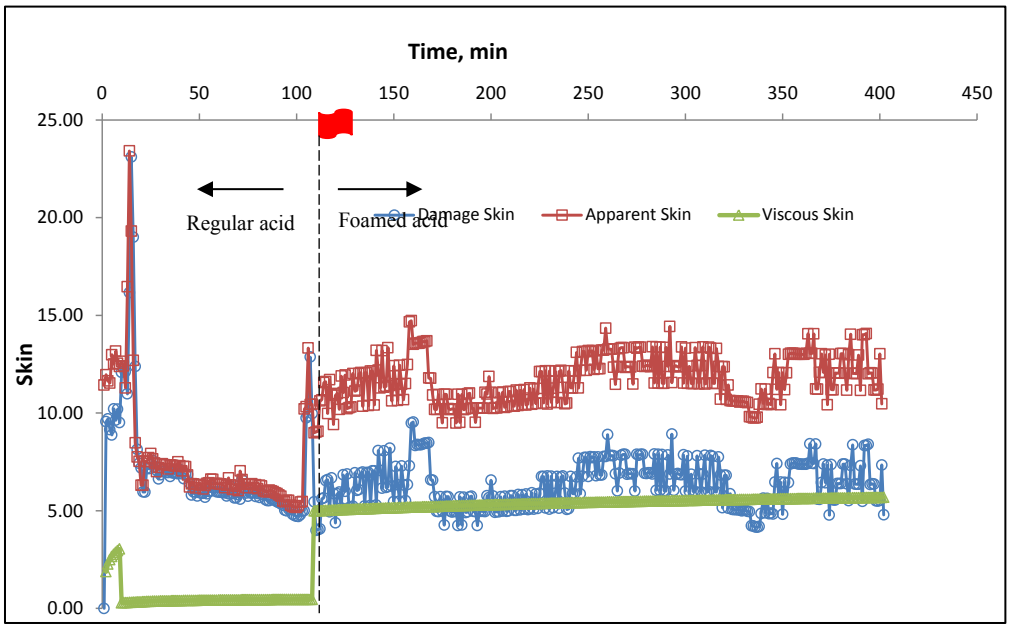

Fig. B43—Skin evolution for Well 7

B7.3 History Matching Results

Fig. B44 and **Fig. B45** show the results of history matching the bottomhole pressure and skin factor.

The bottmhole pressure and skin factor obtained from the acidizing simulator are in good agreement with the actual values estimated from the skin analysis results. The maximum bottomhole pressure had value of 3000 psi and average rate was 5.5 bpm.

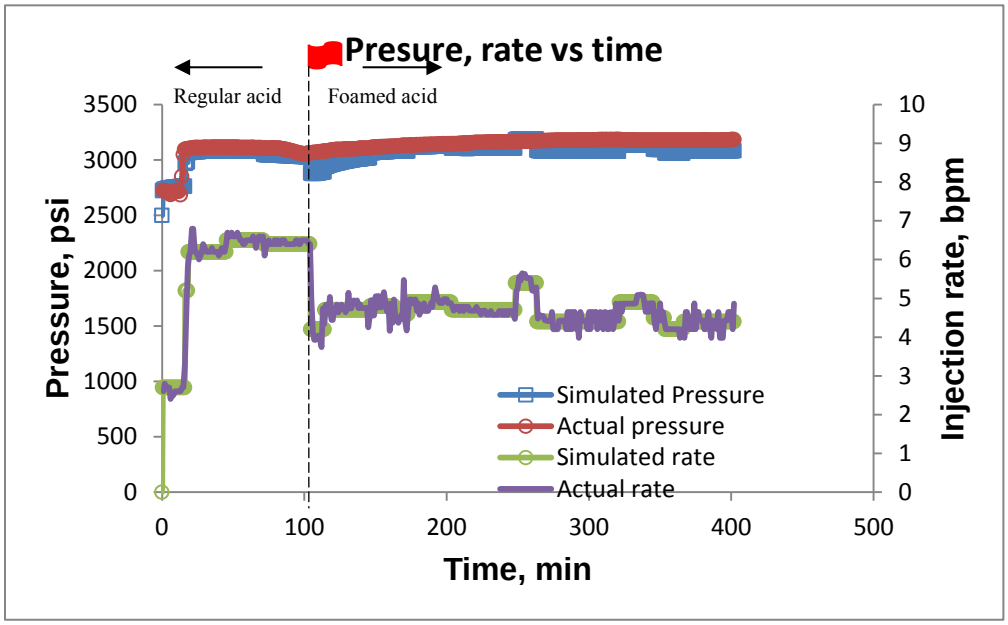

Fig. B44—Pressure and rate history matched results for Well 7

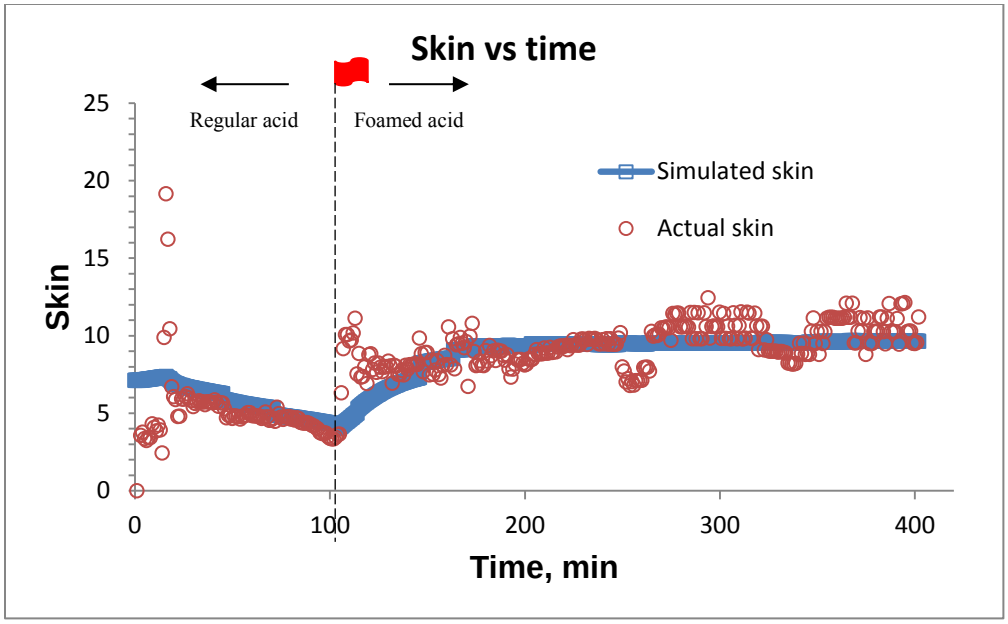

Fig. B45—Skin evolution history matched result for Well 7

B8. Well 8

B8.1 Treatment Description

This well is a horizontal well with an open-hole lateral, as seen in **Fig. B46**. The actual acidizing treatment design comprised of treating the target interval in two stages: first stage with 15% hydrochloric acid (HCl) and second stage with nitrified foam acid using coil-tubing.

The data for the reservoir, the wellbore, and the acid injection is shown in the **Table B18** and **Table B19**.

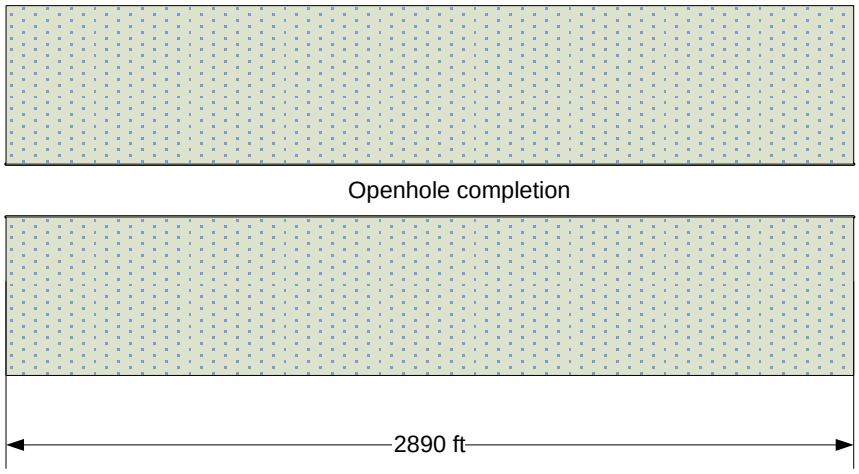

Fig. B46—Well diagram for Well 8

Table B18—Input data for Well 8

Reservoir data	
Initial reservoir pressure, psi	2500
Porosity	0.15
Total compressibility, 1/psi	3.50E-06
Formation thickness, ft	17
Reservoir fluid viscosity, cp	0.46
Reservoir temperature, F	100
Permeability, md	10
Well data	
Casing OD, in	9.625
Casing ID, in	8.681
Liner OD, in	7.000
Liner ID, in	6.184
Tubing OD, in	3.500
Tubing ID, in	2.992
Pipe relative roughness	0.0001
Horizontal section length, ft	2890
Wellbore fluid density, lbm/ft3	63.58
Wellbore fluid viscosity, cp	1.0

Table B19—Injection schedule for Well 8

Fluid Name	Volume Used, gal	Density, lb/ft3	Viscosity, cp	Friction Reducer
HCl	57708	63.58	0.51	0
Foam acid	14406	50.00	0.51	0

B8.2 Skin Monitoring Results

Fig. B47, **Fig. B48** and **Fig. B49** show the measured annular pressure, bottomhole pressure, injection rate, and skin evolution of the treatment.

The production test after the acid job shows that the production rate of this well has increased about 14% (from 287 to 327 BOPD). The annular pressure for the treatment of this well slightly increases, so does the bottomhole pressure (**Fig. B48**).

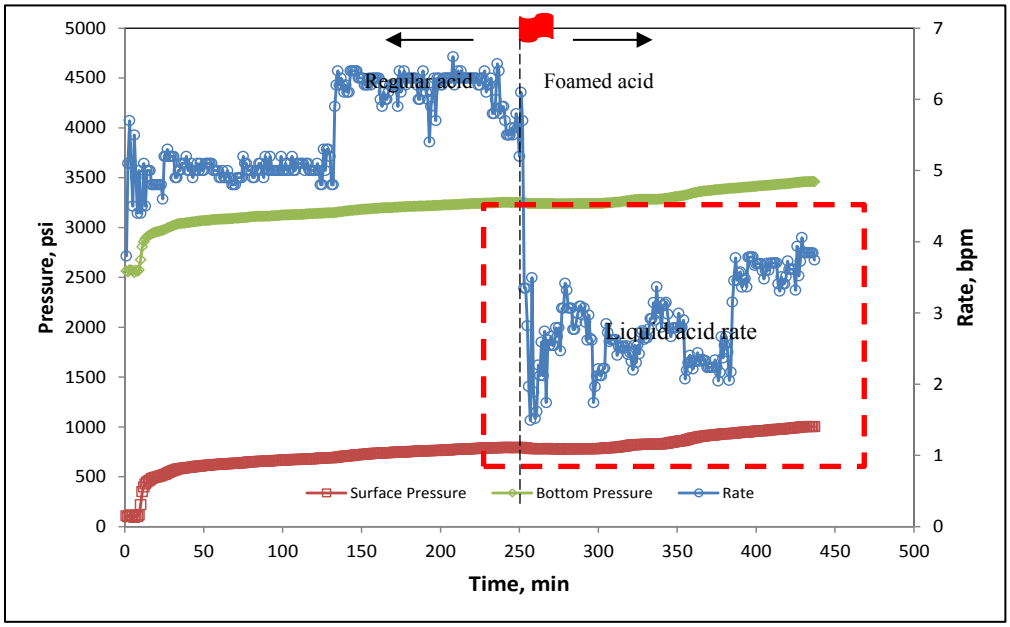

Fig. B47—Treatment data for Well 8

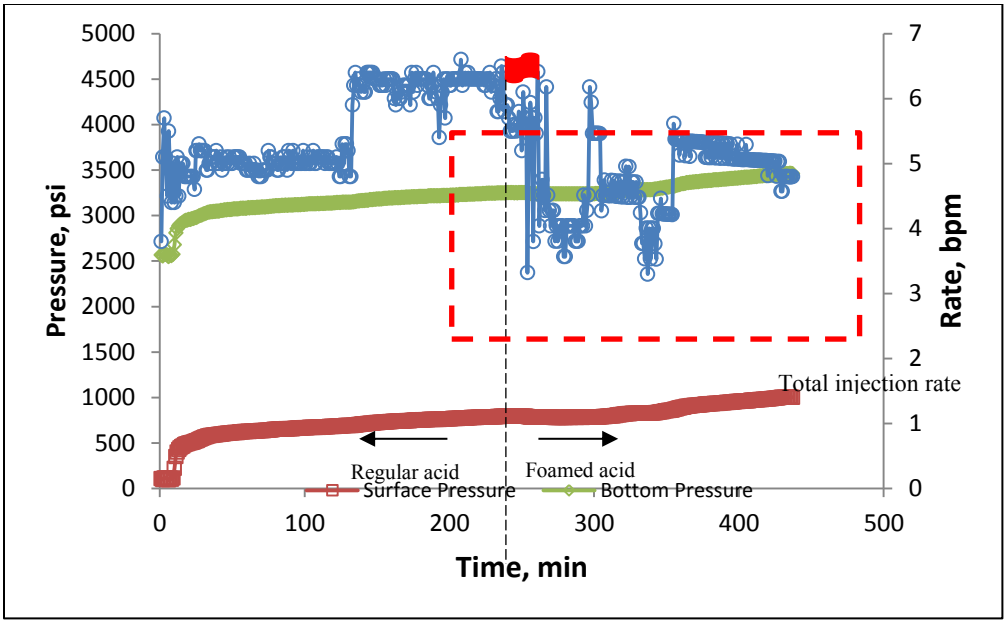

Fig. B48— Treatment data with adjusted total injection rate for Well 8

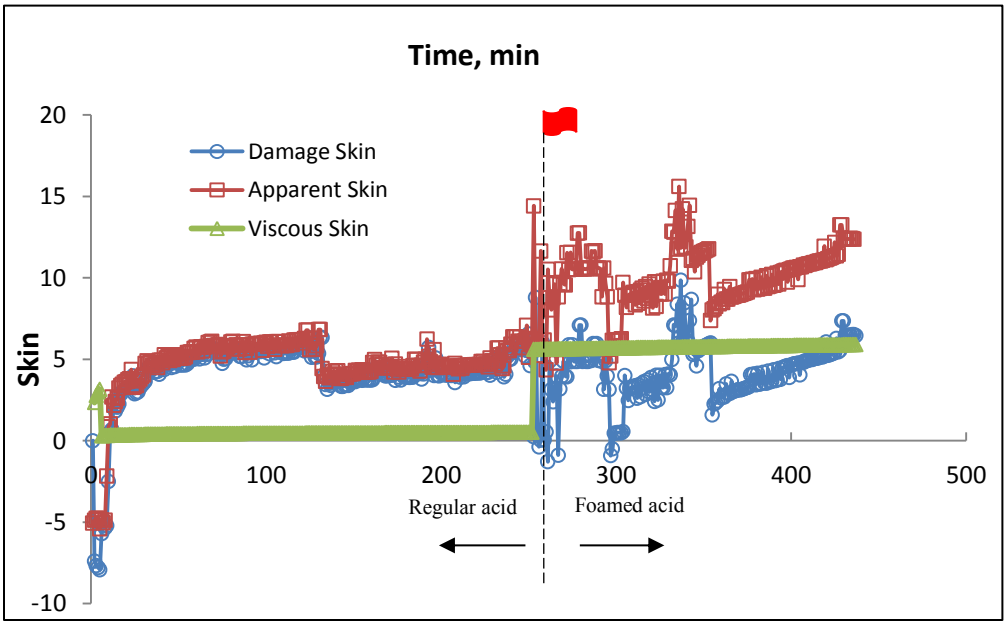

Fig. B49—Skin evolution for Well 8

The estimated apparent skin has the same trend as that of the bottomhole pressure (**Fig. B49**). The increasing trend does not mean that the well has been damaged during the treatment. This is possibly caused by the increasing of the viscosity of the nitrified foamed acid and that viscosity changes overtime during the treatment. The damage skin does slightly decrease after the treatment and causes the slight increase in production (14%).

B8.3 History Matching Results

Fig. B50 and **Fig. B51** show the results of history matching the bottomhole pressure and skin factor.

The bottmhole pressure and skin factor obtained from the acidizing simulator have good agreement with the actual values estimated from the skin analysis results.

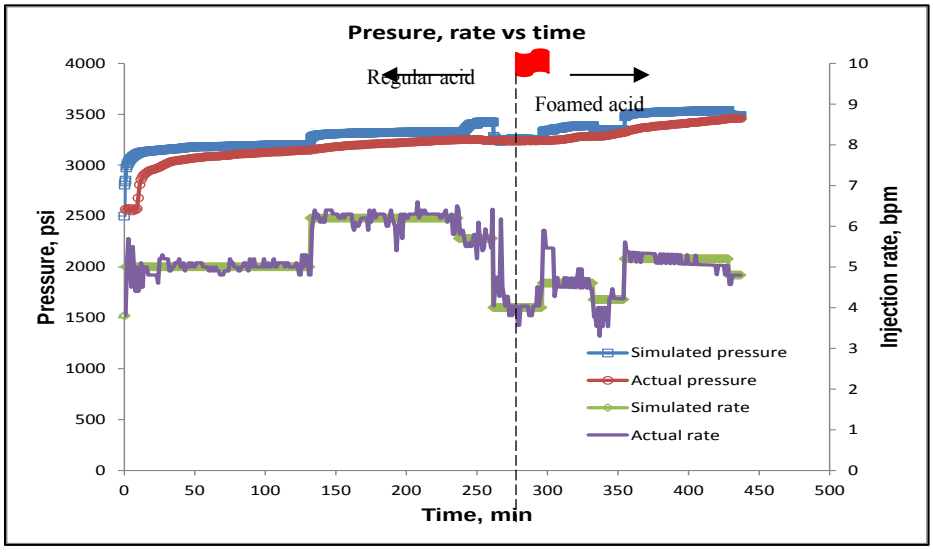

Fig. B50—Pressure and rate history matched results for Well 8

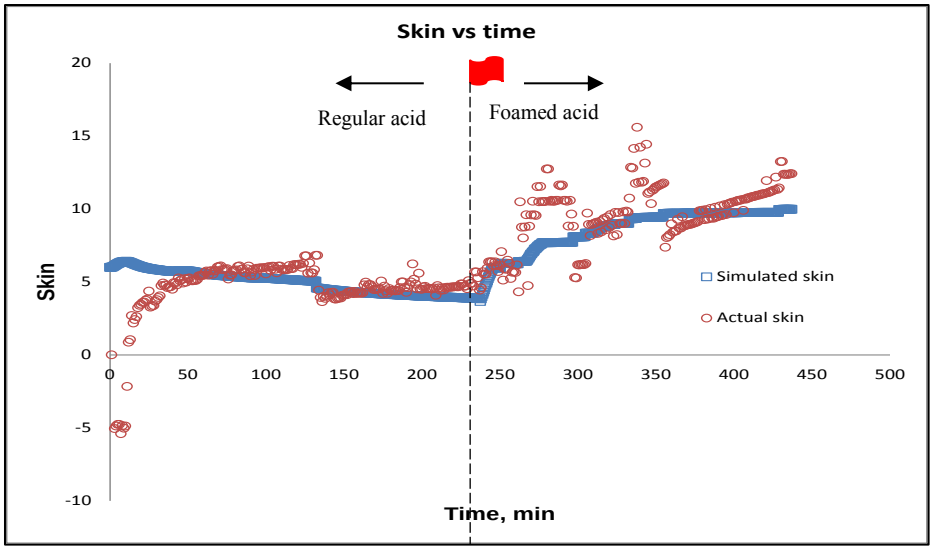

Fig. B51—Skin evolution history matched result for Well 8